Master Thesis

Mineralogy of the Talc-Carbonate-Pyrite-Schist and its spatial distribution in open pit 3 of the Nkomati Nickel Mine in the Uitkomst Complex, South Africa

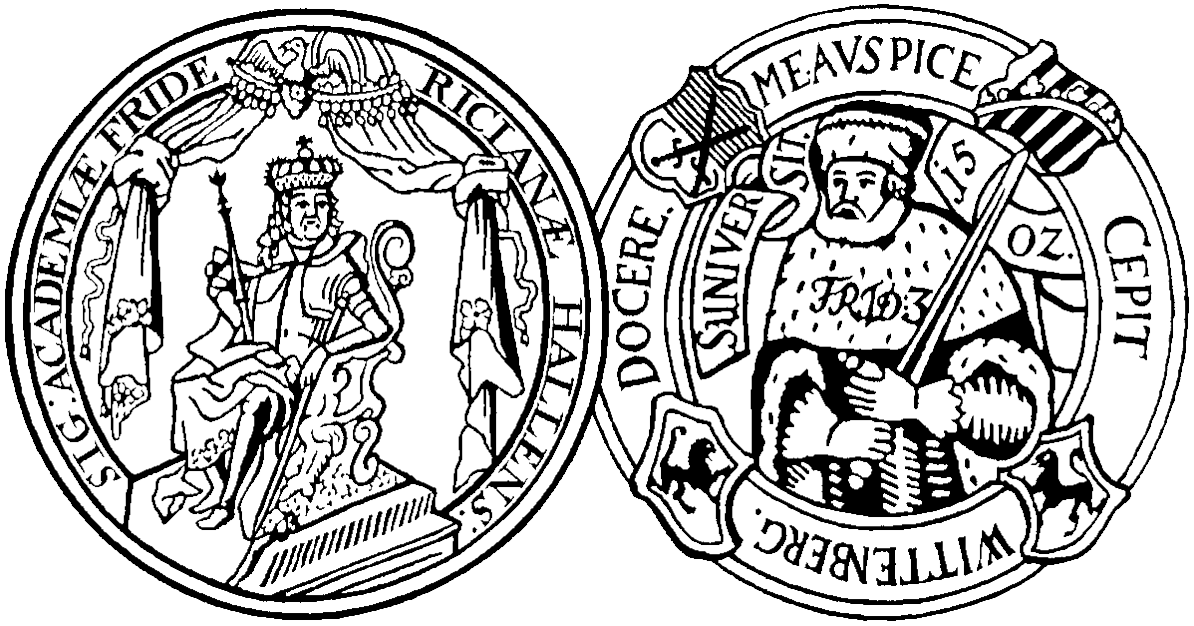

First Redactor: Prof. Gregor Borg
Second Redactor: Prof. Christoph Gauert

Christian Günther
MSc Applied Geosciences
Institute of Geosciences and Geography
Economic Geology and Petrology Research Unit
Martin-Luther-Universität Halle-Wittenberg

Academic honesty declaration

I assure that I wrote the MSc Thesis independently and by myself. I did not use tools or sources which are not cited. The sections I adopted word by word are marked. The thesis has not been submitted to any other examination board.

Name: Christian Günther
Student number: 207207640
Date: 31.03.2013

Content

Abstract

The Uitkomst Complex is an elongated, layered, mineralized, mafic to ultramafic intrusion with a trough or boat-like form in the Mpumalanga Province, South Africa. It bears significant amounts of Ni-, Cu- and PGE-ore. The lower three units of complex are intensely saussuritiсised, amphibolitised, serpentinised, talcified and carbonatised. Talc-carbonate-pyrite schist frequently occurs in the Chromitiferous Peridotite (PCR) unit. Isolated appearances were also observed in the Lower Pyroxenite (LPxt). The pyrite diminishes the total concentration of the nickel in the ore which resulting in local low-grade ore portions in the Nkomati mine.

The alteration zones are very widespread and structurally related to the NE-SW trending main faults as well as to the thrusts in the PCR unit.

According to the XRD data the mineral assemblages are variable in the talc-carbonate schist, which gives rise to different compositions detected by the XRF measurements. The observed mineral assemblage is calcite-dolomite-talc-lizardite/chrysotile-clinochlore-tremolite-biotite-pyrite-pyrrhotite-pentlandite-chalcopyrite.

The rocks have high loss of ignition and high carbonate chlorite pyrite indices (Large et al., 2001) near 100 indicating very high degree of alteration.

The talc-carbonate schist was formed by H_2O and CO_2 rich fluids derived from dolomites, which were assimilated by the ultramafic magma. The carbonates degassed and provided the CO_2, which is necessary for the talc-carbonate alteration.

According to modelled pseudosections in the system SiO_2-MgO-CaO-Al_2O_3-H_2O-CO_2 and the composition of the chromites the formation temperature of the alteration paragenesis is estimated to be about 500°C. The formation of the talc-carbonate-pyrite schist is a retrograde alteration process.

1 Introduction

The Nkomati joint venture is the main nickel producer in South Africa. During the exploitation of the ore body some problems regarding the flotation of the ore appeared. The pyrite in the talc-carbonate schist of the Chromitiferous Peridotite and in the altered parts of the Lower Pyroxenite Unit reduces the total concentration of the nickel in the ore, which results in uneconomic ore portions in the Nkomati mine.

Consequently, this thesis deals with the spatial distribution, geochemistry, mineralogy and p-T-CO_2 conditions of the talc-carbonate-pyrite schist and pyrite rich portions in the PCR and Lower Pyroxenite unit of the Uitkomst Complex. Methodically face mapping pit 3 of the Nkomati open pit, petrographic descriptions of rock samples and thin sections, mineralogical and geochemical measurements of the rock specimen, and modelling of pseudosections were carried out.

A geological and structural map was created in pit 3 on the benches 20 to 25. The main focus was on the occurrence and spatial distribution of the talc-carbonate schist in the PCR unit and the serpentinised portions of the Lower Pyroxenite. The mapping of the talc-carbonate-schist and the pyrite rich portions is a good base to assess the spatial extension of the problematic portions in the pit. The results can be used for sorting out the pyrite rich portions from the ore in situ. Subsequently there is no need to separate the pyrite from the nickel ore during the enriching process.

Therefore the aim of this master project is to investigate the petrography, geochemistry, spatial distribution of the talc-carbonate-schist as well as the source and the stability conditions of the fluids, which led to the formation of the talc-carbonate schist.

The thesis starts with the introduction of the geology of the Uitkomst Complex and the country rocks, which is followed by the description of the general mineralogy and geochemistry of the complex. The next chapter deals with general aspects of serpentinisation and talc-carbonate alteration. The description and interpretation of the macroscopic and microscopic petrography is the next chapter which is followed by the description of the mapping results. The next part of the thesis focusses geochemistry and mineralogy of the sampled specimens. The following chapter contains the modelled pseudosections and the p-T-CO_2 conditions of the talc-carbonate alteration. The last chapters are the discussion, conclusion and a final review to topics, which could be of interest for further scientific work.

2 Exploration and mining history of the Nkomati Ni mine

In the early 20th Century the area around the Uitkomst Farm was explored for asbestos (Internal Nkomati report 2006). During the exploration campaign a sulphide mineralisation was found by Wagner in 1929 (Theart & de Nooy 2001, Li et al. 2002, Maier et al. 2004). The potential of the nickel deposit was noticed by Dr. Louis Coetzee from Anglo American in 1970 (Kenyon et al. 1986). Consequently, a joint venture between Anglo American (Kaffrarian Metal Holdings) and Inco was formed (Internal Nkomati report 2006).

The exploration was performed by INCO and lasted from September 1972 to early 1975. The study resulted in an estimation of a high tonnage, low grade ore body that could be exploited in an open pit. In 1977 Anglo American bought the mineral rights and INCO withdrew from the joint venture in 1980. A full feasibility study was started in May 1989 and lasted until 1991. The report delivered negative results (Internal Nkomati report 2006).

Parallel to the investigations of Anglo and INCO, a second company was active around the area of the Slaaihoek Farm. Since 1929 Eastern Transvaal Consolidated Mines Ltd (ETC) held the mineral rights for gold. In 1975 ETC hired Loxton, Hunting and Associates to create a geological map, carry out a photogeological interpretation and a gravity survey to assess the continuity of the Uitkomst Complex. From 1989 to 1990 ETC increased its efforts, which led to a further feasibility study yielding positive results. In 1993 the companies ETC and MidWits formed the Nico Joint Venture. Anglo American joined in 1995 and acquired 75% of the deposit. The remaining 25% was kept by the former contract partners.

The first feasibility study, which was produced for the massive sulphide body of the new joint venture, was carried out with positive results in 1995. Production started in 1997 (Internal Nkomati report 2006, Maier et al. 2004). Three massive sulphide bodies at the elevation of the granite and quartzite basement were mined (Gauert 2001). A second report dealt with the disseminated ore bodies, which could be exploited through an underground mining operation. After a further study the conclusion was that an open pit mine was preferable (Internal Nkomati report 2006). In February 1999 a new study was performed, the so called Nkomati Expansion Project. A new interpretation of the geological data and new drilling programmes were initiated. It was concluded that the expansion would be financial viable (Internal Nkomati report 2006).

At the moment the Nkomati Joint Venture includes African Rainbow Minerals and Norilsk Nickel with both contractors owning 50% of the deposit.

3 General Geology

3.1 General

The Uitkomst Complex is an elongated, layered, mineralized, mafic to ultramafic intrusion with a trough or boat like form. The complex bears significant amounts of Ni, Cu and PGE ore (Kenyon et al. 1986, Gauert et al. 1995, Gauert 2001, Theart & de Nooy 2001, Li et al. 2002, Maier et al. 2004). Minor ore volumes are composed of Co and Au (De Nooy 2000, Woolfe pers. comm. 2012). The complex is situated in the eastern Transvaal, South Africa, 35 km east of Machadodorp and 20 km north of Badplaas and outcrops in the farms of Vaalkop, Slaaihoek and Uitkomst for approx. 9 km. The width ranges between 650 and 1600 m (Fig. 3.1). There is evidence for a continuation of the complex under the farm Little Mamre for 3 km (Gauert 2001, Maier et al. 2004). The Uitkomst Complex resides close to the palaeo-margin of the Transvaal Basin (Visser et al. 1956, Hornsey 1999). Because of mineralogical evidence the intrusion is likely a satellite body of the Bushveld Complex (Gauert et al 1995, Li et al. 2002, Sarkar et al. 2008).

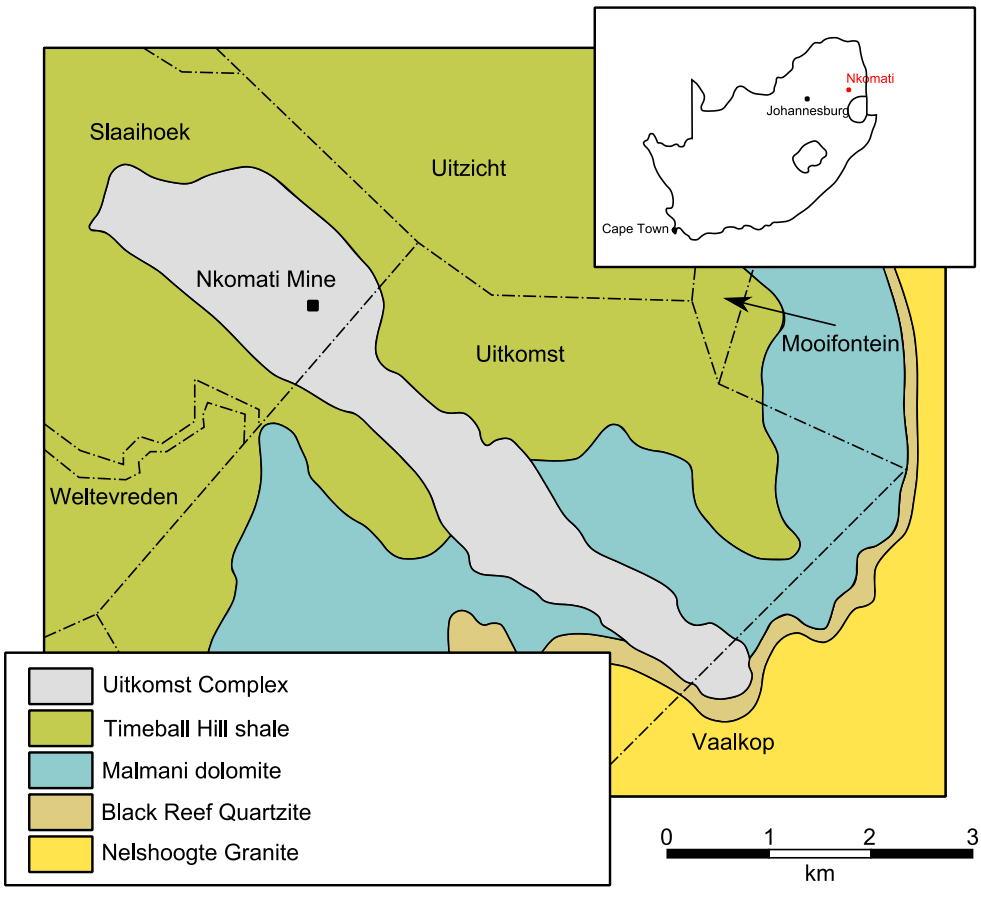

Fig. 3.1: Locality of the Uitkomst Complex (Theart, de Nooy 2001)

The 2.044 Ga old magmatic body intruded into the sediments of the Lower Transvaal Supergroup (Gauert et al. 1995, Gauert & Jordaan 1996, de Waal et al. 2001, Theart & de Nooy 2001, Maier et al. 2004). Their base and the Uitkomst Complex dip (5-10°) to NW (Kenyon et al. 1986, Gauert & Jordaan 1996, de Waal et al. 2001, Li et al. 2002, Theart & de Nooy 2001, Maier et al. 2004, Sarkar et al. 2008).

The base of the Uitkomst Complex is defined by the Black Reef Quartzite Formation which does not belong to the complex. The roof of the intrusion is marked by the Klapperkop Quartzite Member of the Timeball Hill shale. The Uitkomst Complex contains major faults in SW-NE and WNW-ESE directions (Gauert et al. 1995, Sarkar et al. 2008).

Figure 3.2 shows a 3D cross-section of the Uitkomst Complex, its geological units and country rocks.

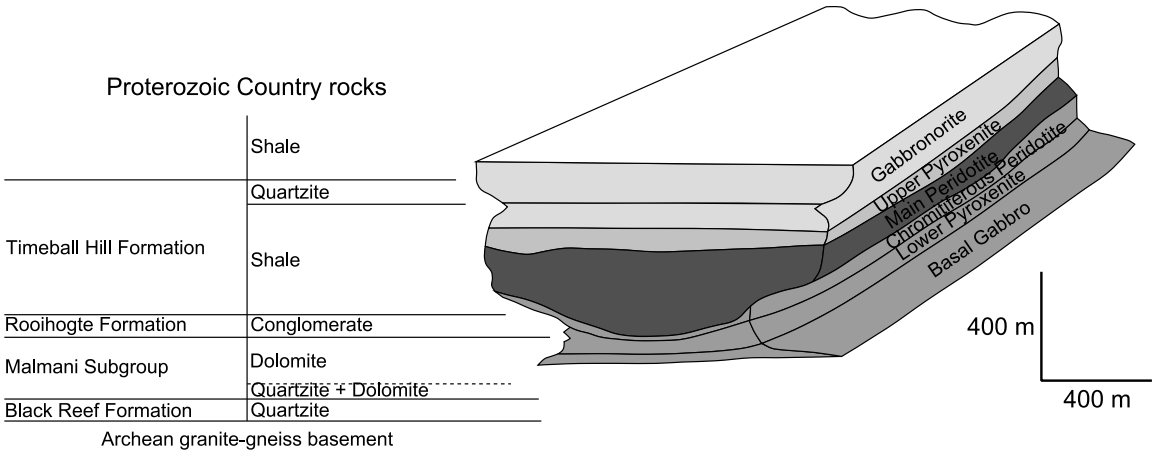

Fig. 3.2: Geology of the Uitkomst Complex (Sarkar et al. 2008)

3.2 Regional Geology

The Uitkomst Complex is situated at the base of the Transvaal Sequence. The surrounding rocks belong to the Malmani Subgroup (Tab. 3.1), which is part of the Chuniespoort Group and the lower Pretoria Group (Kenyon et al. 1986).

In the area of the Uitkomst Complex the Black Reef Quartzite is around 2 m thick and consists mainly of grit and pebble conglomerate at the base followed by quartzite at the top (Li et al. 2002, Maier et al. 2004, Internal Nkomati report 2006). The Oaktree Formation consists of coarse-grained quartzite which is about 3 m thick (Li et al. 2002, Maier et al. 2004), which is followed by the Malmani Dolomite about 150 m thick (Li et al. 2002, Maier et al. 2004, Internal Nkomati report 2006). The subsequent Rooihoogte Formation is present with a 5 to 10 m thick chert conglomerate, the Bevets Conglomerate. The conglomerate is

overlain by at least 1200 m sediments of the Timeball Hill Shale (Li et al. 2002, Maier et al. 2004).

Tab. 3.1: Country rocks of the Uitkomst Complex

<table>
<tr><td rowspan="4">Transvaal Supergroup</td><td rowspan="2">Pretoria Group</td><td>Timeball Hill Formation with Klapperkop Quartzite and Lower Timeball Hill Shale</td></tr>
<tr><td>Rooihoogte Formation with Bevets Conglomerate</td></tr>
<tr><td>Chuniespoort Group</td><td>Malmani Subgroup with Oaktree Formation</td></tr>
<tr><td colspan="2">Black Reef Quartzite</td></tr>
</table>

Transvaal Sequence

The Transvaal Sequence is situated in the Transvaal Basin in South Africa and Botswana and in the Kanye Basin. The sequence consists of up to 15 km thick rocks including low grade metamorphosed mudrocks, sandstones, volcanic, dolomites and iron formations. The hanging units are the very widespread developed Black Reef Quartzite, followed by a unit consisting of chemical sediments and a clastic sedimentary and volcanic unit, the Pretoria Group. Crosscutting intrusiva of the Bushveld Units led to metamorphism of the Chuniespoort Group (Eriksson et al. 1993).

Black Reef Quartzite

The Black Reef Quartzite is regarded as the base of the Pretoria Group and consists of arenaceous rocks, which lie unconformably on the stratigraphically lower rocks. The thickness varies from a few meters up to 30 m (Eriksson et al. 1993).
The Black Reef Quartzite is divided into six lithologies: clast-supported conglomerates, matrix-supported conglomerates, trough cross-bedded sandstones, planar cross-bedded sandstones, plane laminated arenites and laminated arenaceous carbonate rocks. The Black Reef Quartzite passes at its top into the Oaktree Formation of the Malmani Subgroup (Eriksson et al. 1993, Kenyon et al. 1986). The depositional environment is interpreted as a fluvial system (Eriksson et al. 1993).

Malmani Subgroup

The Malmani Subgroup is a part of the Chuniespoort Group and consists of dolomites, cherts and mudrocks. The rocks were deposited over a large area of the Kapvaal Craton. The subgroup is interpreted as an emplacement of epeiric marine sediments (Eriksson et al. 1993). The unit is dated at 2.450 Ga (Walraven & Martini 1995).
Button (1973) described five different formations in the Malmani Subgroup, which are distinguished by their chert content and the appearance of the stromatolites which are, from bottom to top, the Oaktree Formation, the Mont Christo Formation, the Lyttelton Formation, the Eccles Formation and the Frisco Formation.
The most supported model for the development of the subgroup includes a tidally influenced palaeo-environment. This facies is subdivided into four different zones: an intertidal zone with columnar stromatolites; a high energy zone with oolites, oncolites, ripples and breccias; a shallow, subtidal zone with elongated stromatolitic domes; and a deep, subtidal one with elongated stromatolitic mounds and dolomites. The first three zones are characterized by limestones and dolomitic limestones (Eriksson et al. 1993).

Pretoria Group

The lower part of the Pretoria Group is now described because the upper lithologies do not verge on the Uitkomst Complex.
The Pretoria Group is defined as the hanging unit relative to the chemical sediments of the Chuniespoort Group. The border between the two groups is unconformable. In most cases the Pretoria Group consists of an alternation of mudrocks and sandstones. There are minor quantities of volcanic sequences, diamictites and conglomerates. In the basin significant changes of lithology were discovered. The thicknesses of the sediments are also very variable.
The base of the Pretoria Group is defined by the Rooihoogte Formation. The lower part comprises a chert breccia-reworked conglomerate member and is followed by mudrocks and an upper arenaceous sequence. The breccias are generated as in situ sediments which overlie the karsts of the Malmani dolomites. The conglomerates were deposited in alluvial fans and fan deltas (Eriksson et al. 1993).
The Timeball Hill Formation is a higher stratigraphic level being composed of carbonaceous mudrocks which pass upwards into alternating, interbedded ferruginous mudrocks and sandstones. The alternating sequences grade into the Klapperkop Sandstone Member. In some places the carbonaceous mudrocks contain relatively high contents of pyrite, which indicates anoxic conditions during sedimentation. The mudrock-sandstone-sequence was

sedimented in a turbiditic environment. The Timeball Hill Formation evolved in an environment with a deep basin which was filled with fluvio-deltaic sediments from the north, northwest and east. Diamictites in the Timeball Hill mudrocks are glacial, glaciofluvial and glaciomarine sediments (Eriksson et al. 1993).

Contact metamorphism

Around the Uitkomst Complex an approx. 100 m thick contact aureole is developed. The metamorphosed country rocks are composed of a corundum-bearing muscovite-chlorite fels and tremolite- and serpentinite-marbles. The fels was formed from argillaceous rocks. Tremolite and serpentinite marbles originated from silica-rich dolomites (Gauert et al. 1995).

3.3 Lithological Units of the Uitkomst Complex

The Uitkomst Complex hosts six different lithological units (Fig. 3.3). The names of the titles in brackets are used by the Nkomati Geology Department. The Uitkomst Complex is divided into six units from bottom to top: Basal Gabbro, Lower Harzburgite (Lower Pyroxenite), Chromitiferous Harzburgite, Main Harzburgite (Main Peridotite), Upper Pyroxenite and Gabbronorite (Gauert et al. 1995, de Waal et al. 2001, Gauert 2001).

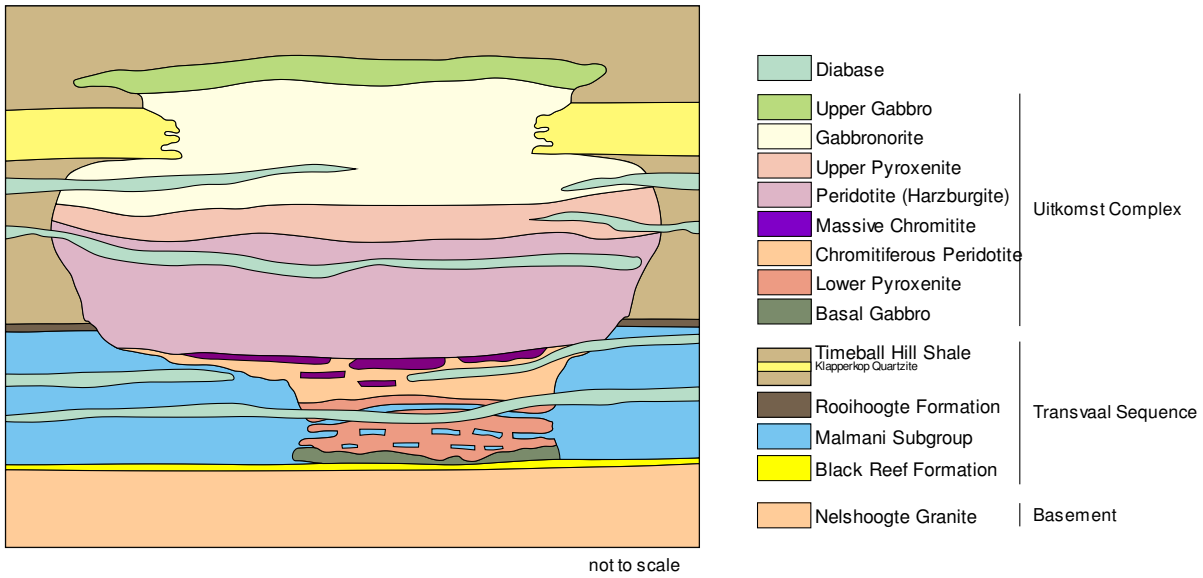

Fig. 3.3: Idealised cross-section of the Uitkomst Complex with country rocks (Internal Nkomati Report 2006)

3.3.1 Basal Gabbro

The thickness varies between 0 and 15 m with an average of 5.6 m (Gauert et al 1995, Gauert & Jordaan 1996, de Waal & Gauert 1997, Li et al. 2002). The unit is, with exceptions, continuous over the whole complex (Gauert & Jordaan 1996, de Waal & Gauert 1997). The bottom contact of the Basal Gabbro to the Black Reef Quartzite is characterized by a sheared talc-chlorite-carbonate rock (Gauert et al 1995). On top of the contact a chilled margin zone of up to 1.5 m is developed (Gauert et al 1995). The contact is interpreted as the rapidly cooled margin of the complex (de Waal & Gauert 1997). Occasionally there is carbonate veining around the chilled zone. The contact to the hanging Lower Harzburgite Unit is gradational (Gauert et al 1995, Li et al. 2002).
The Basal Gabbro Unit is fine to coarse grained, possesses a gabbroic composition (Gauert & Jordaan 1996, de Waal & Gauert 1997), is poorly layered (de Waal et al. 2001), and saussuritized as well as uralitized (Gauert et al 1995, de Waal & Gauert 1997). The subophitic structure of the rock is still visible (Gauert et al 1995). The primary mineral composition is clinopyroxene (20-30 modal %), orthopyroxene (10 modal %), plagioclase (up to 50 modal %), and sulphides like pyrrhotite, pentlandite, chalcopyrite, pyrite and arsenopyrite (de Waal et al. 2001, Sarkar et al. 2008). Towards the top olivine occurs as an additional mineral phase (de Waal et al. 2001). The secondary minerals are amphibole, chlorite, sericite, serpentine, talc, quartz, carbonate, alkali feldspar and epidote-clinozoisite (de Waal & Gauert 1997, Maier et al. 2004). The composition shows variable degrees of chromite and sulphide segregation (de Waal & Gauert 1997).
A remarkable feature is the inverse Cu/Ni ratio. The Cu content exceeds the Ni content in the rock (Kenyon et al. 1986).

3.3.2 Lower Harzburgite (Lower Pyroxenite)

The average thickness of the Lower Harzburgite Unit is 50 m. In places where the stratigraphy is duplicated the thickness varies up to 90 m (Gauert et al 1995, Gauert & Jordaan 1996, Maier et al. 2004). The contact to the Basal Gabbro is gradational (Gauert et al 1995, Gauert & Jordaan 1996) but can be identified by a higher concentration of xenoliths and pegmatoidal rocks (Maier et al. 2004, Edwards pers. comm. 2012).
The Harzburgite Unit has a poikilitic structure consisting of feldspar bearing lherzolite, sulphide rich feldspathic olivine-wehrlite, amphibolite, and pegmatoidal pyroxenite (Gauert et al 1995, de Waal et al. 2001, Li et al. 2002, Maier et al. 2004). The latter is developed around xenoliths and contains coarse-grained clinopyroxene, orthopyroxene, amphibole and plagioclase crystals, which bear interstitial pyrrhotite, pentlandite, chalcopyrite and magnetite

(Gauert et al 1995, Gauert & Jordaan 1996, de Waal et al. 2001). The average content of olivine as a cumulus mineral is up to 50 modal %. Ortho- and clinopyroxene as intercumulus minerals compose 30 modal % or 40 modal %, respectively, of the unit. Chromian spinel and plagioclase are at 10 modal % each (de Waal et al. 2001, Maier et al. 2004). Feldspar becomes more abundant towards the bottom of the unit (Kenyon et al. 1986).
The unit is highly altered. Despite the pervasive alteration (Gauert et al 1995, Maier et al. 2004) (uralitisation, saussuritisation and serpentinisation) the original texture of the magmatic minerals is still visible (Gauert et al 1995). The altered pyroxenites consist of serpentine, tremolite, talc, phlogopite and residual olivine and pyroxene (Kenyon et al. 1986).
The Lower Pyroxenite hosts metamorphosed carbonaceous and quartzitic xenoliths from the country rocks (Gauert et al 1995, Gauert & Jordaan 1996, Li et al. 2002, Maier et al. 2004, Sarkar et al. 2008) that are flattened in the direction of original sedimentary layering and forming rafts. These structures are similarly orientated as the magmatic layering (Gauert et al 1995). The xenoliths can amount to one third of the unit. Around the xenoliths mica and amphibole are apparent in larger amounts (Maier et al. 2004, Sarkar et al. 2008).

3.3.3 Chromitiferous Peridotite (Chromitiferous Harzburgite)

The average thickness of this unit is 60 m. The contact to the Lower Harzburgite is gradational (Gauert et al 1995, Gauert & Jordaan 1996, de Waal et al. 2001, Li et al. 2002).
The unit hosts medium-grained harzburgite which is highly altered to a serpentine-talc-chlorite-carbonate rock (Maier et al. 2004). Originally the unit was composed of disseminated chromite and olivine (de Waal et al. 2001, Maier et al. 2004, Sarkar et al. 2008) which were set in a matrix of amphibole, phlogopite and disseminated sulphides (Maier et al. 2004, Sarkar et al. 2008). The main intercumulus phase is orthopyroxene which encloses chromite and olivine poikilitically (de Waal et al. 2001). The Chromitiferous Harzburgite also contains sheared chromitite lenses and layers (Gauert et al 1995, Gauert & Jordaan 1996, de Waal et al. 2001, Li et al. 2002) which possess a fine layering hosting alternating sequences of intercumulus pyroxene and chromititic pyroxenite (Kenyon et al. 1986). The chromitites have a schlieren-type structure. The lenses are surrounded by strongly altered harzburgite. Towards the top the lenses become more substantial. The upper portion of the unit is made of massive chromitite with a thickness of 3-4 m (Gauert et al 1995).
Because of the pervasive alteration the magmatic minerals were replaced by talc, carbonate, phlogopite, serpentine and chlorite (Kenyon et al. 1986, Gauert et al 1995). There are two strongly altered rock types; a talc-amphibole-chlorite-rock (in this study called talc-carbonate) and serpentinite. Amphibole replaced olivine and pyroxene. The talc was created by

hydrothermal alteration of amphibole and also replaced olivine and pyroxene. In some cases the outlines of the original magmatic minerals are still visible (Kenyon et al. 1986).

3.3.4 Main Harzburgite (Main Peridotite)

The average thickness of the Main Harzburgite Unit is 330 m, more than one third of the Uitkomst Complex.

The unit is a continuous sequence of harzburgite in places grading into dunite and contains feldspathic parts. The unit is a medium to coarse-grained orthocumulate. Pyroxenes and plagioclase enclose the olivine and chromian spinel grains poikilitically (Kenyon et al. 1986, Gauert et al 1995, de Waal et al. 2001, Li et al. 2002, Maier et al. 2004, Sarkar et al. 2008). Orthopyroxene occurs as the main interstitial phase and forms in some parts an additional cumulus phase (Maier et al. 2004). The unit has a weak meter-scale and grain-size layering (de Waal et al. 2001), which is caused by variations in grain size and composition (Gauert et al 1995). Thin chromite bands also occur (Li et al. 2002, Maier et al. 2004, Sarkar et al. 2008). There is no mineralisation except for the lower 10 m of the unit (Kenyon et al. 1986, Gauert et al 1995) and an additional sulphide enriched zone from 50 to 90 m below the top of the unit (Li et al. 2002, Maier et al. 2004).

The main alteration type is serpentinisation (Gauert et al 1995) which ranges from poorly altered parts to local and rare occurrences of serpentinites (Kenyon et al. 1986).

3.3.5 Pyroxenite (Upper Pyroxenite)

The Pyroxenite is up to 60 m thick. The contact of this unit to the Main Harzburgite is sharp transitional (Gauert et al 1995, Li et al. 2002, Maier et al. 2004).

The unit is made up of orthopyroxenite orthocumulate and mesocumulate (Gauert & Jordaan 1996, Maier et al. 2004), with its base defined by an increase of the SiO_2-content simultaneously to the increase of orthopyroxene. The plagioclase remains constant at the base but increases to the centre of the unit. Chromite and clinopyroxene are minor constituents (de Waal et al. 2001). Olivine disappears in the system. Minor sulphides occur in the upper part of the unit (Sarkar et al. 2008).

The Pyroxenite can be subdivided into three subunits: a Lower Olivine-Orthopyroxene, a Pure Orthopyroxene and an Upper Norite to Gabbronorite (Gauert et al 1995, Li et al. 2002). The latter is characterized by an increase of plagioclase, clinopyroxene and quartz. The Pyroxenite unit shows the transition from the ultramafic rocks to the more mafic rocks at the top of the Uitkomst Complex (Gauert et al 1995).

The unit is unaffected by secondary alteration (Gauert et al 1995, Maier et al. 2004).

3.3.6 Gabbronorite

The Gabbronorite Unit is the uppermost sequence of the Uitkomst Complex with an average thickness of 250 m. The contact to the Pyroxenite Unit is gradational (Gauert et al 1995, Li et al. 2002, Maier et al. 2004). The top contact to the Lower Timeball Hill Shale is widely chilled (Gauert et al 1995).

The Gabbronorite is characterized in form as a sill-like body (Gauert et al 1995) and can be subdivided in a main unit and an upper unit (Sarkar et al. 2008). The rock types range from a basal norite through a gabbroic rock to a diorite at the top (de Waal et al. 2001, Li et al. 2002).

The lower part of the Main Gabbronorite is relatively fresh and consists of norite, gabbronorite and olivine gabbro. The contact between the main part of the unit and the upper part is characterised by a brecciated diorite zone of about 5 m thickness (Li et al. 2002, Maier et al. 2004, Sarkar et al. 2008). The Upper Gabbronorite is highly altered with a secondary mineral assemblage consisting of saussuritized plagioclase, chlorite, biotite and tremolite. hosting an up to 3 m thick chilled margin to the hanging sediments (Maier et al. 2004, Sarkar et al. 2008). Secondary minerals are amphibole, albite, quartz, minor chlorite and epidote (Maier et al. 2004, Sarkar et al. 2008). There are also xenoliths with a quartzitic or argillaceous composition (Gauert et al 1995, Li et al. 2002). The sulphide content is less than 1 %. In the lower portion a thin layer of magnetite is developed (de Waal et al. 2001).

The diorites are the most evolved igneous rocks in the intrusion with enrichments in Zr, P, Nb, Y, and LREE (Maier et al. 2004).

3.3.7 Marginal Gabbro

The name was chosen to make a distinction to the Basal Gabbro. The Marginal Gabbro forms a subunit of the Lower Pyroxenite and Main Peridotite. The petrography is similar to the Basal Gabbro. The rocks are medium to coarse-grained, feldspar rich, with a gabbroic composition, low mineralised and graphite as a rare component (de Waal & Gauert 1997, de Waal et al. 2001).

3.3.8 Diabase

There are numerous primary and secondary diabase sills and dykes (Kenyon et al. 1986, Gauert & Jordaan 1996). Some run parallel to the elongation of the Uitkomst Complex (Kenyon et al. 1986). These structures did not play an important role in the evolution of the complex and can be regarded as isolated subsystems (de Waal et al. 2001).

The diabases are grey to green, fine to medium-grained and contain altered plagioclase, hornblende, biotite as well as opaque minerals. Further constituents are quartz, pyroxene, calcite epidote, chlorite and a few sulphides (Kenyon et al. 1986).

3.4 Mineralised Zones, ore bodies

3.4.1 Massive Sulphide Body (MSB)

The extension of the MSB is approximately 400x250x20 m (Gauert 2001, Maier et al. 2004, Internal Nkomati report 2006). The MSB is composed of three single, lens-shaped ore bodies that are situated mainly in the footwall rocks of the Uitkomst Complex (Theart & de Nooy 2001, Internal Nkomati report 2006). There are some smaller lenses within the Basal Gabbro and the Lower Pyroxenite Unit. The lenses are separated by dolomite, quartzite, diabase and granite. The MSB contains 2.9 Mt ore at 2.04 % Ni, 1.13 % Cu and 6.17 g/t combined Au and PGE (De Waal et al. 2001, Li et al. 2002, Maier et al. 2004).
A distinction was made between a massive ore and a stringer ore, which is further divided into a lower and an upper stringer zone. The massive ore consists of pyrrhotite, pentlandite, chalcopyrite, pyrite and magnetite. The pyrrhotite occurs as anhedral, coarse and interlocked grains. Pentlandite is found in pyrrhotite as stringers and clusters, sometime occuring as exsolution flames in the pyrrhotite. Chalcopyrite is present as anhedral blebs in pyrrhotite. Additionally there are PGE-bearing minerals like merenskyite and smaller amounts of michenerite, testibiopalladinite and sperrylite (Theart & de Nooy 2001, Internal Nkomati report 2006). The PGMs are present as irregular to sub-rounded grains residing in sulphide or less common in silicate minerals. The MSB is enriched in PGE minerals in the Lower Stringer Zone and in the western end of the ore body (Theart & de Nooy 2001).
The massive sulphides are relatively metal rich compared to other massive sulphide deposits that are related to mafic to ultramafic intrusions (Maier et al. 2004).

3.4.2 Basal Mineralised Zone (BMZ)

The Basal Mineralised Zone is situated in the Basal Gabbro Unit (Theart & de Nooy 2001, Maier et al. 2004, Internal Nkomati report 2006). The sulphides contain 23-37 % chalcopyrite, 21-32 % pyrrhotite, 17-25 % pentlandite and 2-15 % pyrite and small amounts of cobaltite. Co-Ni-Fe-arsenosulphides, (titano-)magnetite and ilmenite were also observed (Internal Nkomati report 2006). The sulphides become more abundant to the top of the Basal Gabbro (Maier et al. 2004).

The sulphide minerals have an interstitial texture. In net-textured portions they can have a part of up to 20 % of the total rock volume (Internal Nkomati report 2006). The other ore textures range from disseminated parts to blebs, stringers and clusters in the upper parts of the Basal Gabbro. Chalcopyrite is partially remobilised into stringers and appears together with secondary minerals in the form of blebs and intergrowths. Occurrences of arsenopyrite and pyrite are limited to the proximity of the xenoliths where the development of sulphides has more favourable conditions. Ilmenite occurs as oxidation exsolution lamellae in titanomagnetite and also appears in grains. Anhedral magnetite stringers and grains are of secondary nature. A minor and rare constituent is chromite (de Waal & Gauert 1997).

3.4.3 Main Mineralised Zone (MMZ)

The Main Mineralised Zone resides in the Lower Pyroxenite Unit (Theart & de Nooy 2001, Maier et al. 2004, Internal Nkomati report 2006) and hosts mainly Ni rich sulphides. In some parts the MMZ ranges over the whole thickness of the LPxt Unit. In other parts there are just small bands. The economically most important parts can be found in the centre of the trough and can also occur where the Lower Pyroxenite undercuts the Malmani Dolomite. The MMZ is pretty continuous throughout the whole magmatic body except for smaller areas (Internal Nkomati report 2006). The highest content of sulphides can be found in the clinopyroxene rich parts of the Lower Pyroxenite (Gauert 2001).

The following mineralisation types were observed: net-textured, high grade ore, semi-massive to massive lenses, blebby sulphides as well as disseminated sulfides. The semi-massive to massive lenses are associated with high grade ore. Ores next to xenoliths can be semi-massive in the form of pegmatoidal grains (Li et al. 2002, Internal Nkomati report 2006).

The MMZ contains the following sulphide minerals in decreasing order: pyrrhotite (by far the most occurring), pentlandite, chalcopyrite and pyrite (Kenyon et al. 1986, Maier et al. 2004, Internal Nkomati report 2006). There are also minor cobaltite, titanomagnetite, sphalerite, galena, native Cu, awaruite, chromite grains and Pd-Bi-Te phases as well as fine-grained magnetite as a result of serpentinisation processes. Pyrrhotite occurs mostly as filling in interstices between the silicate minerals while pentlandite appears as coarse grains around the pyrrhotite minerals as well as fine-grained exsolution flames (Kenyon et al. 1986, Internal Nkomati report 2006). Chalcopyrite occurs as anhedral grains within the pyrrhotite and as inclusions within the silicate minerals (Internal Nkomati report 2006).

3.4.4 Chromititic Peridotite Mineralised Zone (PCMZ)

The Chromititic Peridotite Mineralised Zone occurs in the Chromitiferous Peridotite Unit (Theart & de Nooy 2001, Maier et al. 2004, Internal Nkomati report 2006). The PCMZ is characterised by chromite bands, lenses, pods, wisps as well as schlieren, and is less continuous than the MMZ.

The dominant sulphide minerals are pyrrhotite, pentlandite, chalcopyrite and pyrite (Li et al. 2002, Internal Nkomati report 2006). In some parts a millerite-pyrite-chalcopyrite assemblage was observed. Minor amounts of cobaltite, gersdorffite, ullmanite, tucekite, galena, and stibiopalladinite were observed (Internal Nkomati report 2006).

The sulphides appear in larger amounts in less chrome rich parts of the PCR Unit and form disseminated, anhedral intergrowths (Li et al. 2002, Internal Nkomati report 2006).

The Massive Chromitite at the top of the PCR Unit marks the transition to the overlying Main Peridotite, and in some parts is bounded by ductile, schistose shear zones. The thickness varies between 0 and 6 m reaching up to 12 m. In the high grade volumes chromite has a part of up to 85 % of the whole rock. Within the weathered zones the sulphides are replaced by clays and limonitic hydroxides. The chromites remain mainly unaffected (Internal Nkomati report 2006). The alteration of the silicate minerals is related to the resorption of chromites. The chromites are normally unzoned (Kenyon et al. 1986).

Euhedral to rounded chromite grains form the semi-massive chromitite (Internal Nkomati report 2006). The typical grain size is more or less constant (Kenyon et al. 1986).

3.4.5 Peridotite Mineralised Zone (PRDMZ)

The PRDMZ is characterised by a low grade, disseminated to bleb-like sulphide mineralisation and is situated in the Main Peridotite.

The main ore minerals are pyrrhotite, pentlandite, mackinawite, chalcopyrite and ubiquitous chromite, which are interstitial to the silicate minerals. Primary magnetite can be found as large grains. In locations with a higher concentration of sulphide minerals the grains occur in fine net textures. In response to the alteration of the olivine grains there are microscopic veins of serpentine, calcite and magnetite that intersect the sulphide minerals. The mineralisation is affected by alteration. Pentlandite is replaced by mackinawite in small veins. Also chalcopyrite can be found but is partially substituted by secondary cubanite, chalcocite, covellite, bornite and valleriite (Internal Nkomati report 2006).

3.4.6 Oxidised and partially oxidised sulphide ores

Sulphidic ores, situated near to the surface, are partially to fully oxidised. Therefore a distinction was made between unoxidised (sulphides completely preserved), partially oxidised (sulphides partially present) and fully oxidised (sulphides completely replaced) sulphide ores.
The extension of the oxidised ores is dependent on different factors such as the density of fractures and shear zones as well as the availability of meteoric water.
At the base of the oxidised formations a supergene enriched saprolite was found with minor economic value. These zones contain secondary, water-soluble copper minerals (Internal Nkomati report 2006).

3.5 Structure

The Uitkomst Complex is an elongated, boat-like, northwest-southeast trending structure. The layering dips at a low angle towards northwest. The layered rocks have a trough-like form with the axis following the major axis of the magmatic body (Gauert et al 1995). The lowermost parts of the complex show a rectangular shape. Towards higher elevations the body flares out horizontally. The rectangular form results from two northwest-southeast trending fault systems (Gauert et al 1995, de Waal & Gauert 1997). The faults can be recognised in the south-western part of the Uitkomst Complex. The orientation of these structures is similar to those in the eastern Transvaal (de Waal & Gauert 1997) with steep dips. The NW-SE trending faults have parallel orientation to the faulting pattern in this area as well as being responsible for major displacements (Gauert et al 1995). The faults are related to the Uitkomst lineament and possess a significant importance with respect to the intrusive history of the area. The strong influence of the lineament which could be responsible for the emplacement of the Boesmanskop syenite (Anhaeusser et al. 1979) led to the idea of a major crustal discontinuity (Hornsey 1999). Steeply dipping faults, which are orientated normal to the magmatic body, also cause vertical displacement and lead to graben and horst structures (Gauert et al 1995). The estimated depth at the point of emplacement is about 6 km (Gauert & Jordaan 1996). At the point of emplacement the stress regime was overall horizontal anisotropic and compressive with the NW-SE directed maximum stress parallel to the layering of the magmatic rocks (Hornsey 1999).
Table 3.2 shows the relevant structures and their ages around the investigation area.

Tab. 3.2: Relevant regional structures around the investigation area (after the summary of Hornsey 1999)

Age	**Structural/Intrusive event**
Mesozoic	NW-SE faulting, fracture set NNE-SSW aligned strike-slip-faulting N-S dykes
Bushveld	Layer-parallel thrust faulting
Pre Bushveld	Diabase sill intrusion, possibly associated with NNE trending dykes Development of NW-SE and NE-SW interference folding, intrusion of the Uitkomst Complex
Godwan	Deposition controlled by NE-SW, NW-SE, and E-W aligned structures

The structures which strike NW-SE, ENE-WSW, and NE-SW are likely to be reactivated older structures which were developed during the genesis of the gneissic fabric in the Nelshoogte pluton. The fault orientations during the Godwan Formation sedimentation were NE-SW, E-W, and ENE-WSW (Visser et al. 1956, Hornsey 1999). During the pre-Bushveld age structures like interference folding in NW-SE and NE-SW direction are apparent in the area around the Bushveld Complex. The present diabase sills are N-S-orientated and reveal an en-echelon-staggering. The dykes are linked to the sills and strike NNE-SSW. The dykes, sills, and folding structures are deformed by later layer-parallel shears which are of Bushveld age. One of these shears is the Basal Shear Zone in the Uitkomst Complex which is described further down. There are also other shear zones which change their character with respect to their host lithologies. In the ultramafic rocks of the Uitkomst Complex the shears appear as talc schists. The first mesozoic structure is a NW-SE-orientated joint system and can be found especially in the Uitkomst Complex. The field observations point to a sinistral shear. A further orthogonal, NW-striking joint set which is crosscut by the NE-orientated fault zone is apparent (Hornsey 1999).

For a more detailed description of the different structural features the Master Thesis of Hornsey (1999) is recommended.

Thrust events and faulting are responsible for partial duplication of the igneous stratigraphy, the displacement of subvertical features and thickening of rock units. One such subvertical feature is the Basal Shear Zone, probably a part of a regional thrust plane near the base of the Transvaal Supergroup. The shear zone is in the Malmani Dolomite near to the contact to the Black Reef Quartzite. The thickness of the shear zone ranges from 0.2 to 3 m (Hornsey 1999, Theart & de Nooy 2001). The Basal Shear Zone, which is related to shear zones in higher stratigraphies of the Uitkomst Complex, developed as a result of compression from

SE and postdates the intrusion of the MSB. The displacement is at least 300 m (Hornsey 1999).

The Uitkomst Complex intruded into a nearly rectangular, tubular opening which was approximately 750 m deep, 1 km wide and 12 km long (Gauert 2001). The opening was created when a bedding plane fault was intersected and offset by a near vertical NW-SE trending fracture zone (Fig. 3.4). Subsequent horizontal faulting and shearing could be a result of tensional conditions during the uplift that resulted from increased heat flow during the emplacement of the Bushveld Complex (de Waal et al. 2001). The depth of the process is estimated to be at least 8 km (Gauert 2001). The following magma flow through the conduit eroded the side walls and led to the present shape of the complex (de Waal et al. 2001, Gauert 2001). It is conceivable that the gabbroic magma was first deposited at the base, top and side walls of the Uitkomst Complex (de Waal et al. 2001, Gauert 2001).

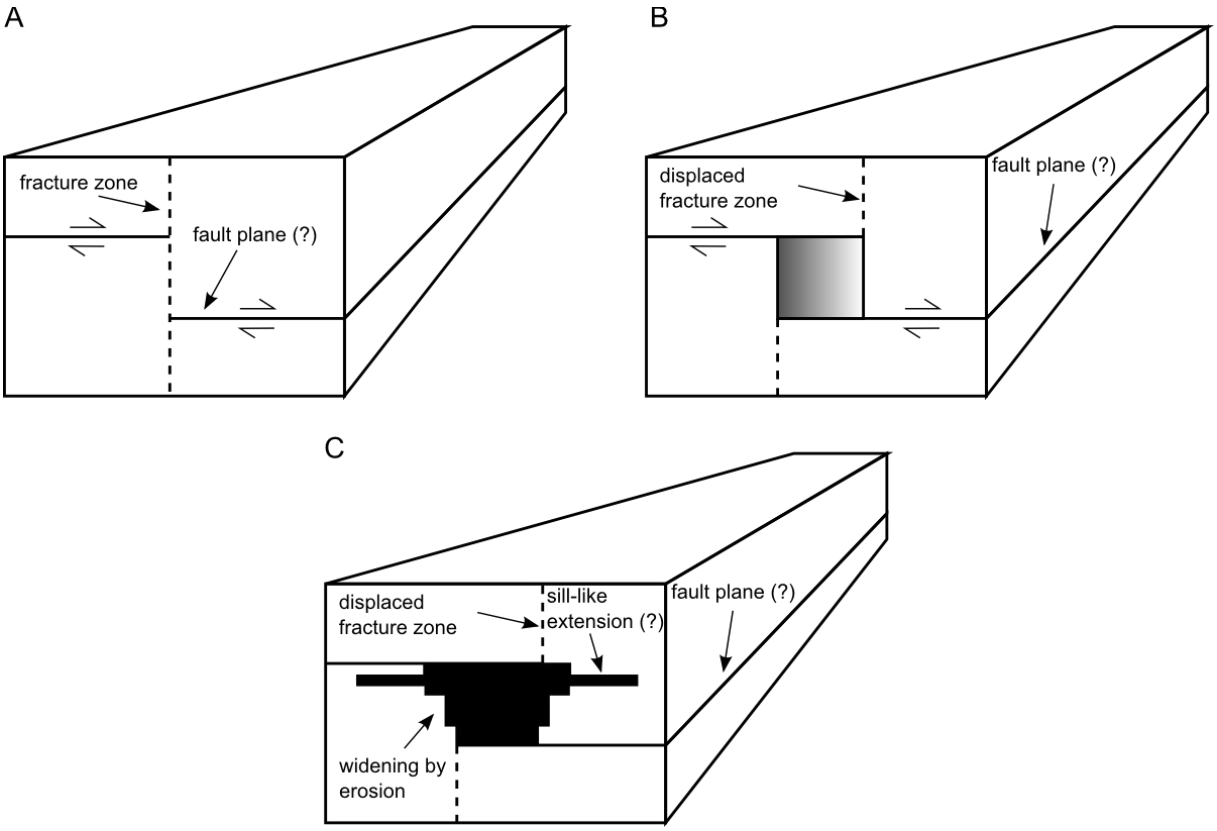

Fig. 3.4: Structural model of the emplacement of the Uitkomst Complex (de Waal et al. 2001)

Another model is proposed by Hornsey (1999). The first pulse (Basal Gabbro) orientated perpendicular to the least minimum stress. During the deposition of the Basal Gabbro and the overlying sediments were domed which resulted in tension cracks. These zones of weakness were intruded by the Lower Pyroxenite which resulted in further doming and fracturing of the hanging units. The rapid increase in magma volumes of the upper sequences of the Uitkomst Complex resulted in flushing-out-events of blocks of wall rock.

After Hornsey (1999) assimilation of country rock in the lower units (BGab and LPxt) of the Uitkomst Complex to create space is not very likely due to the following rapid cooling and the subsequent solidification of the magma which would cause a standstill of the magma flow.
Hornsey (1999) proposed a three stage structural model of the Uitkomst Complex beginning with the diabase intrusion, followed by layer-parallel faulting and subsequent strike-slip faulting. The NE trending dykes seem to be emplaced at the same time as the diabase sills intruded. The largest dyke is the so called “shaft dyke”, which has a strike of 47° and a dip of 70-80° to SE. The strike of smaller dykes varies between 60° and 65° and the range of the dip is from 70° to 80°. The layer-parallel faulting is apparent throughout the whole complex. Some of the shear zones in the higher stratigraphies are composed of talc schist if they are situated in the ultramafic rocks. Along the shear zones the rocks are mylonitised. In some cases these shear zones are responsible for the duplication of the sedimentary sequences. The regional stress regime remained the same during the emplacement of the sills and dykes and the layer-parallel faulting. The strike-slip faults, which displace the Uitkomst Complex, strike from 50° to 60°. There is no significant vertical displacement of the igneous rocks. According to the temporal progression the strike-slip faults displace all other structural features.
Post-Bushveld diabase sills and dykes are developed throughout the whole Uitkomst Complex, and led to a considerable thickening of the complex (Gauert et al 1995). One of these diabase sills is responsible for an uplift of the contact to the Black Reef Quartzite on the north-western part of the complex of around 30 m (de Waal & Gauert 1997).

3.6 Mechanism of ore precipitation

The sulphide segregation in the Basal Gabbro, Lower Pyroxenite and Chromitiferous Peridotite can have several factors. These factors are: mixing of magmas with different composition; a rapid cooling at the margins of the intrusion; a decrease of the FeO content due to precipitation of chromite and magnetite; and the assimilation of siliceous, sulphide-bearing or dolomitic country rocks. The original magma had $\delta^{34}S$ values near 0 ‰. During the emplacement contamination occurred by with ^{32}S enriched sedimentary S with $\delta^{34}S$ values lower than -10 ‰. There is a large quantity of sulphides compared to the thickness of the complex that can be explained by separation and fractionation of a magma pool at greater depth with entrapment and deposition in the Uitkomst conduit (Gauert 2001).
The mixing of magmas with different compositions is supported by the sulphide mineral assemblage in the transition zone from the Basal gabbro to the Lower Pyroxenite where different magmas could have interacted. The first magma pulses had a similar composition to the evolved B1/B2 Bushveld parental magmas. Later pulses were more primitive (Gauert

2001, Maier et al. 2004). Li et al. (2002) also favoured a model with an internal source for S including the contamination of the magma by siliceous xenoliths.

The formation of ores in the complex due to a rapid decrease of temperature is supported by the occurrence of sulphide mineralisation at the base of the intrusion.

A decrease of the FeO content because of precipitation of magnetite and chromite is supported by locally higher contents of sulphides in the PCR unit.

The assimilation of country rocks is the most important factor for ore formation in the Uitkomst Complex (Gauert 2001). The abundant xenoliths are a clear evidence for magma-country rock interaction. To achieve the $\delta^{34}S$ values from -8 to -4 ‰ of the magmatic rocks a minimal assimilation of 10 % country rock at $\delta^{34}S$ values of -11.1 ‰ (dolomite) and -14.5 ‰ (shale) would be necessary (Gauert 2001). Li et al. (2002) confirmed this model. They calculated that 10 % assimilation of the shaly interlayer of the Malmani dolomite or 5 % assimilation of the Timeball Hill Shale would be necessary to produce $\delta^{34}S$ values of -6 ‰ for the Lower Pyroxenite and Chromitiferous Peridotite.

There are severable conceivable sources for the S which is needed for the formation of the sulphidic ores. The bulk of the sulphides could have formed at larger depths where they were separated from a larger magma body and were entrapped in the ascending magma which was deposited in the magma channel (Gauert 2001, Maier et al. 2004). A second process could be the separation of the sulphides from a streaming magma in the conduit (Gauert 2001).

For the segregation the magma has to reach the condition of S supersaturation. This could be obtained, as already mentioned above, by mixing of different magmas and by the assimilation of country rock. The most likely sources for the S are the Timeball Hill Shale and the Malmani Dolomite (Gauert & Jordaan 1996, Gauert 2001) which was probably the more important one (Maier et al. 2004).

The formation of the ores could have taken place in the following way. Due to assimilation of dolomitic xenoliths from the Malmani Dolomite, which degassed because of the high surrounding temperatures, the content of volatiles in the magma increased and the O fugacity raised which triggered the precipitation of oxides like magnetite (Gauert et al 1995, Gauert 2001, Maier et al. 2004). As a result the FeO content in the magma decreased. These factors lowered the sulphide carrying capacity of the melt. Assimilation of shales from the country rocks decreased the S solubility because of the consequent increases of the Si content in the magma (Gauert 2001). At the same time the xenoliths of the Malmani Dolomite and the Timeball Hill Shale acted as suppliers for additional S whereas the S supersaturation was reached (Gauert 2001, Li et al. 2002). These mechanisms acted as triggers for the precipitation of the sulphides in the Lower Harzburgite Unit and chromitites on the top of the Chromitiferous Harzburgite Unit (Gauert et al 1995, Maier et al. 2004). The immiscible

sulphide droplets were transported in the magma. As the magma slowed down the droplets segregated and deposited at the base of the complex (Li et al. 2002, Maier et al. 2004). The sulphides of the Massive Sulphide Body could have formed by descending sulphur droplets from the Lower Pyroxenite through the semi-consolidated Basal Gabbro to the base of the intrusion (Hornsey 1999, Maier et al. 2004).

The sulphide mineralisation of the Main Peridotite, Upper Pyroxenite and Gabbronorite could be a product of a sulphur enriched fluid which led to a supersaturation of the magma and the precipitation of sulphides. This model is supported by the relatively low $\delta^{18}O$ values in the upper part of the Uitkomst Complex. If there were a significant bulk assimilation of sedimentary country rock then the $\delta^{18}O$ values would be higher. The $\delta^{34}S$ values of specimens from the base of the Main Peridotite through to the Gabbronorite are around 0±2.5 ‰. They do not show signs for assimilation of country rock or distinct magma inputs (Sarkar et al. 2008).

3.7 History of emplacement and genesis

The first magma emplacement in the NW consists of the Basal Gabbro. A mixture of the Bushveld B2-magma and a fractionated variation of the parental B1-liquid shows geochemical similarities to the composition of the Basal Gabbro Unit. It is thought that the already fractionated B1 magma was emplaced simultaneously with the B2 magma in the Uitkomst conduit where they could mix (de Waal & Gauert 1997, de Waal et al. 2001, Li et al. 2002, Maier et al. 2004). The first pulses cooled down very rapidly. With increasing temperature because of the intrusion of new magma the Basal Gabbro developed into a phaneritic rock and merged into the Lower Pyroxenite (de Waal & Gauert 1997). This process introduced the conduit stage. Several magma pulses containing olivine, chromite and sulphides moved through the conduit. The suspended load was concentrated in the magma by flow segregation (de Waal et al. 2001). With the time further magma pulses moved towards SE. This was caused by two parallel fault zones which strike from NW to SE. Because of the movement of the magma emplacement a conduit was scoured out. The magma conduit became bigger and replaced the units of the hanging dolomite and schists. The Lower Harzburgite Unit is a highly contaminated, sulphide-rich cumulate rock. Because of the massive nature of the surrounding carbonate and conglomerate rocks the lateral extension of the body was small (Gauert et al 1995, Maier et al. 2004). As the magma reached the schists the horizontal expansion became much bigger (Gauert et al 1995). The hanging Main Harzburgite Unit was emplaced by later magma pulses of nearly constant composition. This is an evidence for an infinite magma source from where large quantities of magma flowed through the conduit (Gauert et al 1995, Gauert 2001, Maier et al. 2004). After

the Main Peridotite was deposited the magma became slower and gave rise for closed system conditions at a level of 420 m above the base of the intrusion (Fig. 3.5). The following Pyroxenite Unit and Gabbronorite Unit show normal fractionation processes (Gauert et al 1995, de Waal et al. 2001, Li et al. 2002, Maier et al. 2004). The Upper Pyroxenite may have been formed by a normal crystallisation prior to the formation of the bulk of the complex (Maier et al. 2004).

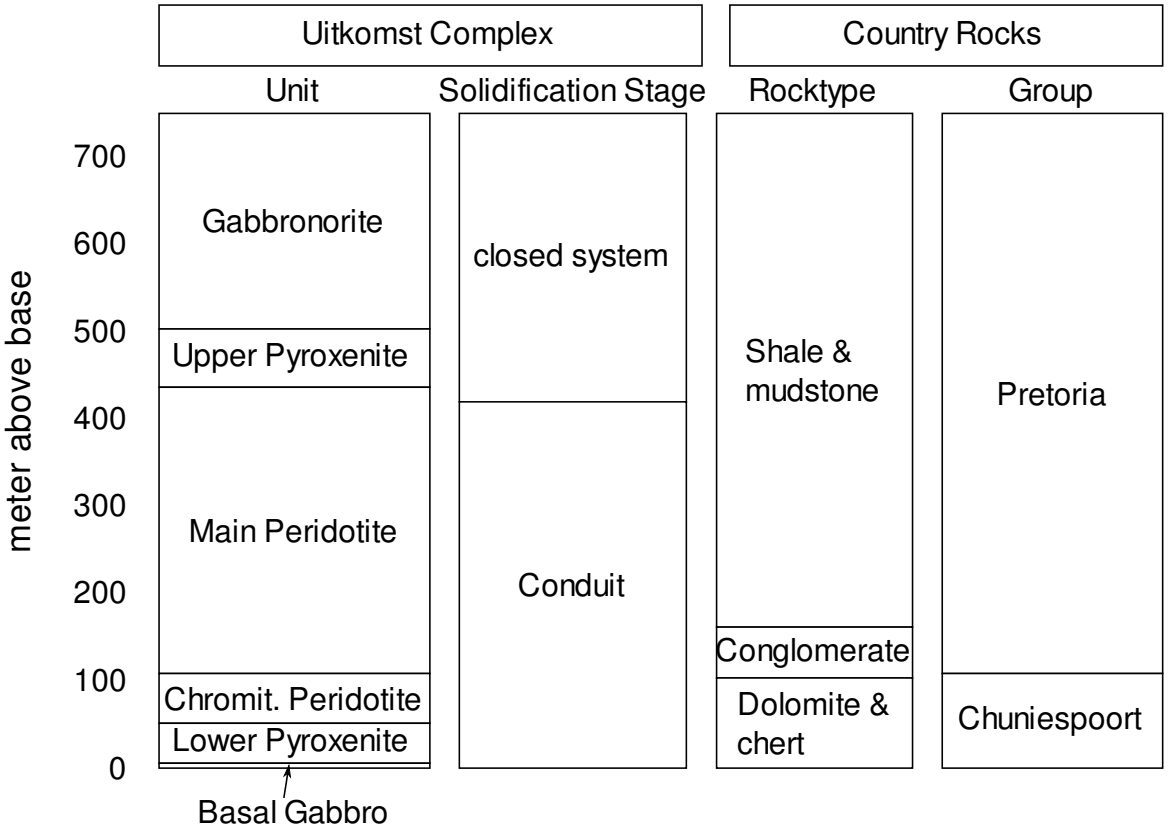

Fig. 3.5: Lithological units, rock types and solidification stages of the Uitkomst Complex (de Waal et al 2001)

3.8 Mineralogy and Geochemistry

The Uitkomst Complex hosts different minerals in different lithotypes. A summary is given in table 3.3:

Tab. 3.3: Mineral occurrences in the Uitkomst Complex sorted by rock types (after Gauert et al. 1995)

Rock type	Cumulus minerals	Intercumulus minerals	Alteration minerals
Chromitiferous harzburgite	olivine, chromite	clinopyroxene, orthopyroxene, amphibole, pyrrhotite, pentlandite, chalcopyrite	serpentine, magnetite, talc, carbonate, chlorite, mica, ferrit-chromite, violarite, mackinawite
Harzburgite dunite	olivine	clinopyroxene, orthopyroxene, chromite, plagioclase, phlogopite, pyrrhotite, pentlandite, chalcopyrite	serpentine, amphibole, talc, ferrit-chromite, magnetite, sericite, epidote, K-feldspar chromitiferous mica, chlorite, violarite, mackinawite
Olivine-orthopyroxenite	olivine, orthopyroxene	plagioclase, clinopyroxene, pyrrhotite, pentlandite	ferrit-chromite, magnetite, fuchsitic mica, chlorite, sericite, epidote, K-feldspar, amphibole, violarite, mackinawite
Orthopyroxenite	orthopyroxene	chromite, phlogopite	magnetite
Norite, Gabbronorite	orthopyroxene, plagioclase, clinopyroxene	phlogopite, titanomagnetite, pentlandite, chalcopyrite, micropegmatite	amphibole, chlorite, sericite, epidote, K-feldspar, fuchsitic mica
Gabbro	plagioclase, clinopyroxene, orthopyroxene, olivine	titanomagnetite, ilmenite, micropegmatite	magnetite, leucoxene violarite, mackinawite, saussurite, chlorite, spinel

3.8.1 Whole rock geochemistry

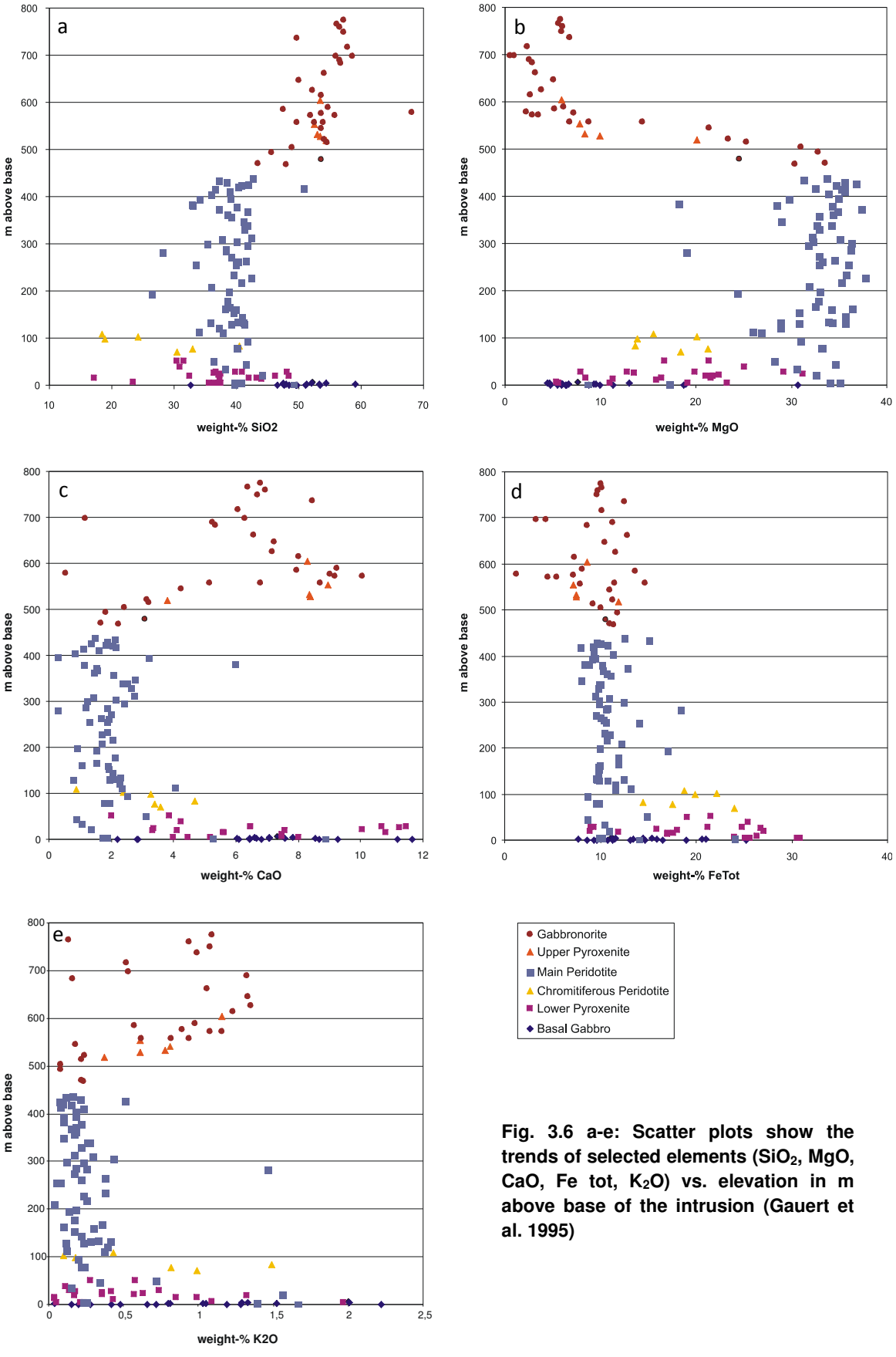

Fig. 3.6 a-e: Scatter plots show the trends of selected elements (SiO_2, MgO, CaO, Fe tot, K_2O) vs. elevation in m above base of the intrusion (Gauert et al. 1995)

The whole rock geochemistry reveals a symmetrical pattern in that the base and the top of the Uitkomst Complex are more evolved whereas the centre is relatively primitive. As a result, Mg, Cr and Ni contents are highest in the middle part of the intrusion. Incompatible elements like Rb, Zr and Y as well as Ti and V are concentrated at the bottom and at the top of the complex. Because of the intense alteration of the Uitkomst Complex the original ultramafic composition is overprinted (Gauert et al. 1995).

The following descriptions are based on the work of Gauert et al. (1995). Figure 3.6a to 3.6e show the element trends of the Uitkomst Complex represented by scatter plots of selected elements versus their height above the base of the intrusion.

Silica values show a rapid decrease from the Basal Gabbro to the Lower Pyroxenite Unit. There is a large scatter of the Si content in the LPxt and PCR. The trend of Si in the Main Peridotite Unit is almost constant. From the Upper Pyroxenite to the Gabbronorite there is an abrupt increase in Si. This trend is maintained up to the top of the intrusion.

Mg shows a large scatter in the Basal Gabbro. The scatter is less pronounced in the LPxt and PCR Unit. The Main Peridotite possesses a constant Mg pattern. From the Upper Pyroxenite to the top of the intrusion there is a sharp decrease of the Mg values.

Fe contents are also characterised by a significant variation in the lowermost three units. In the uppermost three units it seems that there is no major trend. In the Upper Pyroxenite and Gabbronorite the scatter increases.

Ca shows a large variation in the Basal Gabbro. The values decrease sharply in the Lower Pyroxenite and Chromitiferous Peridotite. The Ca contents remain stable until the Upper Pyroxenite is reached. At this point the values increase sharply. Above the base of the Gabbronorite the values decrease.

K shows a similar geochemical behaviour as Ca except for the distinct inflexion at the bottom of the Gabbronorite. The K values increase until they begin to scatter over a wide range (Gauert et al. 1995).

The first inflexion point is characteristic for all elements and occurs less than 50 m above the base of the complex. Below this point the slopes are strongly negative or positive. The large scatters in the Lower Pyroxenite and Chromitiferous Peridotite can be explained by dilution of the elements due to high concentrations of sulphides and chromite. In the Main Peridotite Unit the values for most elements remain constant. Ti, Al, K, and P show slight negative slopes. Additionally their inflexion points are at ca. 500 m instead of 400 m above the base. K, P and Ti also show inflexion points to negative slopes at about 680 m. In contrast to Ca and Al have similar inflexion points at 550 m. Fe and Mn do not possess clear inflexion points. Ni, Cu and S show very similar geochemical patterns. There is a large scatter in the lowermost three units of the Uitkomst Complex. Through the rest of the sequence these

elements remain constant at low values. Cr shows a related pattern but has higher concentrations in the PCR Unit than in the LPxt (Gauert et al. 1995).
The Basal Gabbro has S concentrations of up to approx. 3.5 wt. %. The highest contents were found in the Lower Pyroxenite (4-12.7 wt. %). The PCR unit and the Main Peridotite possess similar S contents as the Basal Gabbro. The upper part of the PRD and the base of the Upper Pyroxenite contain between 100 and 700 ppm S. The concentrations of S increase again to the top of the Upper Pyroxenite to values up to 4000 ppm. The S content decreases in the Gabbronorite from approx. 500 to 1600 ppm to less than 50 ppm in the uppermost portions of the Gabbronorite unit (Maier et al. 2004).
The Cu contents show similar patterns as the S with higher Cu concentrations in the BGab, LPxt, lower parts of the PRD and the upper portion of the UPxt. The non-mineralised parts of the Uitkomst Complex contain less than 50 ppm Cu (Maier et al. 2004).
The highest PGE contents were found in the sulfide-enriched rocks of the Lower Pyroxenite. The chromites host up to 600 ppb PGE. The sulphides can be seen as the main collector phases of PGEs. In the olivine-rich and S-poor rocks chrome reveals good correlations with Os, Ir, and Ru, supporting the thesis that the disseminated chromite controls the Os, Ir, and Ru contents of these samples. Additionally, there is evidence for a Pt-Pd-(Rh)-rich phase whose contents are too high to be explained by trapped melt alone (Maier et al. 2004).

3.8.2 Mineral chemistry

Olivine ranges from Fo80 (80 % of the cations in the solid solution of olivine between its end members forsterite $Mg_2[SiO_4]$ and fayalite $Fe_2[SiO_4]$ are Mg) in the transition zone between the BGab and LPxt Unit to Fo89-90 at the base of the Main Peridotite. This value remains stable nearly through the whole PRD Unit. At an elevation 400 m above the base of the intrusion the value decreases sharply to Fo82 at the lower parts of the Upper Pyroxenite (Gauert et al. 1995). Li et al. (2002) measured similar values (Fo86-92). Mg and Si also show significant inflexion points around this elevation (Gauert et al. 1995). The olivines of the Gabbronorite are highly fractionated with values of less than Fo30 and less than 300 ppm Ni (Li et al. 2002).
The Ni contents in olivine are highly variable. The most Ni depleted olivines reside in the mineralised parts of the Harzburgitic units, which contain more than 1 wt. % sulphides. Olivines with high Ni contents occur in the non-mineralised zones of the Main Harzburgite and the overlying units.
The enstatite content in pyroxene shows a related pattern to the forsterite content in olivine. The minimum values En65 (orthopyroxenites contain 65 mol % Mg in the solid solution between enstatite $Mg_2[Si_2O_6]$ and ferrosillite $Fe_2[Si_2O_6]$) occur in the Basal Gabbro Unit

followed by an increase to En85-90 in the Main Peridotite with a maximum value at 400 m above the base. Above this elevation there is a scatter with a final decrease to En50-60 in the Gabbronorite (Gauert et al. 1995). The Mg number (Mg/(Mg+Fe)) of orthopyroxene in the Main Peridotite unit is stable at a value close to 0.88. The number decreases in the Upper Pyroxenite to 0.71. Lower values can be found in the overlying Main Gabbronorite where the Mg number decreases from 0.5 at the bottom to 0.2 in the middle of the unit. The Mg number of clinopyroxene shows similar patterns (Sarkar et al. 2008).

Regarding its mineral chemistry plagioclase shows the biggest scatter from up to 30 mol %. The composition ranges in the BGab from An70-80 (plagioclases contain 70-80 mol % Ca in the solid solution between anorthite $Ca[Al_2Si_2O_8]$ and albite $Na[AlSi_3O_8]$). The value increases in the harzburgitic units to An92. Some measurements reveal a high content of albite. This may be a result of saussuritisation (Gauert et al. 1995). The An content in the Upper Pyroxenite and the Main Gabbronorite remains constant at values between An62-77. The value decreases from An63 at the base of the Main Gabbronorite to An56 in the middle of the unit. There are no preserved plagioclases in the highly altered upper part of the Main Gabbronorite. As a result the An content ranges between An2-4. In the Upper Gabbronorite the value increases to An79 (Sarkar et al. 2008).

The chromite composition is highly variable.

Amphiboles which replace the primary magmatic minerals show a wide scatter in their composition ranging from hornblende to actinolite (Gauert et al. 1995).

3.8.3 Sulphur isotope data

The $\delta^{34}S$ values in the Basal Gabbro are between -19.5 and +1.8 ‰. There are two clusters at -6.0 and 0 ‰. The strong negative measurement, which are indicative of a sedimentary signature, result from a nearby xenolith of quartzitic composition (Gauert et al. 1995, Gauert & Jordaan 1996). Li et al. (2002) determined $\delta^{34}S$ values from -0.9 ‰ to +2.7 ‰ for the Basal Gabbro. The Lower Pyroxenite Unit reveals $\delta^{34}S$ values from -4.5±1.8 ‰. The mode is at -6.0 ‰ (Gauert et al. 1995). Gauert & Jordaan (1996) measured values between -7.9 and -0.9 ‰. Sarkar et al. (2008) determined similar values (-4 ‰ to -2.8 ‰). The variable values of the Basal Gabbro indicate that there was not enough time for equilibration. The Lower Pyroxenite shows less variability, evidence for a better equilibration during slower cooling rates (Gauert & Jordaan 1996). The $\delta^{34}S$ values of the Main Peridotite range between -7.4 and +1.2 ‰ (Gauert et al. 1995, Gauert & Jordaan 1996). Sarkar et al. (2008) determined values from -7.1 ‰ to -4.5 ‰. The lowest values could be determined for the country rock (-11.5 to -15.5 ‰) (Gauert et al. 1995). Another study (Sarkar et al. 2008) revealed $\delta^{34}S$ values of -11 ‰ for the Malmani Dolomite and -18 ‰ for the Timeball Hill Shale. Gauert & Jordaan

(1996) determined values from -13.3 ‰ to -15.6 ‰ for the Timeball Hill Shale and -11.1 ‰ for the Malmani Dolomite. Sarkar et al. (2008) measured the $\delta^{34}S$ values of the Main Peridotite at around 0±2 ‰. Specimens from the upper part of the Main Peridotite show $\delta^{34}S$ values from -2.4 to 9.1 ‰. Samples from the lower part are characterised by $\delta^{34}S$ values from 0 to 2 ‰. The $\delta^{34}S$-values for the Pyroxenite unit and the Upper Gabbronorite unit show a range between -1.5 and 2 ‰. Li et al. (2002) determined similar $\delta^{34}S$ values (Basal Gabbro, Upper Pyroxenite, Gabbronorite: -0.9 ‰ to 2.7 ‰; non-mineralised Main Harzburgite: -0.2 ‰ to 2.8 ‰; mineralised Main Harzburgite: -7.11 ‰ to -4.45 ‰; Lower Pyroxenite: -5.58 ‰ to 2.8 ‰, Chromitiferous Peridotite: -5.50 ‰ to -5.68 ‰).

As a result, an appropriate model is mixing of a sedimentary sulphur source with an ultramafic magma. According to mass balance calculations an assimilation of around 10 % would be necessary to produce the observed values (Gauert et al. 1995).

An overview of the S isotope measurements from different authors is given in table 3.4.

Tab. 3.4: S isotope values of rocks from the Uitkomst Complex. The used publications are named in the headline.

Rock unit	**Gauert (1995)**	**Gauert & Jordaan (1996)**	**Li et al. (2002)**	**Sarkar et al. (2008)**
BGab	-19.5 to +1.8 ‰	-19.5 to +1.8 ‰	-0.9 to 2.7 ‰	0.2 to 2.7
LPxt	-4.5±1.8 ‰	-7.9 to -0.9 ‰	-5.58 to 2.8 ‰	-4 to -2.8 ‰
PCR			-5.50 to -5.68 ‰	-7.1 to -4.5 ‰
PRD	-7.4 to +1.2 ‰	-7.4 to +1.2 ‰	-7.11 to -4.45 ‰ (mineralised) -0.2 to 2.8 ‰ (unmineralised)	0 to 2 ‰ (lower part) -2.4 to 9.1 ‰ (upper part)
UPxt			-0.9 ‰ to 2.7 ‰	-1.5 to 2 ‰
GabNor			-0.9 ‰ to 2.7 ‰	-1.5 to 2 ‰
Timeball-Hill shale	-11.5 to -15.5 ‰	-13.3 to -15.6 ‰	-18 to -12 ‰	-18 ‰
Malmani dolomite	-11.5 to -15.5 ‰	-11.1 ‰	3 to 10 ‰ (lower quarter) -8 to 0 ‰ (upper three-quarter)	-11 ‰

3.8.4 Oxygen isotope data and Initial Sr isotope ratios

$\delta^{18}O$ isotope data for the Main Peridotite range between 5.2 and 5.9 ‰. The Upper Pyroxenite to Main Gabbronorite show values from 5.4 to 6.9 ‰. Plagioclase possesses slightly higher values. $\delta^{18}O$ values of albite from the altered part of the Main Gabbronorite show a range from 8.8 to 9.7 ‰. Quartz possesses measured $\delta^{18}O$ values between 11.1 and 15.2 ‰. Pyroxene of the Upper Gabbronorite unit shows values between 5.6 and 6.9 ‰.
This supports a model which states that there was no or only low assimilation of country rock with high ^{18}O isotope values. As a result the sulphur as introduced by a fluid did not change the ^{18}O isotopic composition of the magma (Sarkar et al. 2008).
Initial Sr isotope ratios are in the range from 0.704 to 0.715 at 2.050 Ga (Gauert et al. 1995).

4 General aspects of serpentinisation and talc-carbonate alteration

4.1 General

The alteration types, which affected the Uitkomst Complex, are serpentinisation and talc-carbonate-alteration.

Field observations have led to the following alteration sequence, in which the alteration stages become more intensive with an increasing CO_2 content of the alteration fluid: (1) olivine + serpentine + brucite, (2) magnesite + serpentine, (3) magnesite + talc, (4) magnesite + quartz. It is also possible that the most intense degree of alteration (magnesite + quartz) was not reached in some systems because of the lack of silica (Klein & Garrido 2011).

In general, the alteration process in ultramafic rocks begins with the serpentinization of the protolith. Serpentinisation takes place under disequilibrium conditions (Klein & Garrido 2011). Figure 4.1 shows the phase stabilities in the system SiO_2-MgO-H_2O-CO_2.

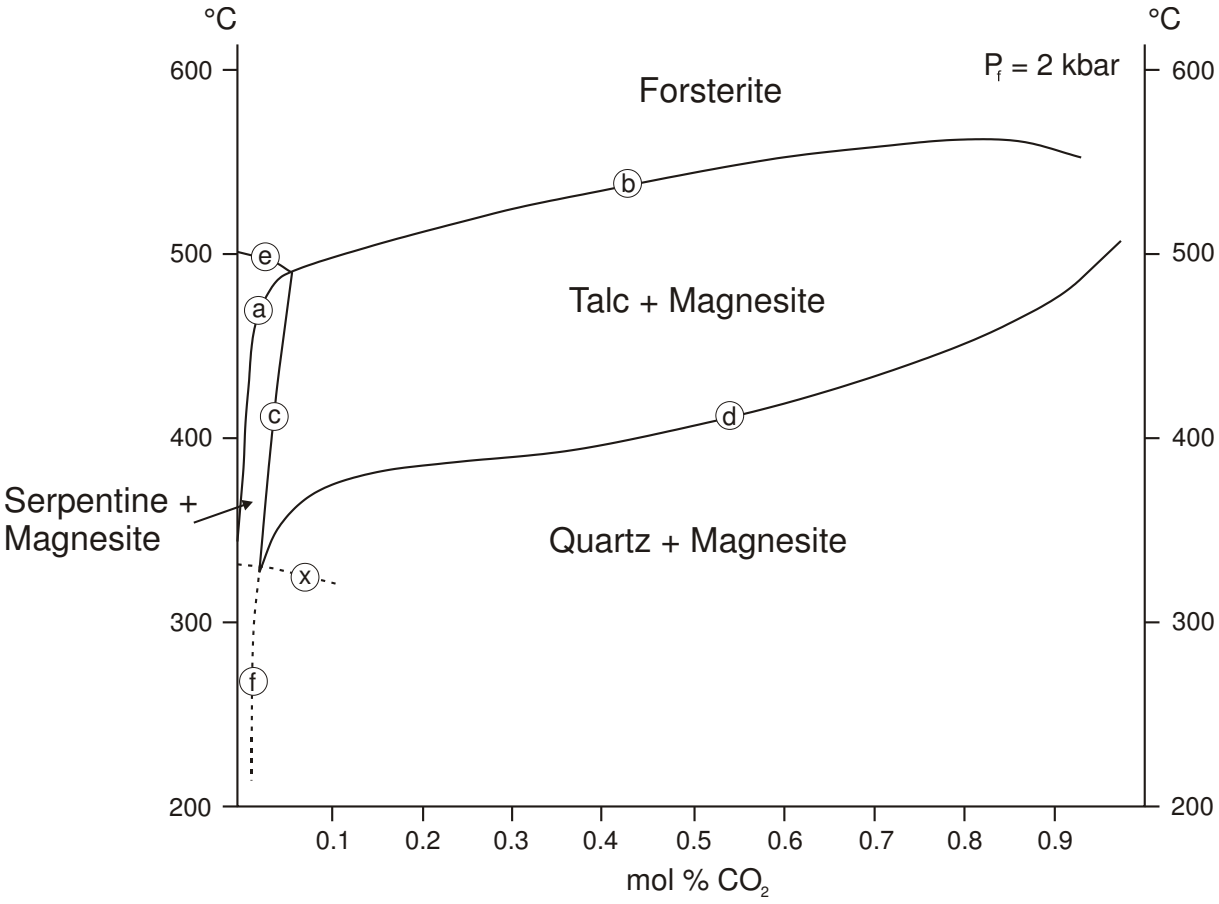

Fig. 4.1: Phase diagram of the system SiO_2-MgO-H_2O-CO_2 after Johannes (1967) showing the influence of a CO_2 enriched fluid on (ultra)mafic rocks.

The first reaction which takes place in the system MgO-SiO_2-H_2O-CO_2 at 2 kbar pressure is (Johannes 1967):

$$reaction\ 4.1: forsterite + brucite \rightleftarrows serpentine + H_2O$$

This reaction is a univariant dehydration reaction. If the aqueous phase is diluted by CO_2 the equilibrium temperature decreases with increasing CO_2 content. Brucite is stable up to a CO_2 content of 0.5 % at a temperature of 400 °C. With higher temperatures and increasing CO_2 content reaction 5.1 is replaced by the first carbonation reaction:

$$reaction\ 4.2: 2\ forsterite + 2\ H_2O + CO_2 \rightleftarrows serpentine + magnesite$$

The lowest temperature, at which the assemblage is stable, is 440°C. The stable conditions of the mineral assemblage end at 490°C and 6 mol% CO_2 (Johannes 1967).
The general reactions (the first three reactions are metastable) which lead to carbonation in ultramafic rocks are as follows (Klein & Garrido 2011):

$$reaction\ 4.3: olivine + 2\ CO_2(aq) \rightleftarrows quartz + 2\ carbonate$$
$$reaction\ 4.4: pyroxene + CO_2 \rightleftarrows quartz + carbonate$$
$$reaction\ 4.5: serpentine + 3\ CO_2(aq) \rightleftarrows 2\ quartz + 3\ carbonate + 2\ H_2O$$
$$reaction\ 4.6: talc + 3\ CO_2(aq) \rightleftarrows 4quartz + 3\ carbonate + H_2O$$
$$reaction\ 4.7: brucite + CO_2(aq) \rightleftarrows carbonate + H_2O$$

The next reaction is:

$$reaction\ 4.8: 4\ forsterite + H_2O + 5\ CO_2 \rightleftarrows talc + 5\ magnesite$$

This reaction takes place when the CO_2 tops 6 mol%. The lowest temperature for reaction 5.8 is 490°C. The equilibrium temperature increases slightly up to a CO_2 content of 71 mol%. At a CO_2 content of 83 mol% the equilibrium line passes through a maximum. After the maximum point the equilibrium temperature decreases (Johannes 1967).
At lower temperatures and CO_2 content between 2 mol% and 6 mol% the reaction is as follows:

$$reaction\ 4.9: 2\ serpentine + 3\ CO_2 \rightleftarrows talc + 3\ magnesite + 3\ H_2O$$

Serpentine is not stable at medium CO_2 concentrations. Under natural conditions fluids with CO_2 contents higher than 6% are likely to occur. Thus serpentine reacts commonly to talc and magnesite. Reaction 5.9 elapses with a constant volume. Because of the steep gradient of the equilibrium line the reaction is mainly dependent on the CO_2 content of the fluid (Johannes 1967).
For the case of a very high supply of CO_2 the final reaction is:

$$reaction\ 4.10: talc + 3CO_2 \rightleftarrows 4\ quartz + 3\ magnesite + H_2O$$

Quartz and magnesite are the final products of the alteration of ultramafic rocks. However this reaction can also occur in carbonatic, quartz- and magnesite-bearing sediments as well as in quartz-bearing magnesite deposits (Johannes 1967). Quartz can also precipitate as amorphous silica, opal-CT or chalcedony (Klein & Garrido 2011). Magnesite is stable over a wide range of CO_2 contents.
A continued flow of fluids at low temperatures can lead to decarbonisation and silicification of the altered rock (Klein & Garrido 2011).
Serpentinisation is known for producing very reducing fluids. These fluids are linked to the formation of large amounts of dihydrogen ions triggered by the oxidation of ferrous iron to ferric iron with water. Therefore native nickel-iron minerals and alloys (Klein & Garrido 2011) are likely to be stable. Fluids produced by serpentinisation have extremely low oxygen, sulphur, silica and CO_2(aq) fugacities. If a CO_2-bearing fluid is present the redox conditions change fundamentally. For example the oxygen fugacity sharply increases because of the liberation of oxygen from the reduction of ferric to ferrous iron in the carbonates because of the connection between the sulfur and oxygen fugacity via reaction

$$reaction\ 4.11: S_2(g) + 2\ H_2O\ (l) \rightleftarrows 2\ H_2S\ (aq) + O_2(g).$$

The sulphur fugacity rises as well. The increase leads to the formation of a sulfur rich hematite-pyrite assemblage from a sulfur poor pentlandite-awaruite-magnetite assemblage. There is also an increase in the activities of silica and CO_2(aq) (Klein & Garrido 2011).
The best thermodynamic conditions for the carbonisation of serpentinised peridotites occur at low to moderate temperatures because the gradients in silica and CO_2(aq) activity are steepest (Fig. 4.2). At high temperatures the solubility of quartz (blue lines) increases. Therefore the talc-quartz-magnesite equilibrium is shifted to very high CO_2(aq) activities which make it difficult to initiate the carbonation reaction except when there is a high content of CO_2(aq) in the fluid (Klein & Garrido 2011).

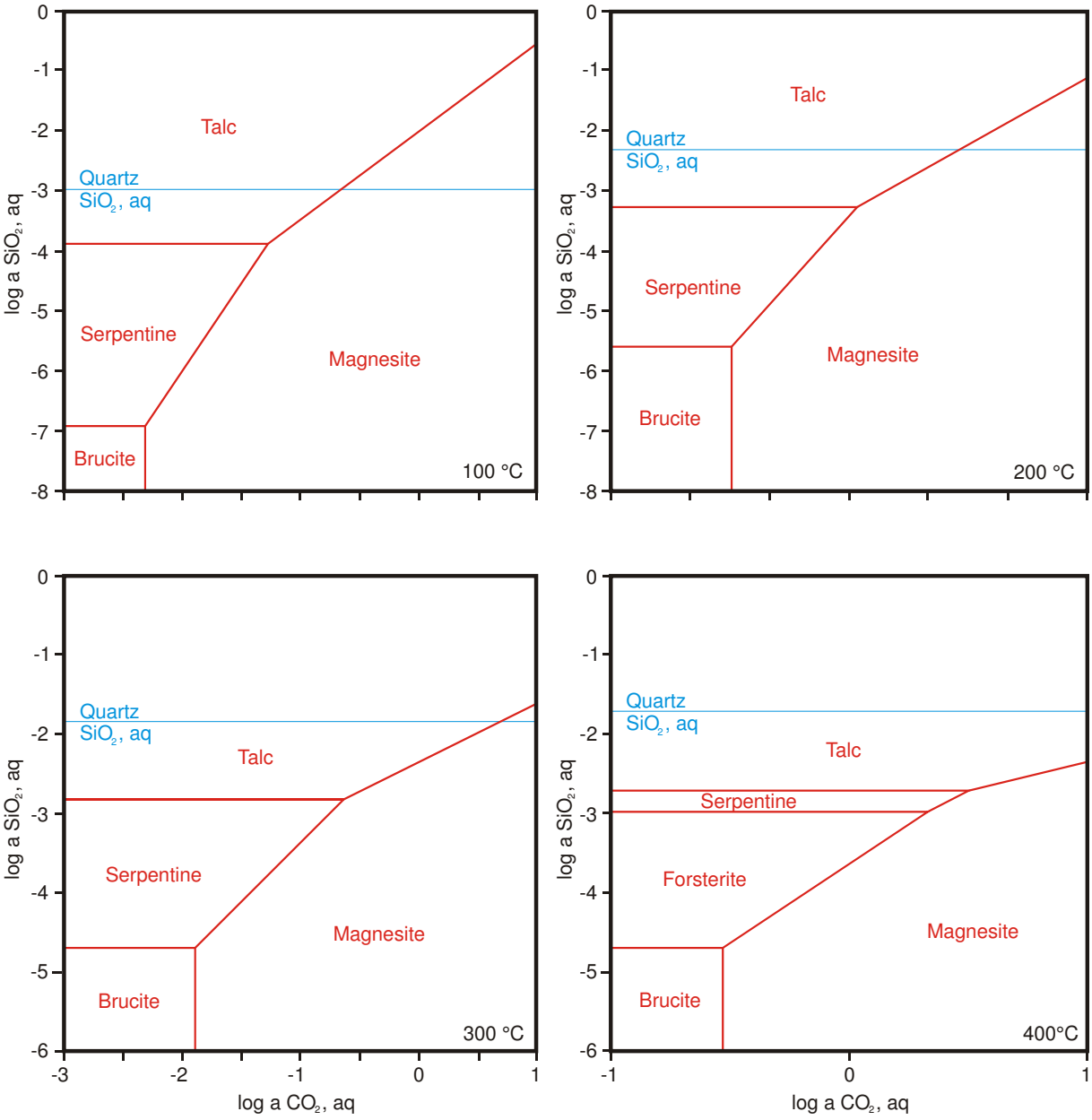

Fig. 4.2: Activity-activity diagrams in the system SiO_2-MgO-H_2O-CO_2 (Klein & Garrido 2011). The red lines define the stability fields and the blue line represents the quartz solubility at different temperatures (stated in the lower right corners)

4.2 Alteration in the Uitkomst Complex

Alteration is a very widespread phenomenon in the Uitkomst Complex. The rocks are serpentinised, altered to talc-carbonates, uralitised and saussuritised (de Waal et al. 2001). The alteration is strongest in the lower three units. The secondary assemblage consists of talc, carbonate, serpentine, actinolite-tremolite, epidote, leucoxene, sericite and saussurite (Gauert & Jordaan 1996).

The Lower Pyroxenite and the PCR unit are altered to talc-carbonate-rocks. This alteration abruptly ends at the level of the Massive Chromite, which caps the PCR unit. The Main

Peridotite is serpentinised. The lower three units of the Uitkomst Complex rest on the carbonates of the Malmani Dolomite. These contact rocks could have been responsible for high CO_2 partial pressures that led to a stabilisation of talc and carbonate (de Waal et al. 2001).

The primary sulphides show a weak alteration with magnetite having replaced pyrrhotite along grain margins. Pyrite forms secondary, idiomorphic grains. In the Basal Gabbro unit magnetite is oxidised to leucoxene (Gauert & Jordaan 1996).

Alteration in the upper parts of the complex is most intense in the central portion of the Gabbronorite unit although there are also alteration phenomena in the lower part of the Gabbronorite unit. In the most altered parts, pyroxene has been converted into actinolite, chlorite and quartz, plagioclase was albitised, and the albite reacted to epidote. Meteoric waters were probably responsible for the alteration of the Gabbronorite and partially for the alteration of the Basal Gabbro. The fluids migrated along pathways into the magmatic body (possibly via cooling cracks) and altered the rocks near the margin of the complex. It is likely that the fluids exchanged elements with the surrounding country rocks (Sarkar et al. 2008).

Measurements of fluid inclusions performed by Sarkar et al. (2008) indicated that the alteration of the upper parts of the Uitkomst Complex took place at around 500°C with a saline fluid of 20 to 25 weight% NaCl.

The fluid:rock ratios are thought to be higher in the upper part of the Main Gabbronorite as indicated by the $\delta^{18}O$ values of albite and quartz. Lower $\delta^{18}O$ values appear locally in the Upper Gabbronorite and in the lower part of the Main Gabbronorite. Similar $\delta^{18}O$ values of plagioclase are observed in the Basal Gabbro unit (6.1 to 8.1‰), supporting the thesis that hydrothermal fluids were of meteoric origin (Sarkar et al. 2008).

The alteration of the BGab, LPxt and PCR unit was investigated by Steenkamp (2012). It is suggested that the CO_2 rich fluids, whose source is the devolatisation of the Malmani dolomite, migrated upwards and were entrapped by Massive Chromitite layer and the reaction skarn around the Uitkomst Complex, which led to an extensive alteration of the PCR unit. The relative lower degree of alteration of the LPxt compared to the PCR is explained by the more effective escape of the alteration fluids along structural features and along the flow of the conduit. The developed alteration assemblages were overprinted by later events like intrusion of diabase sills and tectonic reactivating of older structures. The shear zones in the Massive Chromitite layer have been developed by the increase in volume of the PCR unit due to the alteration. The determined temperatures of the alterations fluids are between 540 and 660°C (Steenkamp 2012).

5 Methodology

5.1 Mapping

The mapping was carried out in open pit 3 in the Nkomati mine. A geological compass, a clino-ruler and a GPS system were used for the mapping. The mapping results were drawn to scale on an A3 sheet. The structural measurements had to be corrected by 18° due to the magnetic declination. The mapping of this unit was reduced to the identification of xenoliths and different alteration stages because the Lower Pyroxenite unit is a very heterogeneous unit and it was difficult to get access to the whole pit due to ongoing mining operations, instable rock slopes and safety issues. After the mapping was finished the results were compared to borehole data to check the accuracy of the mapping.
For the plotting of the structural elements the software Stereonet 7 from Rick Allmendinger was used.

5.2 Sample selection

All talc-carbonate specimens, which could be found, were taken as samples. The author tried to collect representative specimen of all in the open pit available rock units. The main focus was on the Chromitiferous Peridotite and Lower Pyroxenite unit. Single specimens were taken from special places such as the contact of xenoliths and ultramafic rocks or from faults or joint zones. In total 66 rock specimens from different lithotypes were sampled. If the samples were taken from the face they can be geographically assigned. To assign the original location from samples, which were picked up from loose material, is more difficult. Only the bench can be identified. Due to daily mining operations the specimens from loose material were dislocated from their original source. The samples were numbered in the order they were found. On overview over the specimens is given in the appendix (Tab. A1).

5.3 General Preparations of the specimens

After the sampling the rock specimen were inscribed and cut in two pieces to have backup-samples if there should be some difficulties concerning the measurements. After that the rocks were crushed and milled with a steel pot for circa 30 s. The final grain size should be lower than 2 µm. A total of 30 to 50 g rock powder per specimen was produced. The rock powders were used for XRF and XRD measurements and for the determination of the loss of ignition (LOI). The rest of a specimen was used to cut blocks for thin sections, which were prepared at the Martin-Luther-University Halle-Wittenberg.

5.4 X-Ray Diffraction (XRD)

The XRD measurements were carried out at the University of Free State (Bloemfontein) using the D5000 Bruker AXS diffractometer. The evaluation of the measured data was carried out with the software XPert Highscore Plus at the Martin-Luther-University Halle-Wittenberg. The SiO_2 contents of some samples are overestimated due to problems with the configuration of the XRD measuring instrument.

With the XRD facility one can investigate the reflexion and diffraction of x-rays on crystal lattices. An X-ray tube emits X-rays, which are aimed on the specimen. The X-ray will be reflected or diffracted. In the case of diffraction the former coherent radiation will be phase displaced. The X-ray will be reflected only through integral phase displacement. Therefore the reflexion appears only at certain angles, which are determined by the distance of the reticule. The reflected X-rays can be counted by detectors. On that score one can determine the distance between the atom layers by using the equation of Bragg. The distances are characteristic for each mineral.

5.5 X-Ray Fluorescence (XRF)

The XRF measurements were carried out at the University of Free State (Bloemfontein) with the Panalytical Axios XRF spectrometer and the Super Q analytical software. The evaluation of the measured data was done at the Martin-Luther-University Halle-Wittenberg.

The XRF technology is based on the emission of characteristic secondary X-rays of a certain element. X-rays are emitted on the specimen by an X-ray tube. This is the so called Kα radiation. The radiation hits an electron, which absorbs the energy and leaves the innermost shell. An electron of the next higher energetic shell falls on the lower shell, which is linked to a loss of energy. Now radiation in form of characteristic X-rays is emitted. The energy of the emitted X-rays correlates with the energy difference of the involved shells. If the secondary radiation fulfils the equation of Bragg, it will be detected as a peak by the measurement device.

The samples were analysed with fusion disks. The major elements, which were measured, are SiO2, TiO2, Al2O3, Fe2O3, MnO, MgO, CaO, Na2O, CaO, K2O, P2O5, Cr2O3, and S. The analysed minor elements are V, Sc, Co, Ni, Cu, Zn, As, Br, Rb, Sr, Y, Zr, Nb, Mo, Ag, Cd, Sn, Sb, Ba, Tl, Pb, Th, U.

The main elements K_2O, MnO, TiO_2, Na_2O and P_2O_5 show some negative values in the original data. The negative values were replaced by the half of the calculated deviation that was given in the table. K_2O, TiO_2 and Na_2O have the most values, which were negative.

5.6 Scanning Electron Microscopy (SEM)

The SEM measurements were carried out at the Martin-Luther-University Halle-Wittenberg with a scattering electron microscope of the type JSM-6300 from JEOL. The EDX detector XFlash 5010 from Bruker was used. The software, which was used for the evaluation of the X-ray spectrograms, is Quantax 200 from the company Bruker. The acceleration voltage is 20 keV and the energy resolution is at 123 eV. The evaluation of the diagrams was carried out by Sabine Walther. The interpretation of the determined concentrations of the elements in the targeted minerals was done by the author.

Before measuring the specimens (or thin section) have to be sputtered. This has to be done because of charging effects. If the primary electron ray is too strong, then the specimen will be electrically charged, which disrupts the measuring process. The investigated specimens were sputtered with carbon.

A total of 431 measurements were performed. To analyze the samples the back scatter mode was used. The measurement of each point lasted 90 s. The minerals, which were measured, were mostly chlorite, serpentine, talc, sulphides, oxides, and carbonates. In total 8 prepared thin sections were analysed.

An electron ray is emitted by a heated tungsten wire. This is the so called hot cathode. Around the wire a negative charged Wehnelt-cylinder is installed. The electrons are accelerated by an electric field and focussed by a system of lenses. The scanning of the prepared thin section takes place through the deviation of the electron ray in x and y direction. The primary electron ray is moved row by row over the specimen. To the resulting picture grey values are assigned. They will be presented on the screen.

The microscope is equipped with different detectors. One detector is constructed for recognising back scatter electrons (BSE). The other detector is used for measuring secondary electrons (SE). The BSE detector is a semiconductor detector. The energy rich back scatter electrons hit the detector. This results in a defect, which leads to an electric current, which can be detected. The SE detector consists of a scintillator, a collector, fiber optics and a photo multiplier. Through a voltage in the collector the secondary electrons are accelerated. These electrons lead to lightings in the scintillator, which are enhanced by the photo multiplier.

The electron beam of the SEM does not measure the surface of a mineral. The beam penetrates the grain to certain extent and possesses a certain spatial spread. If the measured minerals are too small or replaced, then the SEM measures a mixture of surrounding minerals. Measurements, which reveal such a mixture are not considered in chapter 8.

For the interpretation of the data the measurements had to be converted. An excel sheet compiled by Barnes (2004) was used for the chromites. The chlorites were recalculated with an excel sheet of Andy Tindle. To convert the weight% of elements into weight% of oxides the method after Kalantar et al. (2008) was used. For the creation of the ternary plots the software GCDkit (Janousek et al. 2006) was used.

5.7 Optical microscopy

For the microscopic identification of the minerals an optical microscope from Leica was used. Polished thin sections of 30 selected specimens were produced at the Martin-Luther-University Halle/Saale by Gerald Berthold. All minerals could be identified by transmitted light except the ore minerals. The opaque phases were identified with the SEM. Pictures were taken for the most important and representative specimens with an Axiophot microscope from Zeiss. The software, which was used, is NIS-Elements F3.0.

5.8 Pseudosections

For the construction of the pseudosection the software Perple_X by James Connolly was used.

The pseudosections are CO_2-T-diagrams, which is why the pressures had to be estimated. Numerous sections were produced to find out the best fitting results. Attempts were made with different pressures, bulk rock compositions and temperature ranges. An attempt was started to evaluate the pressure dependence of the reaction. But it turned out, that the reactions are nearly pressure independent, which is indicated by approximately vertical tie-lines.

Another pseudosection was modelled with two different composition groups at the base of the XRF results. Different pressures between 500 and 1500 bar were estimated. For the reduction of the phases the minor constituents were excluded.

5.9 Pycnometer

The pycnometer test is designed to measure the density fluids and powders. Before the pycnometer test the rock powder has to be dried at 50°C for two days. Therefore the powder will lose the capillarily bounded water.

At first the pycnometer has to be weighted without (m_p) and with the dried rock powder (m_1). The weight of the rock powder is m_d. After the weighting the pycnometer has to be filled with distilled water in a way that the powder is completely covered. Now the water in the filled

pycnometer has to be boiled for at least 20 minutes. The rock powder and the water will be deaerated during the boiling. After this step the pycnometer is filled with distilled water up to the neck. Now the pycnometer has to cool for at least five to ten minutes. For that purpose the pycnometer is placed in a bucket, which is filled with water. Then the temperature of the water in the pycnometer is measured. The density of the water can be estimated via a table. The pycnometer with the water and the rock powder has to be weighted again (m_2). The difference of the pycnometer filled with water and the rock powder and m_1 equals the weight of the water (V_W). Now one can calculate the volume of the water in the pycnometer.

Afterwards the volume of the pycnometer has to be measured. One fills distilled water of a certain temperature (to estimate the density of the water via a chart) in the pycnometer. The pycnometer with water has to be weighted (m_3). The difference to the weight of the pycnometer itself equals the weight of the water. Now one can calculate the volume of the pycnometer (V_P).

The difference of the volume of V_P and V_W is the volume of the rock powder. Now one can calculate the density of the rock powder.

6 Petrography

In this chapter only the mapped lithologies are considered. The description of all specimens is given in the appendix (Tab. A2).

6.1 Macroscopic features

6.1.1 Black Reef Quartzite

The Black Reef Quartzite is a cherty to gritty, easily splittable rock, is very fine-grained and has a milky appearance. The quartzite is the lowermost rock type apparent in open pit 3.

6.1.2 Basal Gabbro

The Basal Gabbro (Fig. 6.1) possesses dark grey and dark green to black (pyroxene, serpentine) and white minerals (feldspar). The rocks are widely serpentinised. Along faults rocks were found, which were very soft, highly altered and oxidised. An apparent mineral, which is linked to the oxidation, is goethite.
It is very difficult to distinguish between the Basal Gabbro and the Lower Pyroxenite if the pyroxenite is feldspar rich. The differentiation was made by the higher Cu mineralisation of the Basal Gabbro.

Fig. 6.1: Picture of a gabbroic rock from the Basal Babbro (specimen H39). The white minerals are feldspar. The dark portions are composed of mafic minerals.

6.1.3 Lower Pyroxenite

The Lower Pyroxenite is composed of calc-silicates, talc-carbonate schists, and different types of pyroxenite with respect to the alteration, grain size, secondary mineralization and mineral assemblages. One common feature is the occurrence of secondary pyrite. In some places the pyroxenite is silicified or crosscutted by up to 5 cm thick quartz or calcite veins.
The first type of pyroxenite (Fig. 6.2) is a fine-grained, highly serpentinised, soft, dark green to black coloured, and weakly mineralised rock. The sulphides are disseminated.

Fig. 6.2: Picture of a fine-grained pyroxenite from the Lower Pyroxenite (specimen H32). In the lower part sulphide minerals are apparent. Large crystals cannot be recognised.

The next pyroxenite type (Fig. 6.3) is coarse-grained, dark green to black and highly mineralised. The sulphide minerals built a network, which partially encloses the rock forming minerals like pyroxene or amphibole. The ore texture is called net-texture.

Fig. 6.3: Picture of a coarse-grained pyroxenite from the Lower Pyroxenite (specimen H31). The disseminated to net-textures sulphide mineralisation is visible.

The third pyroxenite type is fine to medium-grained with a dark green to black colour, weakly altered, and possesses a low to medium mineralisation. The feldspar content is very high (up to 20 %) compared to the other two pyroxenite types. The feldspars and pyroxenes are subhedral to euhedral. The feldspars can be present as globules from up to 5 cm. Serpentine is apparent as well.

6.1.4 Chromitiferous Peridotite

The Chromitiferous Peridotite (Fig. 6.4) is a highly altered, ultramafic rock, which has a dark grey to black colour and is very talceous. Some parts are serpentinised. The original magmatic textures are still preserved. The PCR is mineralised by sulphides and intersected by numerous serpentine veins. The fine-grained chromite crystals are poikilitically enclosed by olivine.

Fig. 6.4: Picture of a rock from the Chromitiferous Peridotite (specimen H12). Small chromite grains are poikilitically enclosed by olivine crystals.

The PCR hosts most of the talc-carbonate schist (Fig. 6.5) present in the Uitkomst Complex. The talc-carbonate is a fine-grained, greasy, soft, and crème-coloured to brownish-grey rock. The primary sulphidic mineral assemblage is pyrrhotin-pentlandite-chalcopyrite. Secondary pyrite, which forms up to 1 cm large, idiomorphic cubes, is also apparent. Other minerals are carbonates, serpentine and tremolite.

The Chromitiferous Peridotite (Fig. 6.6) is chrome rich and hosts semi-massive to massive chromitites. The chromitites are fine-grained, dark brown to black coloured, and very talceous. Around the chromitites big shear zones are developed. In these shear zones the rocks are highly altered, very talceous, and schistose. The sulphide minerals are elongated in the direction of the schistosity due to the movement of the rocks in an environment, which allows plastic flow. Rarely these zones are serpentinised.

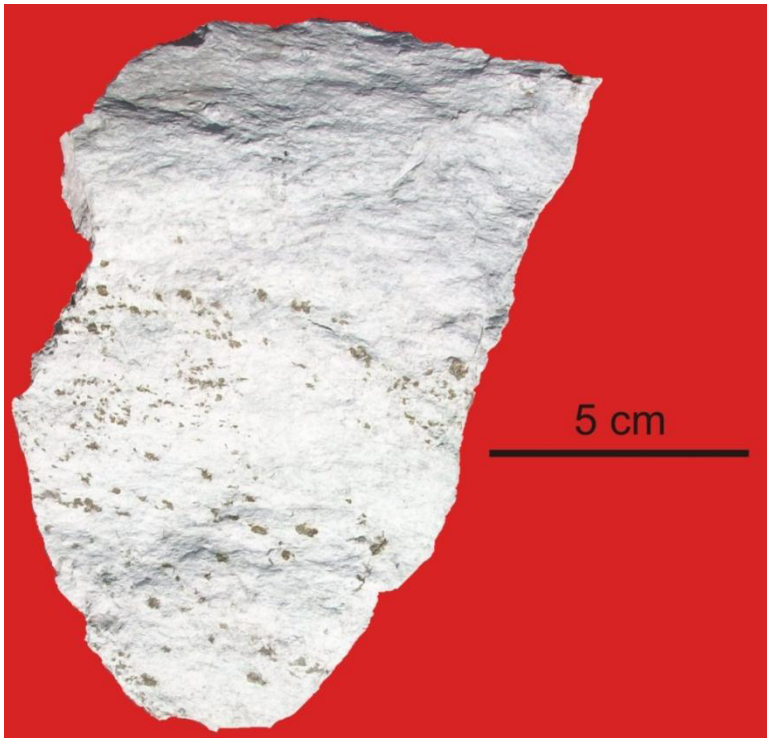

Fig. 6.5: Picture of a talc-carbonate schist from the PCR unit. The specimen, which is shown, is H50. The rock is white to light grey. Sulphides are apparent. The idiomorphic sulphides are pyrite.

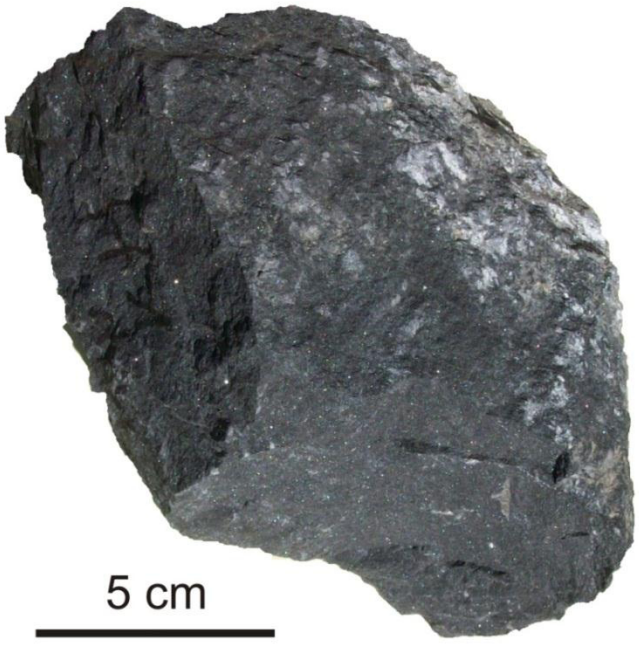

Fig. 6.6: Picture of a Massive Chromitite from the Chromitiferous Peridotite (specimen H1). The rock is dark brown to black and fine-grained. The white areas are very talceous.

6.1.5 Main Harzburgite

The Main Harzburgite (Fig. 6.7) is an ultramafic rock, which is less altered than the LPxt and PCR but also shows signs of serpentinisation indicated by the fatty lustre of the originally primary olivine grains. The harzburgite possesses a dark grey to black colour and is low mineralised. The primary minerals are replaced by amphibole and serpentine. The mineralisation is disseminated and very fine-grained.

Fig. 6.7: Picture of a peridotite from the Main Harzburgite (specimen H4). The sulphides are disseminated. The peridotite is completely composed of mafic minerals.

6.1.6 Calc-silicate fels

The calc-silicate felses are xenoliths, which were assimilated from the country rocks. The apparent minerals are pyroxenes and carbonates such as calcite and dolomite. The originally sedimentary rocks (dolomites) are light to lime green coloured, and massive to layered in their appearance. There are short layers, which are up to 2 m in length, and very continuous layers, which are persistent for at least several tens of meters. The calc-silicate rocks are mostly situated in the LPxt and PCR. The dip of the continuous layers runs parallel to the general dip of the ultramafic intrusion. Some of the short layers a folded.

6.1.7 Diabase

The diabases (Fig. 6.8), which are composed of pyroxene, amphibole and feldspar, are intrusions of basaltic composition crosscutting the ultramafic layered complex. The diabase is dark grey to black (pyroxene, amphibole) and white (feldspar) coloured, not or very weakly altered and in rare cases weakly mineralised by pyrite. The intrusions form sills and dykes.

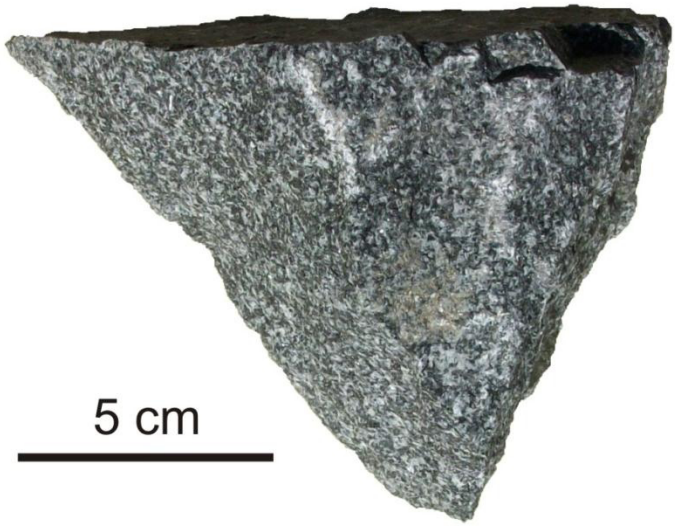

Fig. 6.8: Picture of a diabase (specimen H24). The white minerals are feldspar. The dark portions are composed of mafic minerals (amphibole, pyroxene).

6.2 Microscopic features

The abbreviations, which are used in the following pictures, are derived from Whitney and Evans (2010). An overview of the mineral quantities in the thin sections is given in the appendix (Tab. A3).

6.2.1 Basal Gabbro

Figure 6.9 shows a portion of specimen H39. Altered amphibole, feldspar, quartz, sulphides and serpentine are apparent. The original igneous minerals are replaced by secondary minerals but the magmatic textures are still visible. The feldspar in the central part of the picture is saussuritised. Below the feldspar a strongly altered amphibole grain is apparent. The sulphides seem to be unaffected by the alteration.

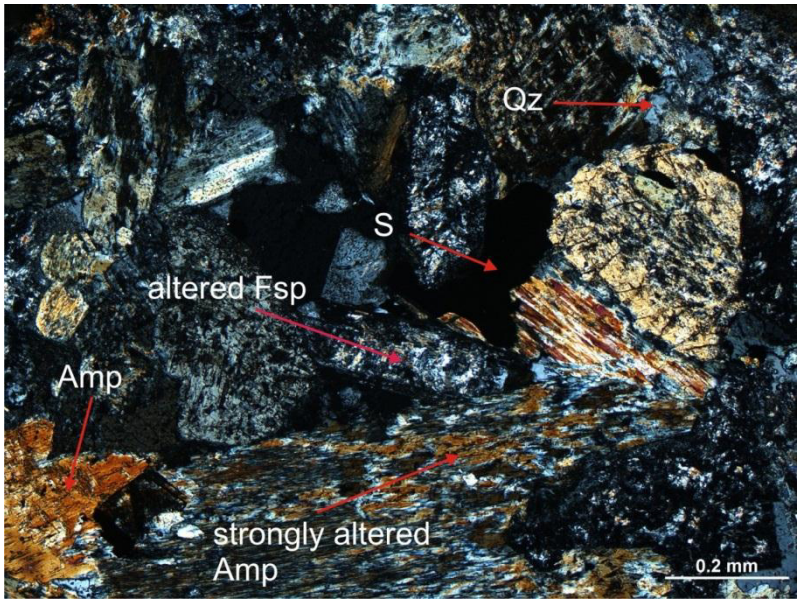

Fig. 6.9: Thin section of specimen H39. The picture was taken under crossed nichols. Altered amphibole (Amp) and altered feldspar (Fsp) are apparent. Some feldspars are twinned. Sulphides (S) are opaque. Quartz (Qz) occurs rarely. The original igneous textures are still apparent.

Figure 6.10 shows another portion of the specimen H 39. Serpentine, amphibole, quartz and sulphide phases are apparent. The amphibole grain in the middle of the figure shows irregular grain boundaries due to the replacement by serpentine. Quartz is located in interstices. The sulphides possess sharp, clearly defined grain boundaries.

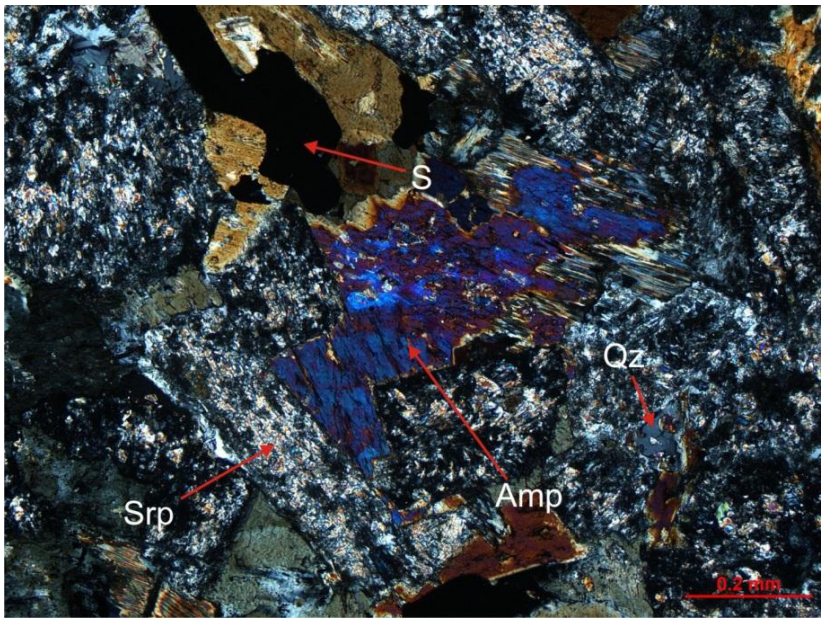

Fig. 6.10: The picture of the thin section from specimen H39, which was taken under crossed nichols, shows sulphide (S), serpentine (Srp), amphibole (Amp) and quartz (Qz). Amphibole is replaced by serpentine.

6.2.2 Lower Pyroxenite

Figure 6.11 shows a portion from a thin section of specimen H59. The minerals talc, serpentine, amphibole, magnetite and olivine are apparent. Olivine is a relic of the primary igneous mineral assemblage. Former rounded olivine grains are replaced by serpentine and rimmed by magnetite, which was produced by serpentinisation processes. The former pyroxenites are converted into amphiboles and serpentine. In the upper half amphibole is replaced by talc and the grain boundaries are irregular. The magmatic textures are still apparent.

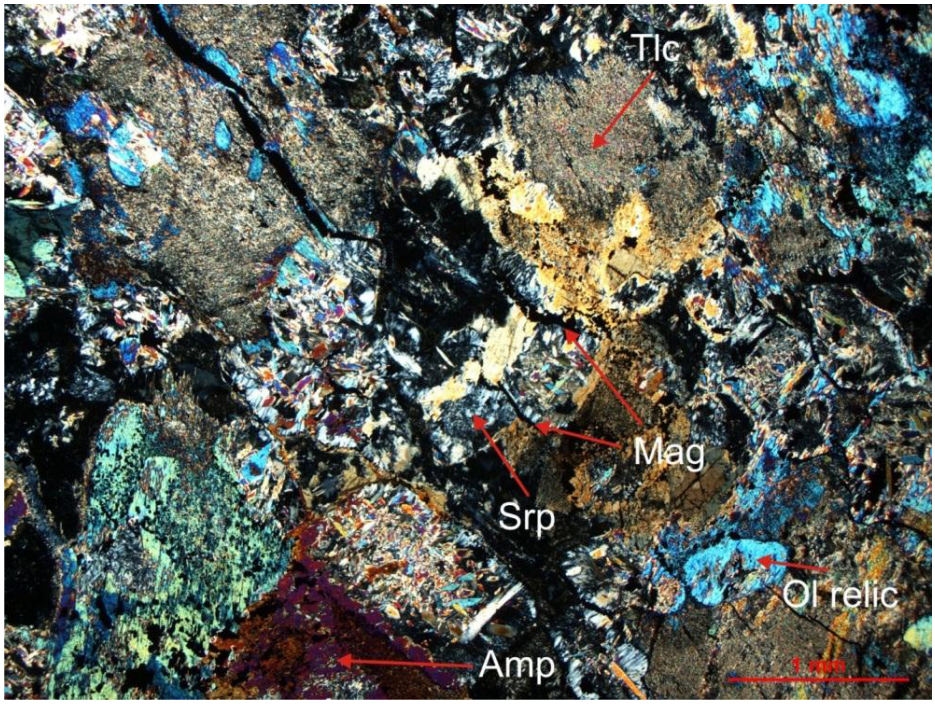

Fig. 6.11: The picture of the thin section of specimen H59, which was taken under crossed nichols, shows the minerals talc (Tlc), serpentine (Srp), relics of olivine (Ol), amphibole (Amp) and magnetite (Mag). Olivine is replaced by serpentine, which is rimmed by magnetite. Talc replaces amphibole in the upper part of the picture.

The next three figures are from specimen H59 as well. They provide a better view on the serpentinisation of olivine. Olivine is mainly replaced by serpentine. The replacement took place from the rim of the grain to the inside (Fig. 6.12). In the right picture magnetite rims are apparent around serpentinised olivine. In the left picture amphibole encloses the replaced olivine crystals.

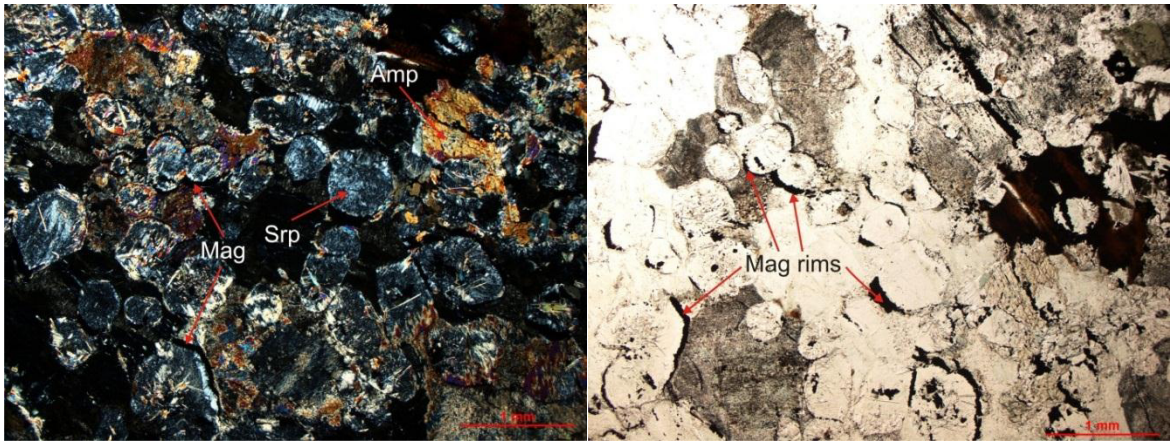

Fig. 6.12: The left picture of the thin section of specimen H59, which was taken under crossed nichols, shows former olivines, which are completely replaced by serpentine. In the right picture, which was taken under normal polarised light, the olivines are rimmed by opaque phases (magnetite).

In the central part of the picture needles of tremolite could be identified (Fig. 6.13). They overgrow the serpentine minerals. The serpentines show a directed growth from the grain boundaries into the centre of the mineral, which was replaced.

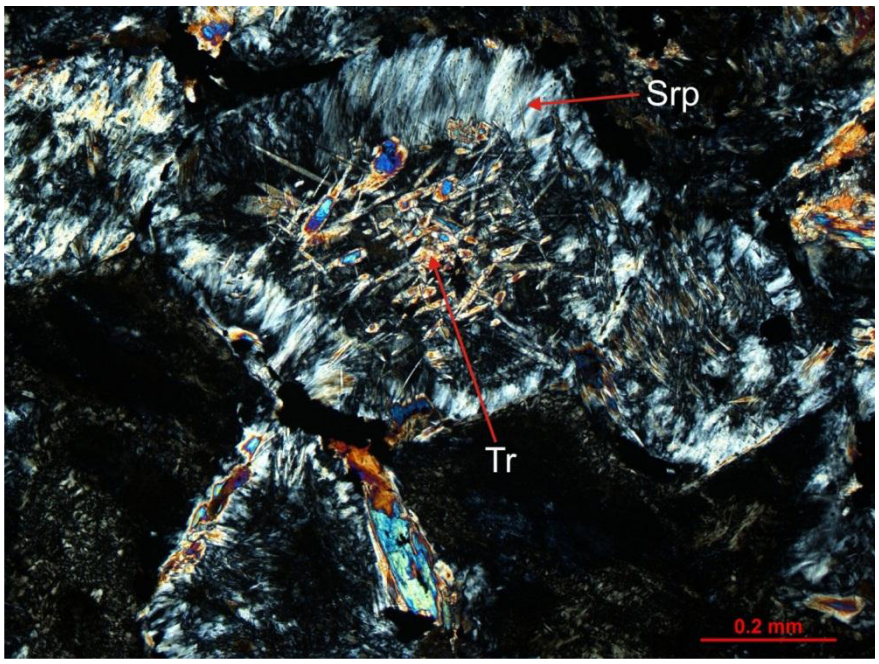

Fig. 6.13: The picture of the thin section of specimen H59, which was taken under crossed nichols, shows a more detailed view of the replacement structures. The olivine is replaced from the grain boundaries to the inner part of the grain. In the centre of the replaced olivine tremolite (Tr) needles are apparent.

6.2.3 Chromitiferous Peridotite

In figure 6.14 euhedral to sub-rounded chromites, olivine and serpentine are apparent. Olivine has a poikiloblastic texture. In areas with less or no chromite the olivine is replaced by serpentine. In the lower left corner a directed growth of serpentine is apparent due to formation of a vein or a directed replacement of a primary mineral.

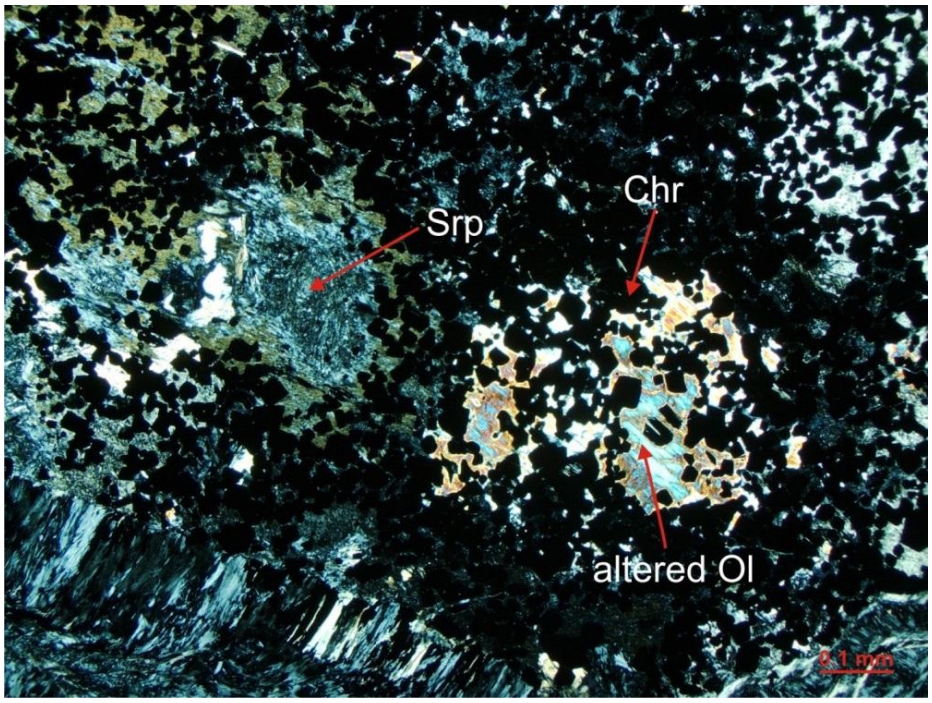

Fig. 6.14: The picture of the thin section of specimen H11, which was taken under crossed nichols, shows serpentine, chromite and olivine relics. In the left side a mineral is apparent, which is replaced by serpentine. The chromite grains are euhedral. In the lower left corner a directed growth of serpentine can be observed.

Figure 6.15 shows a serpentine vein in the PCR. Three different generations are apparent. The first generation trends from the lower left to the upper right corner. The second generation crosscuts the first generation from bottom to top. The third generation crosscuts the other generations of veins from left to right. In the lower right corner a mesh-textured olivine is apparent. A more detailed picture is given in figure 6.16.

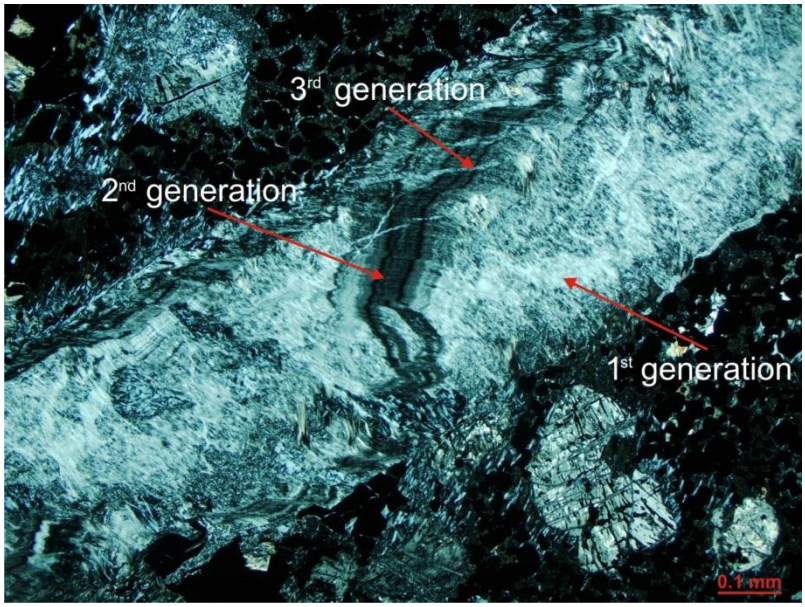

Fig. 6.15: The picture of the thin section of specimen H11, which was taken under crossed nichols, shows three different generations of serpentine veins. In the lower left corner an olivine grain, which is replaced by serpentine, is apparent.

The mesh textured olivine is a typical feature of the serpentinisation of an olivine (Fig. 6.16). The serpentine minerals begin to replace the olivine along cracks and grow from these cracks into the olive grain.

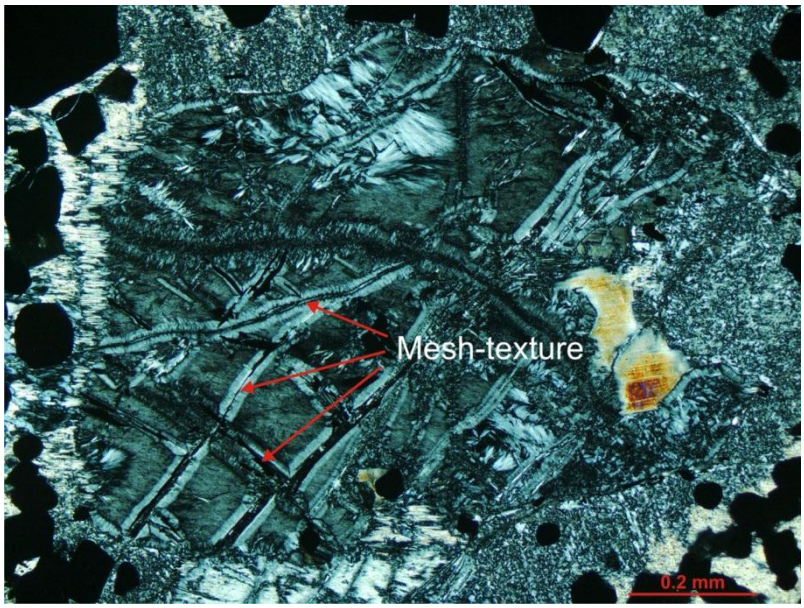

Fig. 6.16: The picture of the thin section of specimen H11, which was taken under crossed nichols, shows a more detailed view of the replaced olivine grain from figure 6.15. The replacement started from the rim of the grain and from cracks. From these areas the serpentine minerals grew into the olivine grain.

Along the serpentine vein chromite grains show dissolution phenomena (Fig. 6.17). The porous chromite was replaced by Cr bearing serpentine, which was identified by SEM measurements. Along the cracks the chromite grains possess a brighter colour, which indicates a modification of the composition in these areas.

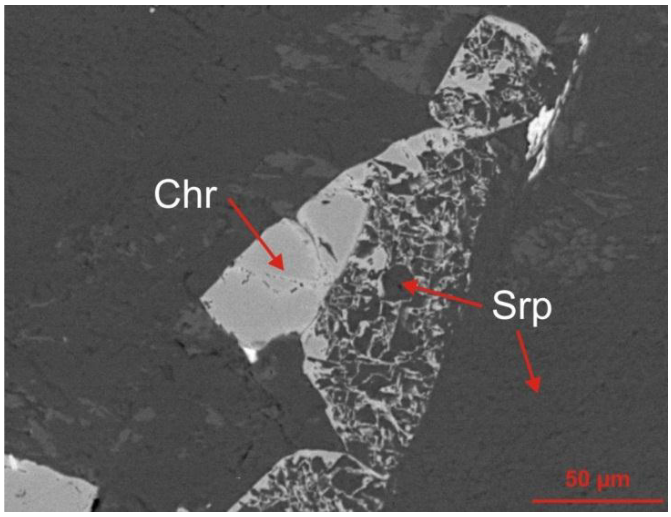

Fig. 6.17: The BSE image of specimen H11 shows a dissoluted chromite grain, which is adjacent to a serpentine vein. The chromite is replaced by Cr bearing serpentine.

An unusual feature is the occurrence of pyrrhotite and pentlandite in the mesh textures of the serpentinised olivines (Fig. 6.18). The sulphides are located along cracks. In the right picture the chromites possess a euhedral to sub-rounded shape.

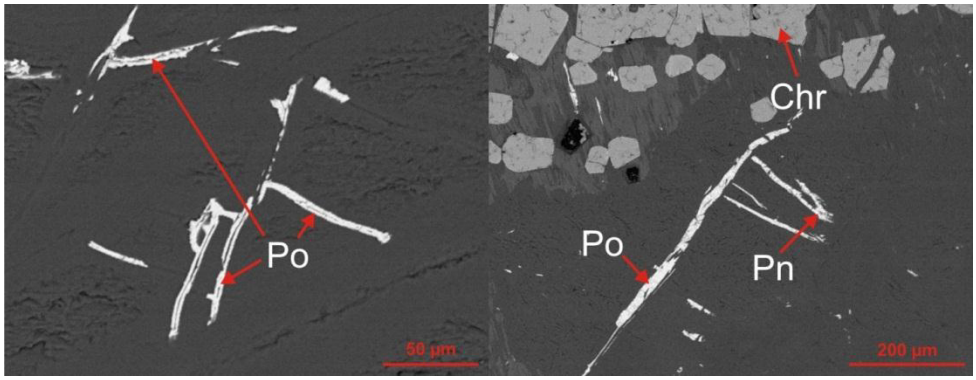

Fig. 6.18: BSE image of specimen H11 shows the occurence of sulphides in a mesh textured olivine. In the right picture the euhedral grains are chromites. In some cases they are weakly rounded. The abbreviations stand for pentlandite (Pn), pyrrhotite (Po) and chromite (Chr).

The Massive Chromitite is largely composed of euhedral chromite grains in a matrix of talc and serpentine (Fig. 6.19). Some chromite grains reveal a resorption texture as it was observed by Kenyon et al. (1986), which can be a result of the alteration processes.
Nearly all chromite grains are less than 200 µm big and have a euhedral to sub-rounded shape (Fig. 6.19), which is typical for chromites experienced greenschist metamorphism conditions (Barnes 2000). If there had been evidence for amphibolite facies metamorphism the chromite grains would have been much bigger with a cluster in grain size between 100 and 200 µm (Barnes 2000). The chromites reveal no zonation in BSE pictures. After Barnes (2000) the chromites can be labelled as “type 1 spinels”.

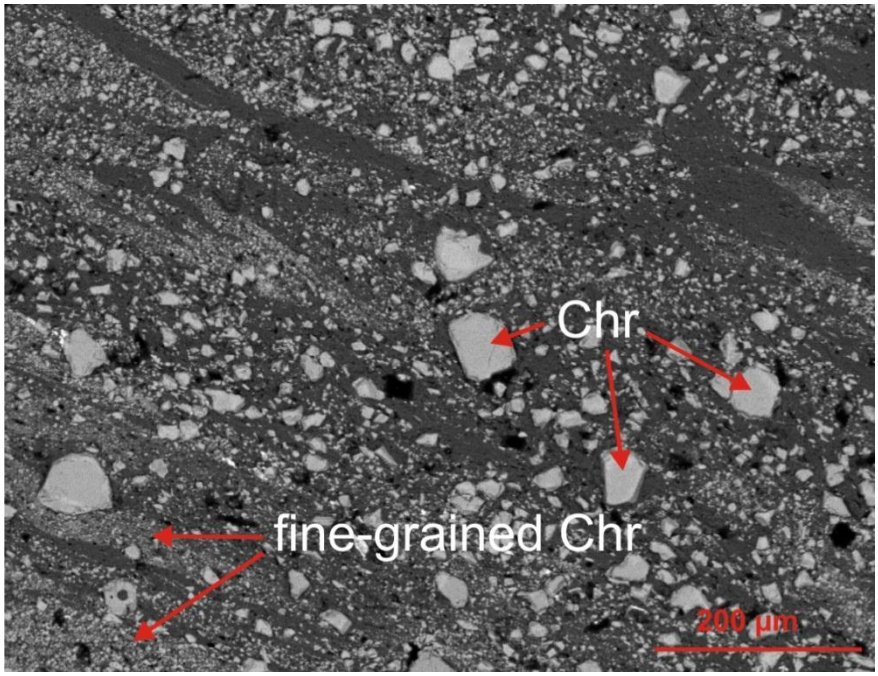

Fig. 6.19: The BSE image of specimen H22 shows an overview of the chromite grains, which are very small and do not exceed 100 µm. The chromites possess a euhedral to sub-rounded shape. The black areas are holes, which emerged during the preparation of the thin section.

In figure 6.20 the primary magmatic minerals are completely pseudomorphically replaced by serpentine and talc. It seems that talc replaced cumulus minerals and serpentine replaced the matrix minerals. The igneous textures are still preserved. The oxidation haloes around the sulfides are indicators for oxidising conditions.

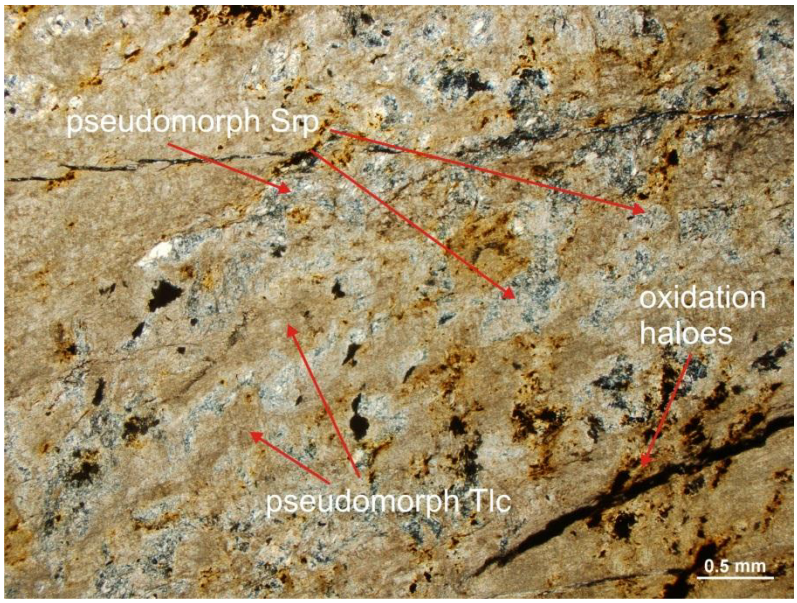

Fig. 6.20: The picture from the thin section of specimen Hx, which was taken under crossed nichols, shows the extensive replacement of primary minerals by talc and serpentine.

In figure 6.21 pyrrhotite, pentlandite, and apatite are apparent. The matrix is composed of talc and serpentine. The crack, which seems to be a vein, is a result of the cutting during the preparation of the thin section.

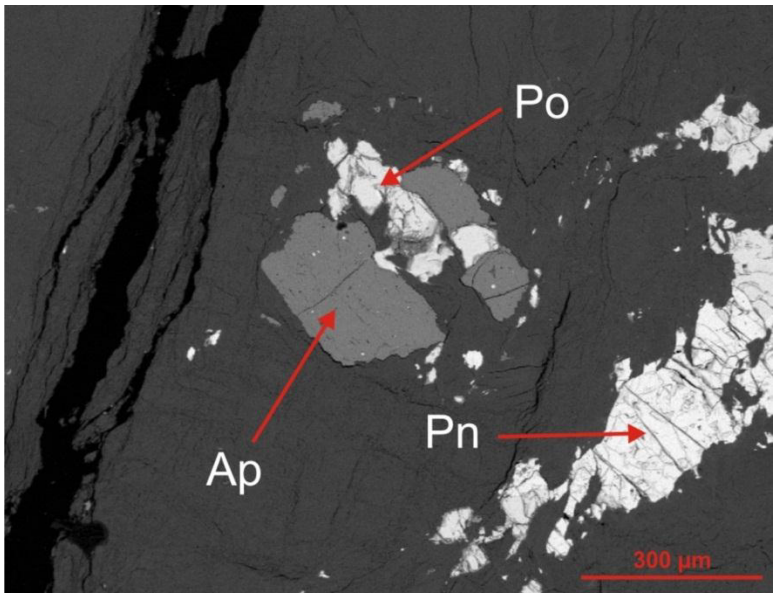

Fig. 6.21: The BSE picture of specimen Hx shows apatite (Ap), pyrrhotite (Po) and pentlandite (Pn). The dark grey areas are a mixture of serpentine and talc. It seems that there is a vein in the left part of the picture but this is a result of the thin section preparation.

6.2.4 Main Peridotite

In figure 6.22 amphibole, altered olivine, quartz, feldspar and a mixture of serpentine and chlorite are apparent. The olivine is already altered to serpentine. Feldspar also shows evidence of saussuritisation. The sulphides possess euhedral shapes. It seems that they replace the amphibole. Serpentine and chlorite are intergrown. The original magmatic textures are still preserved.

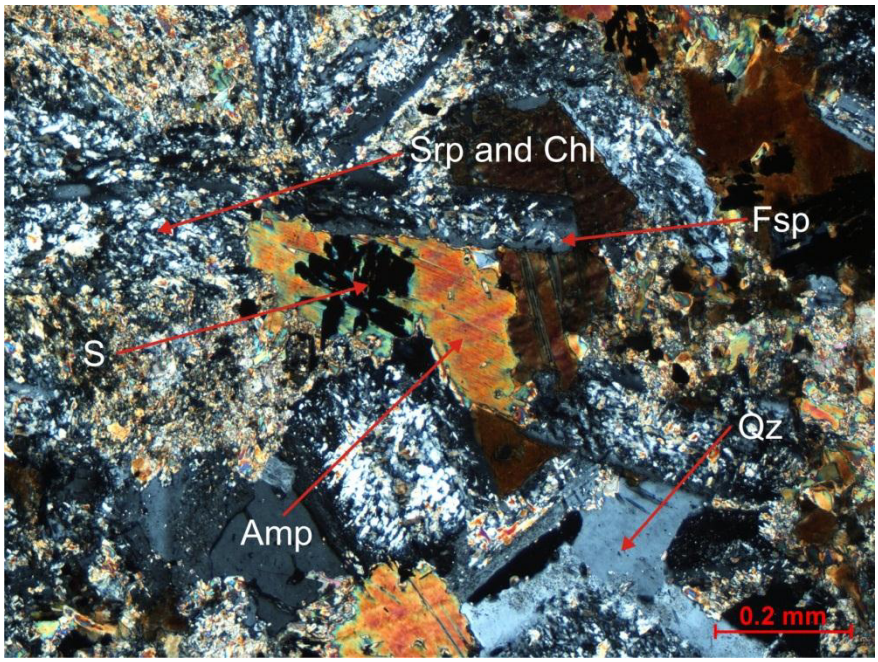

Fig. 6.22: The picture from the thin section of specimen H2, which was taken under crossed nichols, shows altered feldspar, amphibole, quartz, replaced olivine and sulphide. The primary igneous texture is still apparent.

Figure 6.23 shows amphibole, feldspar, sulphides and carbonate. The Main Peridotite is also affected by carbonate alteration albeit in a much lesser extent than the PCR and the LPxt. Feldspar is twinned and partially replaced. Amphibole possesses a zonation, which is apparent by the different interference colours. The primary magmatic textures are preserved. The occurrence of carbonates in the PRD unit indicates that CO_2 enriched fluid escaped through the Massive Chromitite Layer into hanging units of the PCR unit.

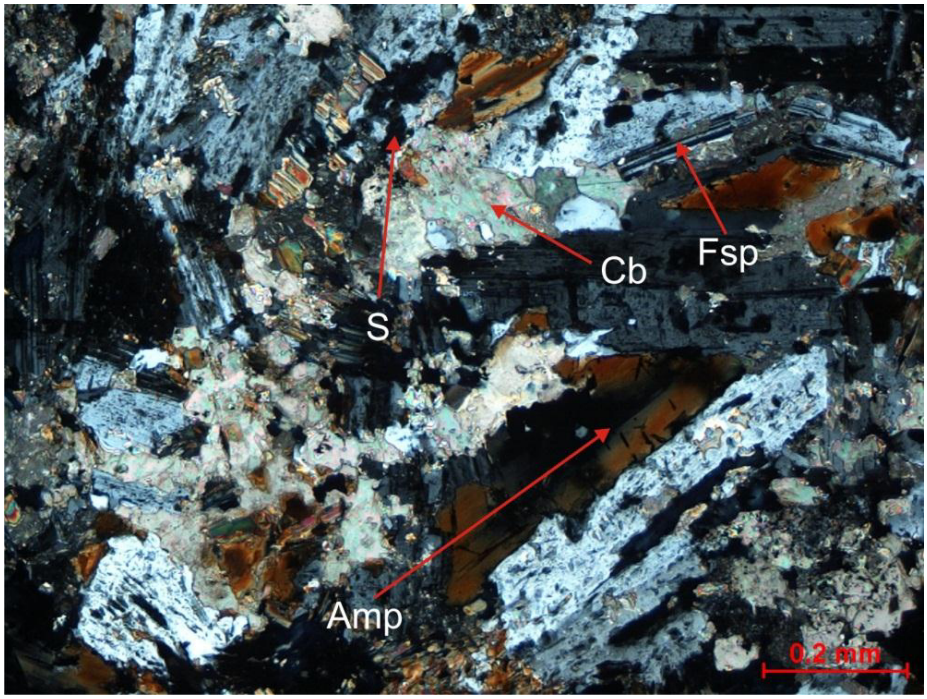

Fig. 6.23: The picture from the thin section of specimen H2, which was taken under crossed nichols, shows feldspar, amphibole, sulphide and carbonate (Cb). The primary igneous textures are still apparent. The occurrence of carbonates indicates that there was an interaction of a CO_2 enriched fluid with lithotypes above the Massive Chromitite layer at the top of the PCR unit.

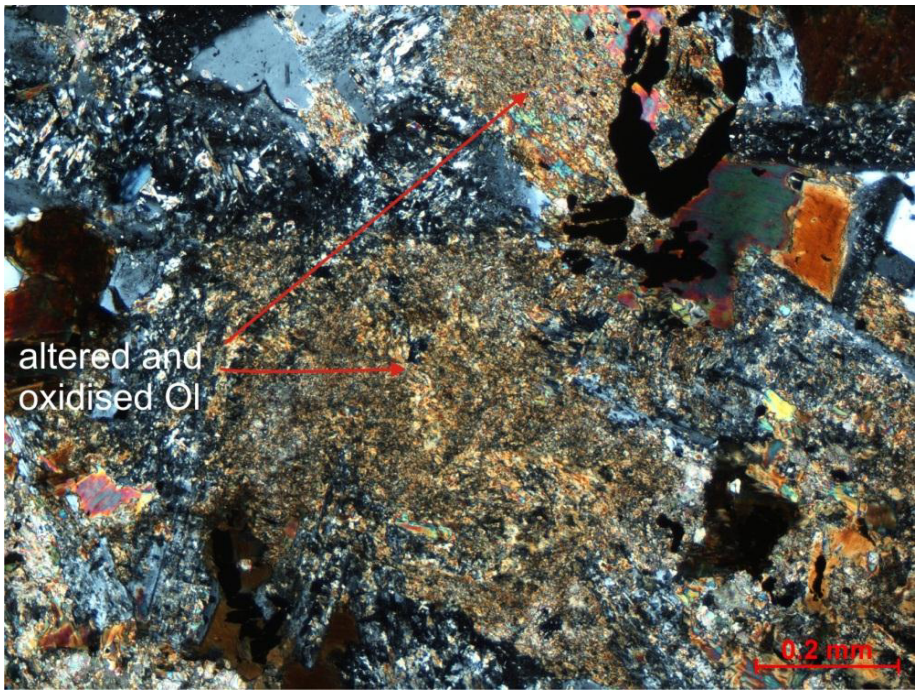

Fig. 6.24: The picture from the thin section of specimen H2, which was taken under crossed nichols, shows altered and oxidised olivine.

In figure 6.24 altered olivine hosts minerals with a strong intrinsic colour. These minerals are possibly clays and iron oxides. The oxidation overprinted the serpentinised olivine. Serpentine, amphibole, quartz, and sulphide are also apparent. Quartz shows some signs of undulose extinction, which is indicative for plastic deformation of the quartz, which implies an alteration of the rock during or before a plastic flow of quartz. The magmatic, intergranular texture of the rock is preserved.

Summary

Several different replacement structures are apparent in the investigated thin sections. The alteration of the lower units of the Uitkomst Complex is also apparent in the thin sections. From figure 6.15 it can be concluded that there were multiple injection of fluids, which precipitated serpentine. Along these veins chromite were dissolved where apparent, which led to a porous texture. The intergrowth of serpentine and chlorite due to replacement reactions is a common feature (Banfield et al. 1994, Bailey et al. 1995). Despite the intensive alteration of the primary mineral assemblage the original magmatic textures are still preserved.

An unusual feature of the some serpentinised, mesh textured olivines is the occurrence of sulphides along cracks (Fig. 6.18). It is possible that the sulphides represent a syn to postgenetic replacement event with respect to the serpentinisation. If this is case, the fluids must have contained S, Fe and Ni. These elements could have their origin in primary sulphide assemblage (Moeskops & Davis 1977).

The occurrence of oxidised olivine (Fig. 6.24) and oxidation haloes around sulphide minerals (Fig. 6.20) indicate an interaction with an oxidising fluid subsequent to the serpentinisation and talc-carbonate alteration of the lower unit of the Uitkomst Complex.

The occurrence of carbonate minerals in the PRD sample indicates that CO_2 rich fluids interacted with rock units above the PCR unit.

7 Mapping results

7.1 Face mapping

The sections are named as follows: B stands for the number of the bench according to the official names used by the Nkomati joint venture, P for the part of the bench and S for the section of the part. Usually, the length of a portion is about 240 m and the length of a section is 120 m. These lengths are chosen by practical reasons. One part consists of two sections due to the size of the mapping sheet. A location map of the faces is depicted in figure 7.1. The colours of the rock units (see legends) are based on the standards of the Nkomati mine. The scale of the section is below or next to the depicted legends.

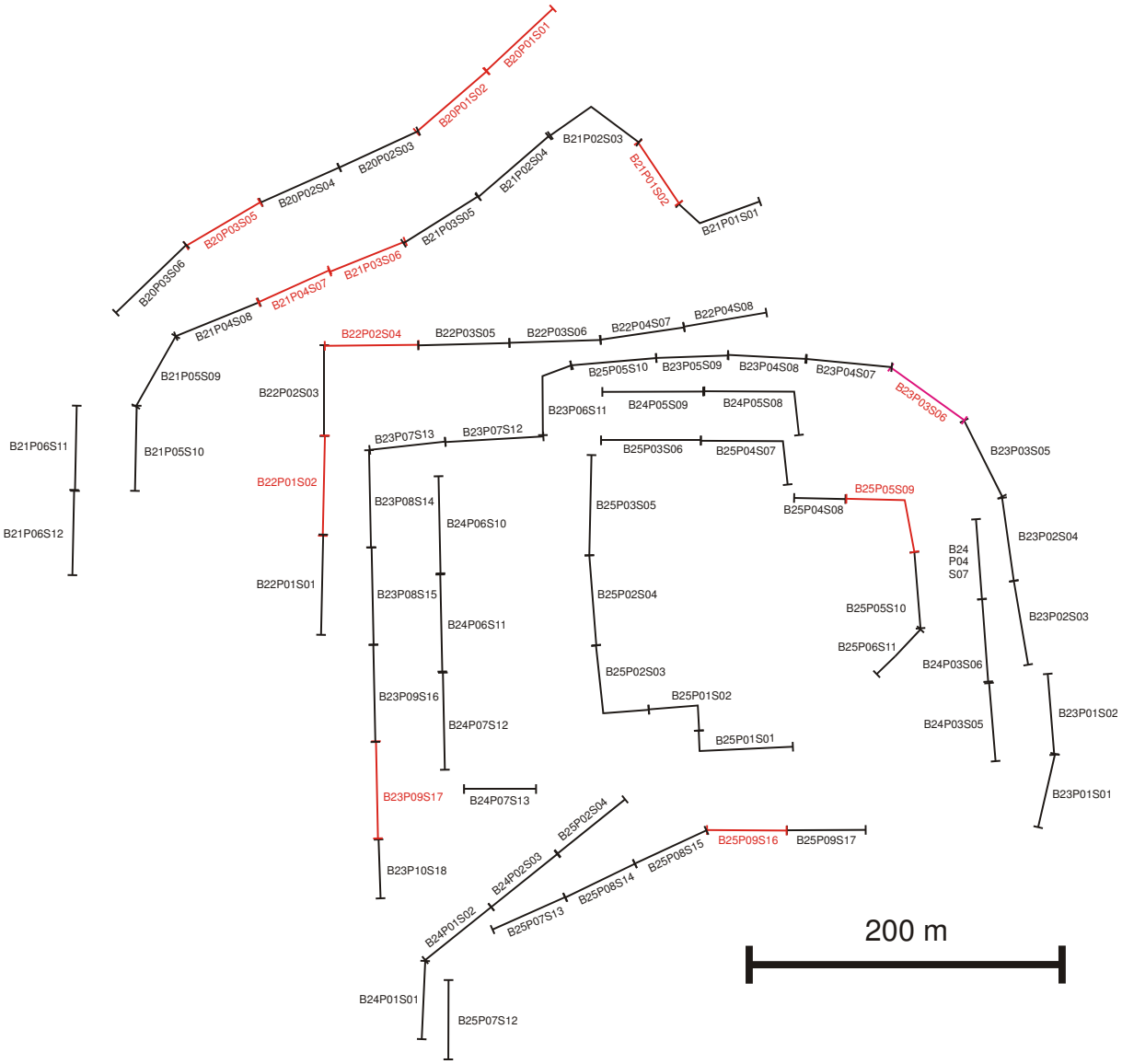

Fig. 7.1: Location map of the investigated faces. The red coloured locations represent the faces, which are described below.

The horizontal scale is 1:200 and the vertical scale is 1:100. The vertical scale is twofold exaggerated.

Only the most important sections, which are representative for the structural and geological development, are depicted. The other maps of the faces can be found in the electronic appendix. The description of the faces, which are not considered in this chapter, can be found in the last section of the appendix.

The term diabase is used for an intrusive, medium-grained rock with a mafic composition. It would be scientifically more correct to describe this rock as basalt, dolerite or gabbro but for a unitary form of the thesis the official terms of the mine are used.

In the following chapters the term fault is used for structural features, which displace the host lithology but their thickness is limited to the structural feature. Zones with thicknesses from 0.5 m and more are termed shear zones.

The section B20P01S01 (Fig. 7.2) is situated in the Main Peridotite (PRD) and Chromitiferous Peridotite (PCR). The face is located in the northernmost part of the open pit. The apparent rocks are chromite-rich peridotite and Massive Chromitite (MChr) of the PCR (Chromitiferous Peridotite) unit and peridotite of the PRD (Main Peridotite). In the PCR the typical, nearly horizontal shear zones are apparent. Along these thrusts the rocks are highly altered. The stratigraphic inversion of the PRD and the PCR unit is unusual. This inversion could be a result of a thrusting event. The direction of movement (NW-SE) is probably perpendicular to the orientation of the face.

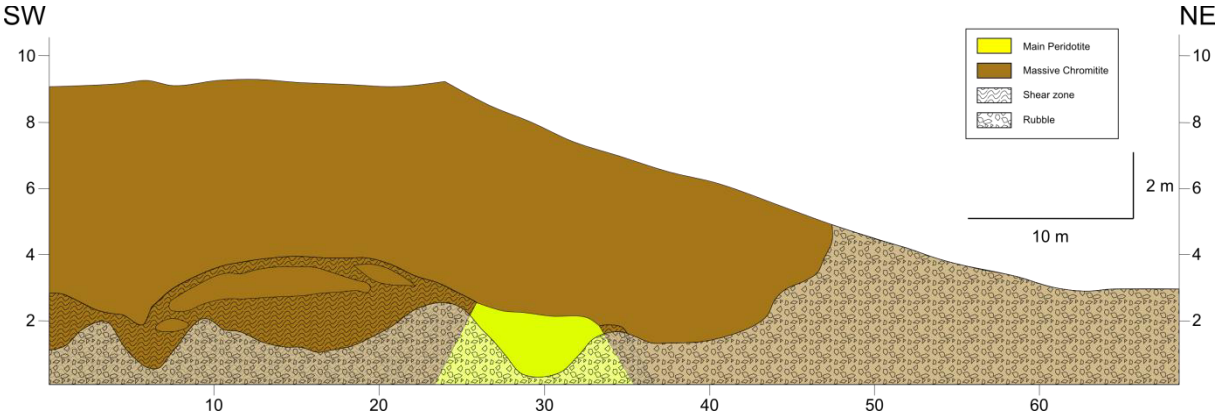

Fig. 7.2: Picture of section B20P01S01. MChr and PRD rocks are apparent. Additionally there is a horizontal shear zone.

Section B20P01S02 (Fig. 7.3) shows a complex geology. The face rests on B20P01S01. Rocks of the PCR (Massive Chromitite) and PRD unit are apparent. The chromitite, which is sheared, occurs in folded layers and lenses, which are generated by thrusts and shear zones. The rocks are strongly altered. There is an intercalated peridotite layer between two chromitite layers. It seems that PRD layer was deposited in this position (after the lower

MChr layer and before the upper sheared chromite layer) and is not a result of thrusting events. The folding of the intercalated layers could be a result of drag folding in SW-NE direction as it is apparent in figure 7.3. There is a reverse fault, which is revealed by the abrupt change of the lithology and the up faulting of the shear zone. Similar structures were observed by Joubert (2013) in the MChr layers. It cannot be ruled out that the fault also possesses a horizontal displacement.

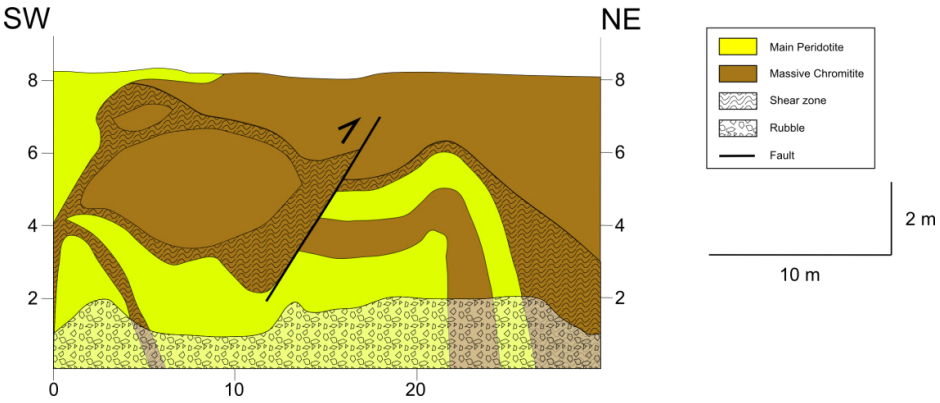

Fig. 7.3: The section B20P01S02 shows a complex geology. Rocks from the MChr and PRD unit are apparent. The layers are strongly folded. Massive chromitite lenses are surrounded by horizontal shear zones. A fault separates the layers from the shear zone at 13 m.

In B20P03S05 (Fig. 7.4), which is located in the SE part of bench 20, partially to strongly oxidised peridotites and a single chromitite layer are apparent. The spatial distribution of the oxidation is depicted below (Fig. 7.20).

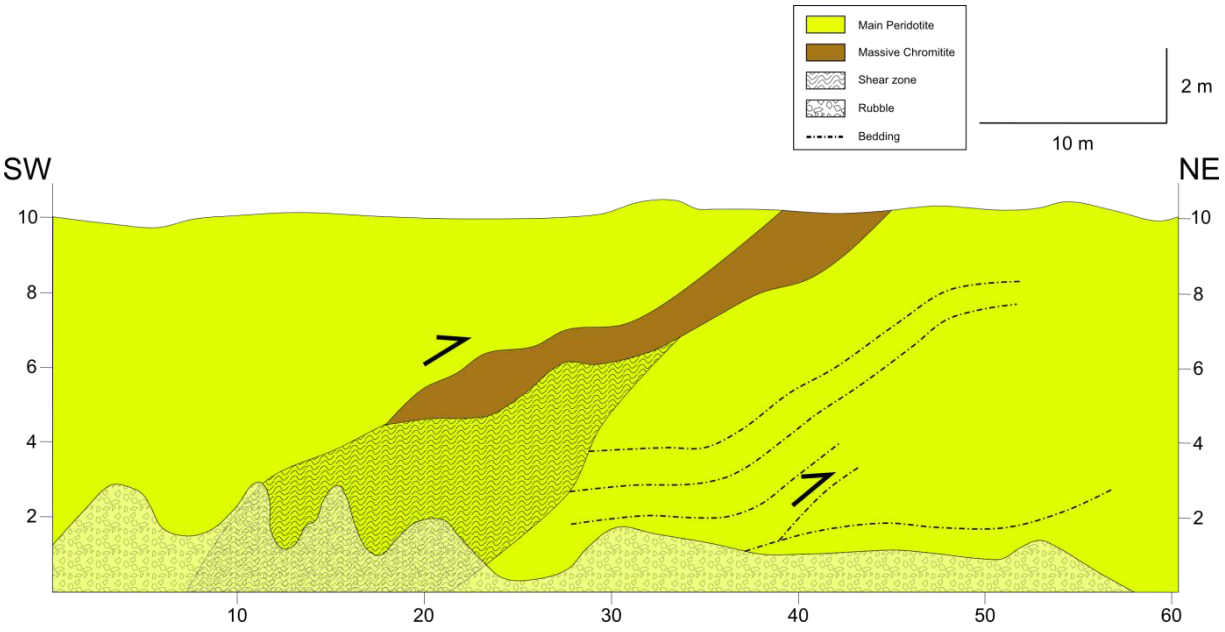

Fig. 7.4: Section B20P03S05 shows a thrusted MChr layer in PRD rocks. A shear zone is developed under the Massive Chromitite layer. The bedding is slightly folded. The black arrows show the relative direction of displacement.

The MChr layer is intercalated into the peridotites, which is evident by the shear zone below the Massive Chromitite. The bedding of the peridotite is still visible and its contact to the shear zone is discordant indicating that the shear zone was developed after the deposition of the PRD layers. The course of the bedding also indicates thrusting events. The differences in the degree of weathering can be attributed to pervasive joints in the peridotite where meteoric fluids could migrate into the rock. In some parts the peridotite is weathered to soil.

Figure 7.5 shows the section B21P01S02, which is situated in the NE part of bench 21. The section hosts rocks of the LPxt (Lower Pyroxenite) unit (pyroxenite), PCR unit (chromite rich peridotite) and diabase. Vertical faults and a nearly horizontal thrust are apparent. The vertical faults are located in the diabase, and along the contact between the diabase and the PCR unit. The vertical faults have orientations of 154/85 (fault in the diabase) and 172/80 (fault along the contact diabase-PCR). The fault between the diabase and the chromitiferous peridotite could be a result of the weakening of the shear strength rock due to heating (Handin & Hager 1958) during the emplacement of the diabase. The shear zone, which is likely displaced by the vertical fault, could not be followed up any further. The following events led to the formation of the rocks: at first the ultramafic igneous rocks were deposited followed by a thrusting event, which displaced the original contact between the LPxt and the PCR. The nearly horizontal shear zone in the PCR could have been generated simultaneously to the aforementioned thrust fault. Subsequent a dyke intruded into the ultramafic rocks. Afterwards the vertical fault zone was developed and displaced the contact PCR-diabase.

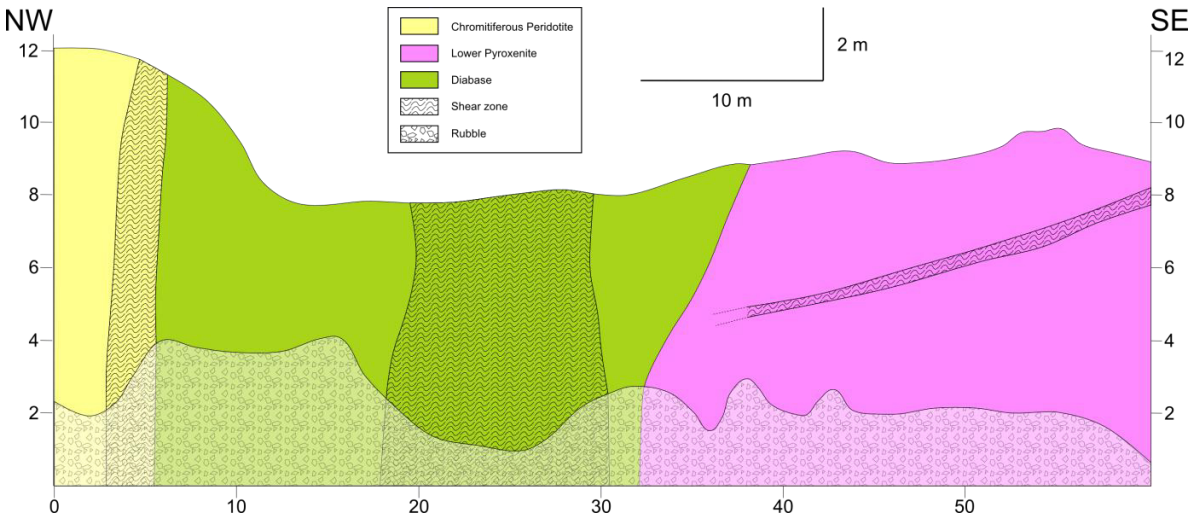

Fig. 7.5: The section B21P01S02 is depicted. Two steep and a low dipping shear zone are apparent. At 5 m a shear zone is developed along the contact between the diabase and the PCR unit. Another vertical shear zone is apparent in the diabase. The LPxt hosts a nearly horizontal shear zone.

B21P03S06, which is situated in the central part of bench 21, hosts altered rocks of the PCR unit and a highly altered pyroxenite layer, which is intercalated into the PCR unit as evident by a shear zone underlying the sheet.

The shear zone and the pyroxenite layer continue in section B21P04S07 (Fig. 7.6). Next to the pyroxenite layer another shear zone (from 7 to 35 m), which hosts PCR lenses, is apparent. The shear zone has a similar shape as the ones in section B20P01S02. The stepped form results from thrusting events along several layers. In the centre of the section there is an oxidation front, which can be linked to oxidising meteoric waters, which migrated along faults and joints.

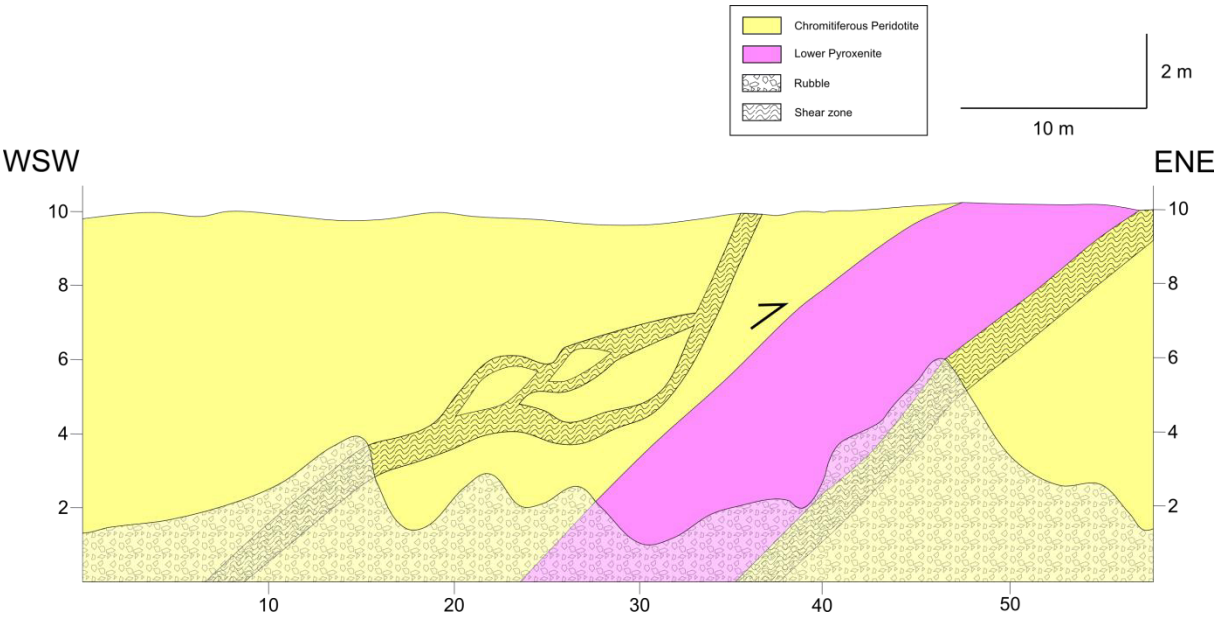

Fig. 7.6: This section contains parts of the sections B21P03S06 and B21P04S07. A large pyroxenite layer is thrusted into the PCR unit. In the SW of the pyroxenite layer a shear zone developed. The black arrow shows the direction of the movement of the wedge.

Figure 7.7 shows section B22P01S02, which is located in the E of bench 22. A large xenolith thins out, which could be due to tensional forces due to the magma flow or irregular assimilation. The pyroxenite in contact to the calc-silicate is fine-grained, which could be a product of rapid cooling during the contact with the xenolith. The layering of the xenolith is still visible as well as two faults. One fault possesses a relatively flat apparent dip. The second fault is nearly vertical. It could not be completely figured out which fault was generated at first. One possible scenario is that the flat dipping fault is a relic of earlier layer-parallel faulting in the country rocks as it was recognised by Hornsey (1999). After the assimilation of the xenoliths the vertical fault was generated.

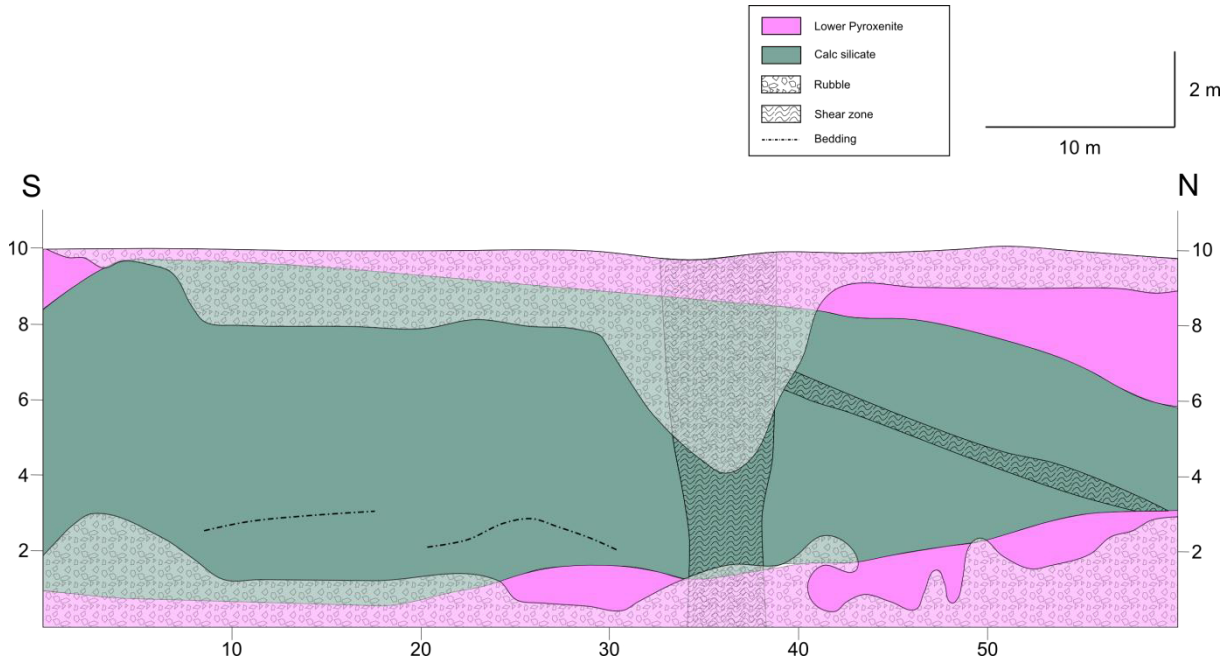

Fig. 7.7: Section B22P01S02 shows a big calc-silicate xenolith with preserved sedimentary layering in the LPxt unit. A shear zone in the xenolith is crosscut by a vertical shear zone.

Section B22P02S04 (Fig. 7.8) is located in the NW part of bench 22 and hosts pyroxenite and calc-silicate xenoliths. Both rock types are interbedded. The rocks show an apparent dip to the W, which indicates, together with the apparent dip of the xenoliths and pyroxenite of section B22P02S03, the low dip of the Uitkomst Complex to the NW. The interbedding results from flushing out events of single calc-silicate layers. A vertical fault zone crosscuts the lithology. Horizontal displacement of the rocks or abrupt ending of the xenolith are the most likely explanations for the change of the lithology in the E of the fault zone.

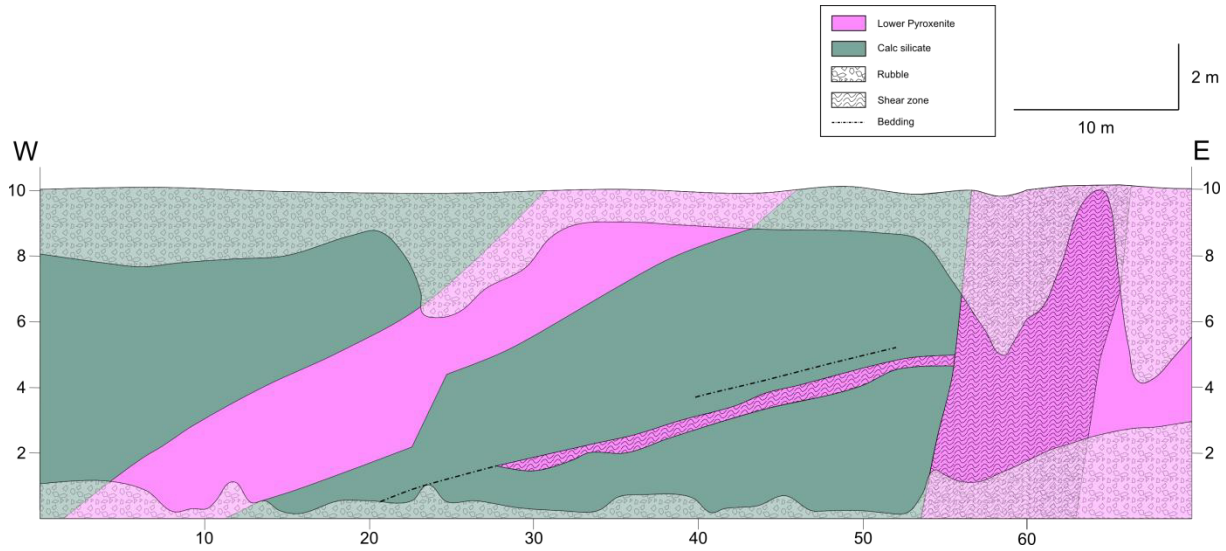

Fig. 7.8: Section B22P02S04 shows a complex geological pattern. From 0 to 53 m big calc-silicate xenoliths are intercalated with pyroxenite layers. The xenoliths end abruptly at the vertical shear zone. The bedding is parallel to the orientation of the xenoliths.

In section B23P03S06 (Fig. 7.9), which is situated in the NE part of bench 23, the number of the calc-silicates becomes less. They are parallel to the folded bedding and nearly horizontal. There is a close standing joint system, which could be indicative for a shear zone, crosscutting the bedding planes. The vertical displacement is minimal. At 40 m the layers form a wedge, which is a result of layer-parallel thrusting.

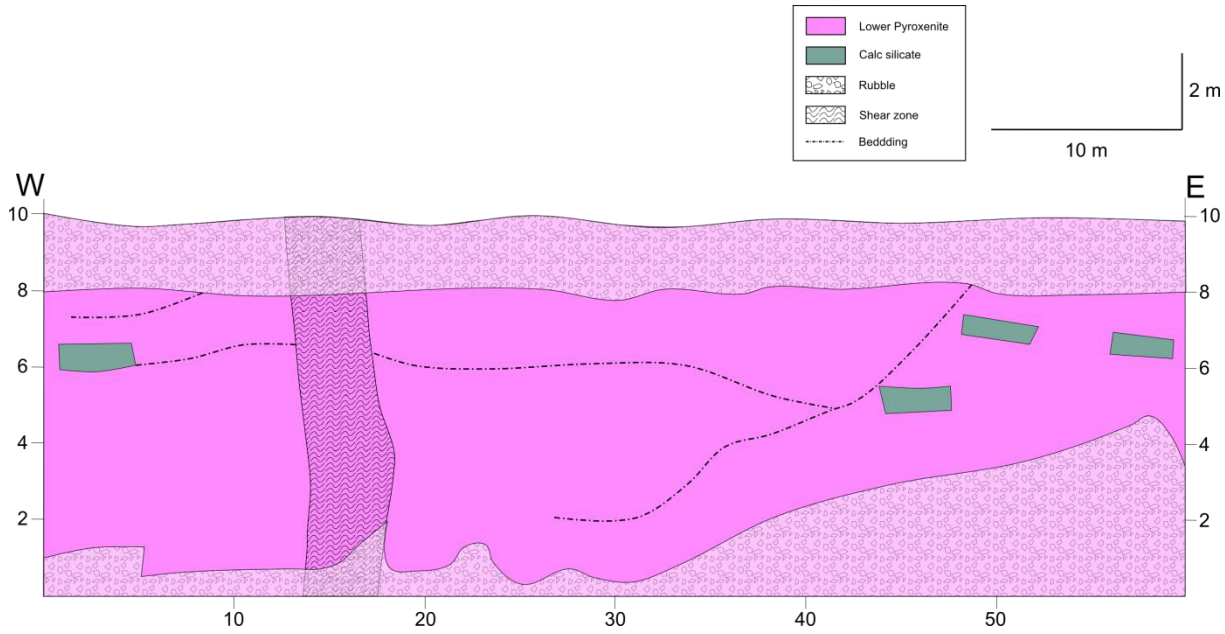

Fig. 7.9: Section B23P03S06 is situated in the LPxt. The calc-silicate xenoliths are nearly horizontal. The bedding is slightly folded.

Figure 7.10 shows section B23P09S17, which is characterised by a thrusted and sheared contact of the LPxt unit and the PCR unit. The face is located in the E part of bench 23. The calcite veins are cut along the shear zone indicating that the calcite veins were generated before the thrust fault. Around the shear zone an oxidation front is developed. The MChr is surrounded by shear zones and seems to be folded. Further to the S a massive shear zone is developed, which begins at 7 m in the section. The thrusted contact of the PCT and LPxt continues on bench 24 and strikes from the E to the W (see Fig. 7.13). The sulphides along this contact are elongated in the direction of the movement of the thrust.

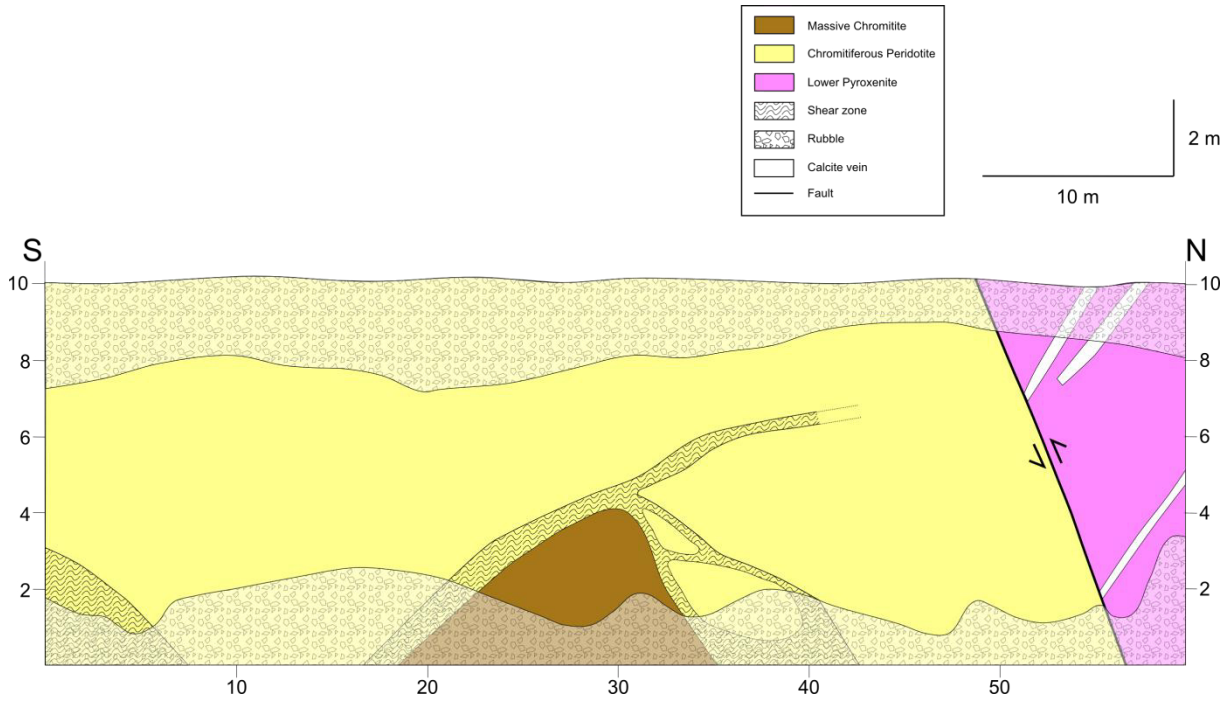

Fig. 7.10: Section B23P09S17 shows rocks from the PCR unit (peridotite and chromitite) and from the LPxt (pyroxenite). The chromitite is surrounded by shear zones. The white areas are 10 cm thick calcite veins, which are cut by a thrust fault, which displaces the LPxt and the PCR unit.

In section B25P05S09 (Fig. 7.11), which is located in the NE part of bench 25, the pyroxenite is relatively fresh. The bedding planes are parallel and displaced by three faults. Along the faults the pyroxenite is highly altered, fine-grained, soft and bears goethite. The faults have similar orientations (from the W to the E 304/90, 128/85, 132/90). These faults are a part of the NW-SE trending main faults and displace the bedding of the pyroxenite by 0.5 and 3 m.

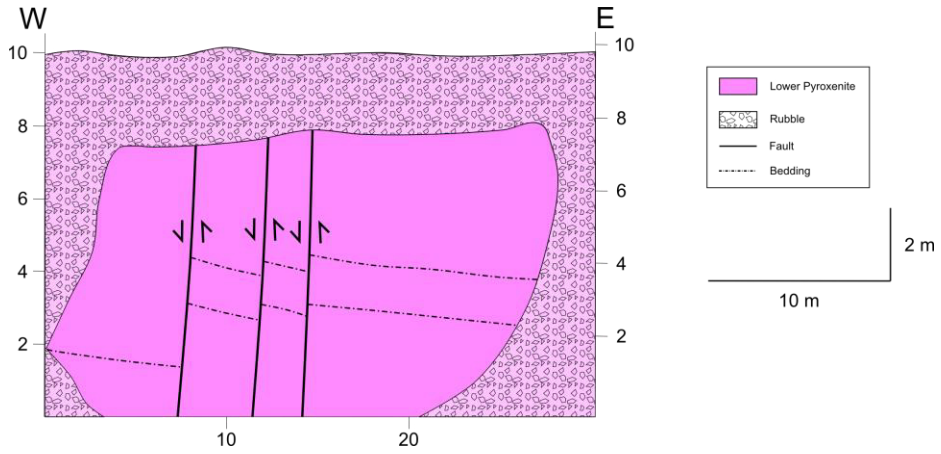

Fig. 7.11: Section B25P05S09 is situated in the LPxt. Three vertical faults with displacements of 0.5 to 3 m are apparent.

The section B25P09S16 (Fig. 7.12), which is located in the NE part of bench 25, contains Massive Chromitite, chrome rich peridotite (PCR unit), pyroxenite (LPxt unit), and diabase. The contacts between Massive Chromitite and chrome rich peridotite as well as the contact

between pyroxenite and diabase are sharp. The rocks of the PCR unit are strongly altered. Possibly, the Massive Chromitite lens is a thrust wedge. The vertical fault at 60 m strikes from NW to SE (137/65) and is a part of the regional strike-slip system in this direction. A vertical displacement of about 3 m, which is line with the findings in section B25P05S09, is possible as it is indicated by the course of the bedding.

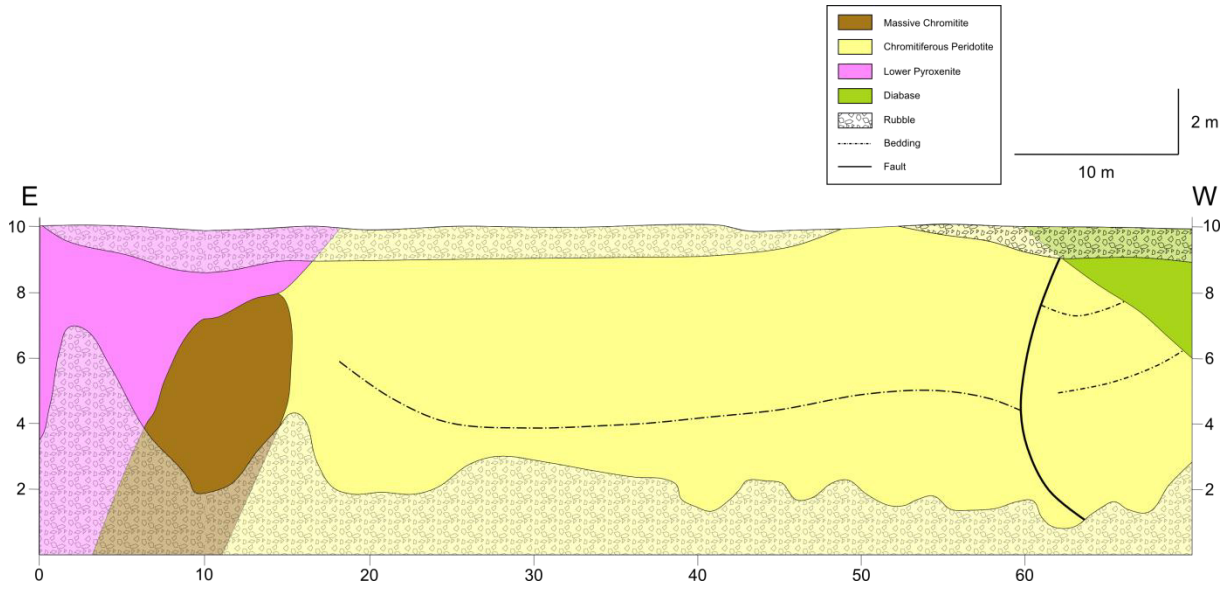

Fig. 7.12: Section B25P09S16 shows a range of lithotypes. Pyroxenite from the LPxt, peridotite and chromitite from the PCR unit, and diabase are apparent. The fault zone from 60 to 64 m is nearly vertical and strikes from NW to SE (in a low angle relative to the face orientation). The bedding is slightly folded.

7.2 Geological map and structures

Every bench is 10 m high. The topographic elevation increases from the inside to the outside. The innermost and southernmost benches belong to bench 25. The bench to the E and to the W of bench 25 is bench 24. Bench 23 encloses bench 24 and 25 with an opening to the S. Bench 22 joins to the NW part of bench 23. Bench 21 and 20 are located in the NW part of the pit. The full lines represent the known trend of the faults. The dashed lines symbolise the most likely, continued trend (Fig. 7.13).

In general the lithological order of pit 3 matches the general lithological order of the Uitkomst Complex. At the base of the pit in the E part of bench 25 Black Reef Quartzite was identified. The first unit of the Uitkomst Complex, the Basal Gabbro, follows directly on top of the quartzite. The Basal Gabbro is followed by the Lower Pyroxenite, Chromitiferous Peridotite with the Massive Chromitite at the top and the Main Peridotite. There are numerous calc-silicate xenoliths, thrust wedges, diabase intrusions and shear zones, which modify the normal lithostratigraphy. The complex dips with 5° to the NW.

Two diabase intrusions were mapped. The diabase south of the centre of the pit in a topographic height of bench 25 and south of bench 24 is a sill. The diabase identified in the E part of bench 21 and 22 as well as in the N part of bench 23 and in the W part of bench 24 is a sill with an apparent dip of 10-15° to the E measured on bench 22 and 24. It is possible that the bedding planes the pyroxenites acted as zones of weakness, which makes it easier for a diabase to intrude into the complex. It is possible that the mapped diabases belong to one sill intrusion, which is bended and therefore not apparent in the E part of bench 25. A 3D animation in the electronic appendix clarifies this assumption.

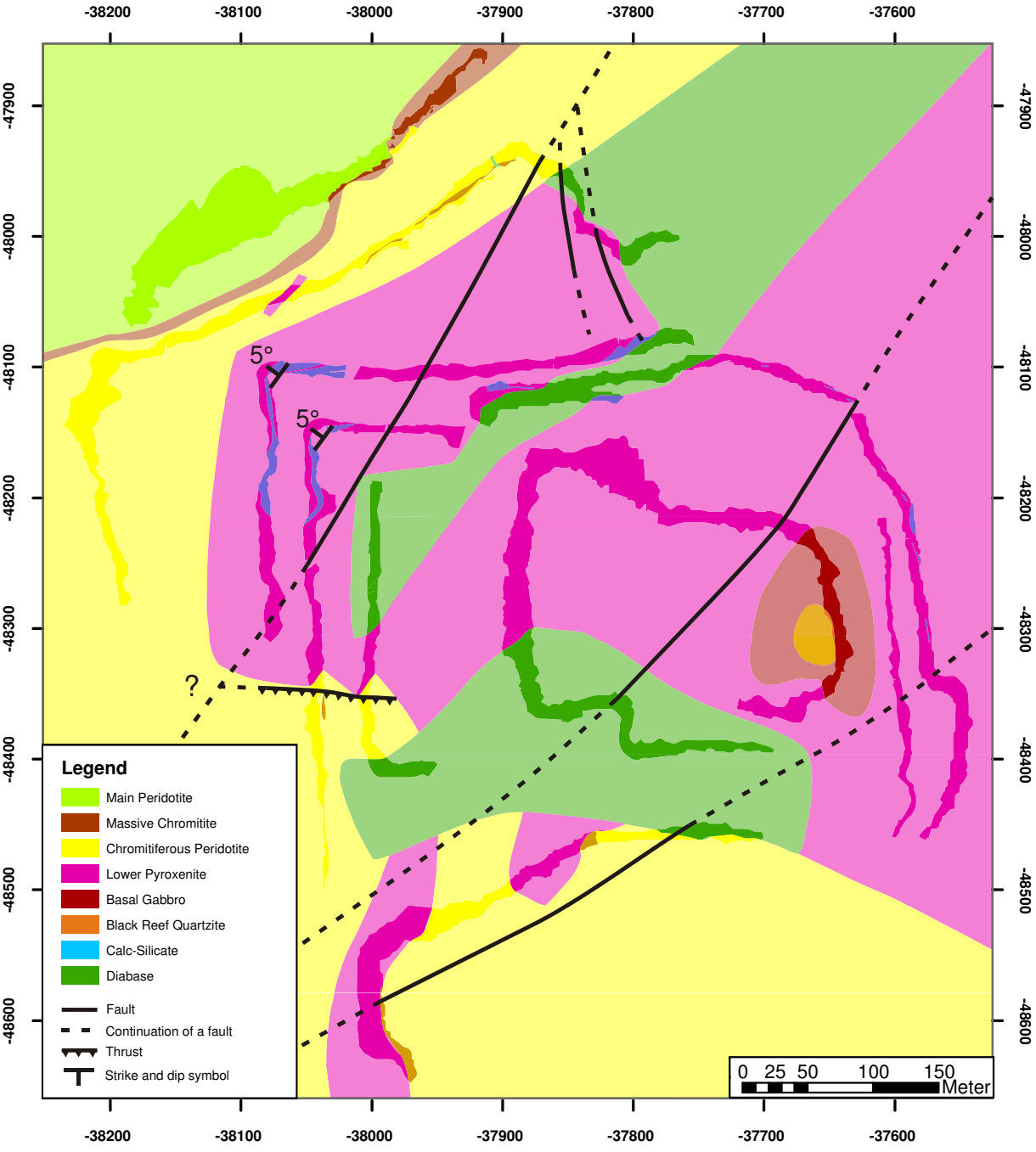

Fig. 7.13: The geological map of pit 3 with the main structural features is shown.

Most of the xenoliths are calc-silicates and quartzites and are mostly located in the LPxt unit. Some xenoliths are apparent in the Basal Gabbro and the PCR unit. The xenoliths are generally nearly horizontal, sometimes folded with a low dip. The bigger and more continuous xenoliths are parallel to the bedding and show the general dip of the complex to the NW. One calc-silicate on bench 21 is vertical, which fits with observations in the underground mine (pers. comm. Cossa 2012). Most of the xenoliths reside on bench 22 and 23. It is possible that there are xenoliths on bench 25 but they could not be observed because they were buried under rubble. As a result, a definite conclusion on the relative abundances of the xenoliths on different topographic levels is not possible.

The talc-carbonate schist is very rare. Most of the schist was already mined out but could be found in loose material of bench 19, 20 and 21. Directly in the outcrop the talc-carbonate schist could be observed on bench 23 in the LPxt unit and on bench 22 in the PCR unit. There are numerous schlieren on bench 21 with high amounts of talc.

Numerous thrust, faults and wedges are apparent. Pyroxenite thrust wedges can be recognised in the PCR unit on bench 21 and south of the diabase from bench 24 and 25, which is a result of pushing forces of the flowing magma in the conduit (pers. comm. Coetzee 2012). The pyroxenite layers were not already consolidated due to the high temperatures. The layer broke along a zone of weakness and was thrusted. There is also an E-W trending thrust fault on bench 23 and 24, where the LPxt unit is upfaulted on the PCR unit. The thrust has an apparent dip to the S. Therefore pressure was exercised from a northern direction. It could not be figured out if the thrust is cut by the northernmost NW-SE trending fault. In the PCR unit chaotic shear zones are developed, which can be linked to the formation of lenses and development of the shear zones around them. Hot fluids could have changed the mechanical properties of a rock into a more ductile regime (Handin & Hager 1958). Due to the high availability of fluids (e.g. Gauert et al. 1995) the formation of ductile shear zone was possible.

Three vertical faults were correlated over several benches. The both northern faults possess a NE-SW trend. The southern fault is trending from ENE to WSW. These orientations correspond with the trends of the regional faults. No vertical displacement can be recognised on the scale of the geological map.

Figure 7.14 was chosen because the software used for construction of stereo plots in the Nkomati mine provides better results than the software used by the author. The poles of the jointing planes are depicted in the figure.

The joints show a couple of clusters in the contour plot. There is a large range in dip and strike directions of the bedding planes and their poles. The most notable clusters are steeply dipping, NW-SE and NE-SW trending joints. Another maximum dips at steep angles to the E. Additionally there are numerous smaller clusters. Four groups dip at medium angles (35° to

50°) to the S, SE, NW and NE. Further clusters dip with steep angles to the S, SSE, WNW, N and NE. All jointing systems are related to regional patterns (pers. comm. Kerry 2012).

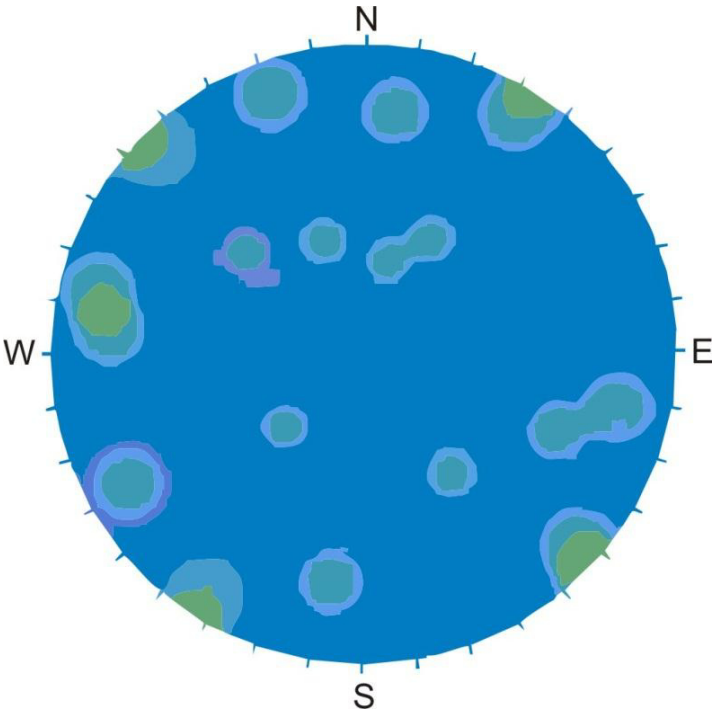

Fig. 7.14: The contour stereo plot of all measured joints (Internal Nkomati report 2012) shows the poles of the planes. The green to violet areas show the clusters of the poles of the joints. There are numerous clusters in different directions. The most important are the ones, whose poles are dipping at very low angles to NW, NE, SE, SW and W.

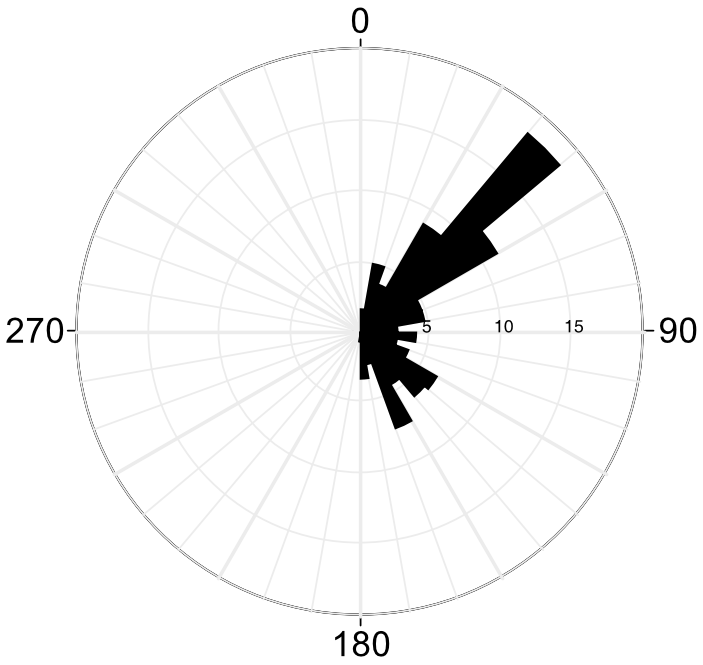

Fig. 7.15: Rose diagram of all measured joints. The black timbers represent the relative proportions of the strike directions. One timber is 10° wide. The main strike direction is NE-SW. Smaller clusters are in the directions NNE-SSW, E-W, SE-NW and SSE-NNW.

The rose diagram in figure 7.15 shows the strike directions of the joints. The main trend is NE-SW, which runs parallel to the main trends of the shear zones and faults (described below). There are also smaller clusters in the directions NNE-SSW, E-W, SE-NW and SSE-NNW. They are in line with other regional jointing systems (pers. comm. Kerry 2012)
Fig. 7.16 shows the strike and the dip of the faults on a Schmidt net projection. The faults dip very steep and possess a NE-SW-trend. Three faults reveal other trends and strike from NNW to SSE, from WNW to ESE or from E to W, respectively. There are also low dipping faults but they could not be measured due to safety issues (instable rock slopes).

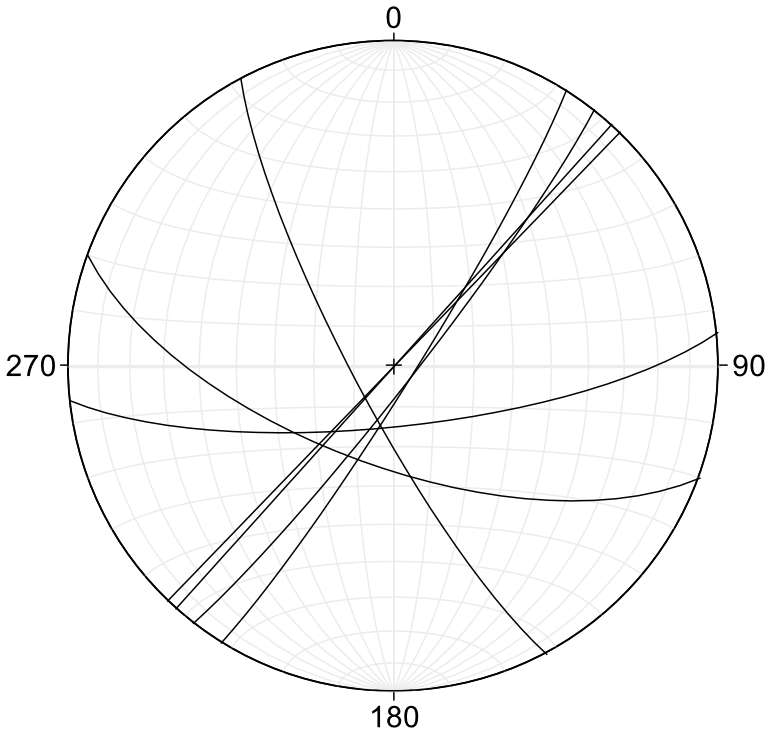

Fig. 7.16: A Schmidt net projection of all measured fault planes. The main strike direction is NE-SW and runs parallel to the main strike direction of the joints. Single faults strike NNW-SSE, WNW-ESE and E-W. The dip is generally very steep.

Fig. 7.17 shows the strike and the dip of the shear zones, which show similar orientations as the faults. The layer-parallel faults are underestimated because in most cases it was not possible to measure them directly. One shear zone strikes from NNE to SSW with a very steep dip of 90°. The only low dipping shear zone with a dip of 10°, which could be measured, possesses a similar strike direction as the steeply dipping shear zones.

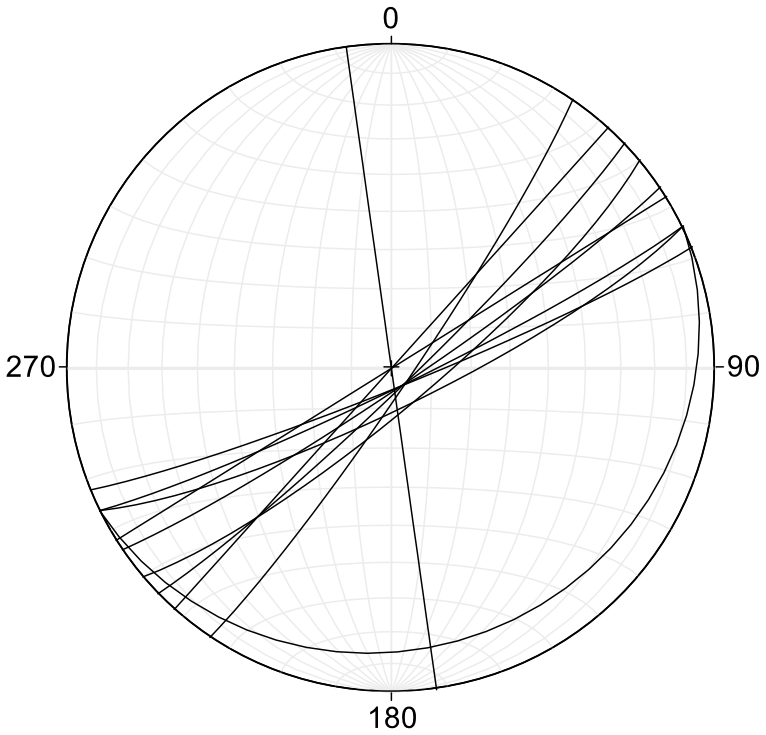

Fig. 7.17: A Schmidt net projection of all measured shear zones is shown. The main strike direction is NE-SW at very steep dips (80-90°) and runs parallel to the main strike directions of the joints and faults. One low dipping shear zone with a similar strike as the steep shear zones is apparent. But the low dipping shear zones are underestimated.

The main trends are clearly in the direction NE-SW. The joints, faults and shear zones show clusters in this direction. There are also minor structural directions from NNE to SSW.

Field observations indicate that there are local parts showing an extensional stress regime evident by normal faults from bench 21 part 4 section 8 (see electronic appendix). This feature can be attributed to push and pull forces (Mattauer 1993) owing to the magma flow. The semi-consolidated rocks possess a low resistance with respect to the tensional forces. Therefore it is likely that some layers tore.

Figure 7.18 shows the poles of all measured bedding planes, which do not show a clear trend. The scatter is a result of the folding of the bedding and thrusting of the magmatic layers. A stretch of the contour lines in WSW-ENE direction is apparent, which proves the boat-shaped form of the Uitkomst Complex (Gauert et al. 1995). Dips to the NW, SE rare compared to the WSW and ENE. Generally the dip is very low (5 to 20°). The steepest dips are 30°, which reside on the flank of thrust wedges.

The measured layer-parallel shear zone possesses a similar orientation as the bedding, which indicates that the low dipping shear zones run parallel to the bedding planes. Thus the low dipping shear zones developed along bedding planes. It could not be figured out, if the layer-parallel faults from the country rocks (Hornsey 1999) are also present in the igneous rocks of the Uitkomst Complex. But it is likely that most of the observed low dipping shear zones in the igneous rocks are local structures and do not continue in the country rocks.

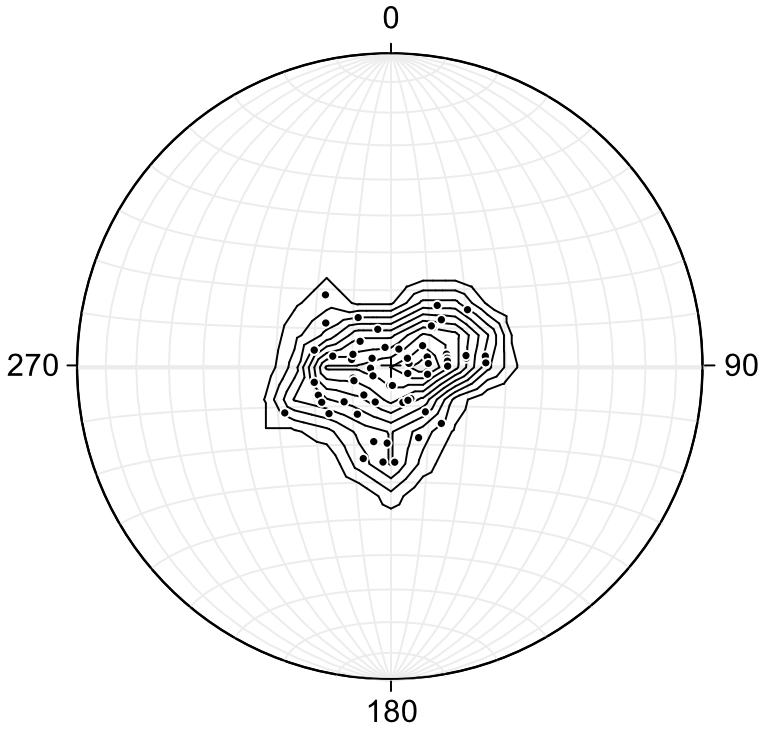

Fig. 7.18: A Schmidt net projection of all measured bedding planes is depicted. The bedding planes are displayed as poles (black dots). There is no clear trend but a stretch of the black contour lines in ENE-SWS direction. The dips of the bedding are generally very low.

7.3 Types and spatial distribution of alteration in open pit 3

The alteration is very widespread (Fig. 7.19). The alteration zones should be regarded as the least spatial distribution of the alteration because investigations of thin sections revealed alteration phenomena in parts of the pit that were regarded as fresh. This was mainly because of the very difficult differentiation of fresh and weakly altered rock specimen. The red areas are assigned to the talc-carbonate alteration and green areas are related to the serpentinised portions of the pit. The brighter areas are interpolated.

The alteration zones possess a NE-SW trend that is parallel to the regional main faults around and in the Uitkomst Complex. The serpentinisation is mainly linked to the LPxt unit and the talc-carbonate alteration is related to the PCR unit. The alteration also occurs around calc-silicate xenoliths. Based on the observations two alteration processes are possible. The first occurred after degassing of the dolomite xenoliths and the migration of the fluids along thrust faults into the PCR unit. The second arose through the formation of NE-SW trending faults and the migration of meteoric waters into the rock units.

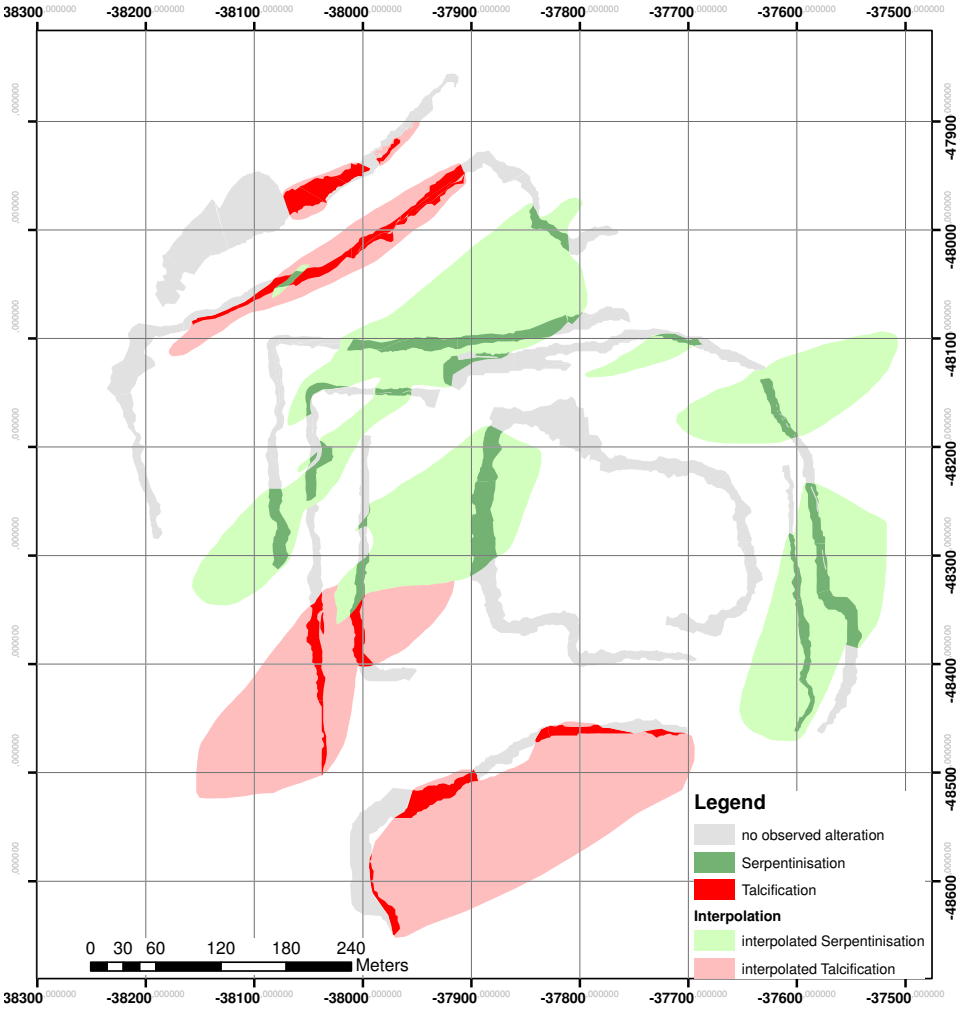

Fig. 7.19: Alteration map of pit 3. The red areas are mapped as talc-carbonate alteration. The green areas were identified as serpentinised portions of the pit. The brighter areas are interpolated based on the mapping in combination with the trends of structural features.

The distribution of pyrite concurs with the alteration zones. Therefore the formation of pyrite is linked to the development of the alteration zones. Due to oxidation events the pyrite is restricted to the areas without weathering. In oxidised zones the pyrite was transformed into oxides and hydroxides.

The alteration grade increases with the stratigraphic height up to the MChr layer, which could have acted as a barrier for the alteration, at the top of the PCR unit. The Main Peridotite is less altered, which is in line with the findings of the petrography.

7.4 Spatial distribution of oxidised rock units in open pit 3

The oxidation occurs mainly in the near of the surface where oxidising, meteoric waters have the strongest influence. The weathering is notably strong in the NW and S parts of the open pit (Fig. 7.20). These portions were likely exposed near the surface.

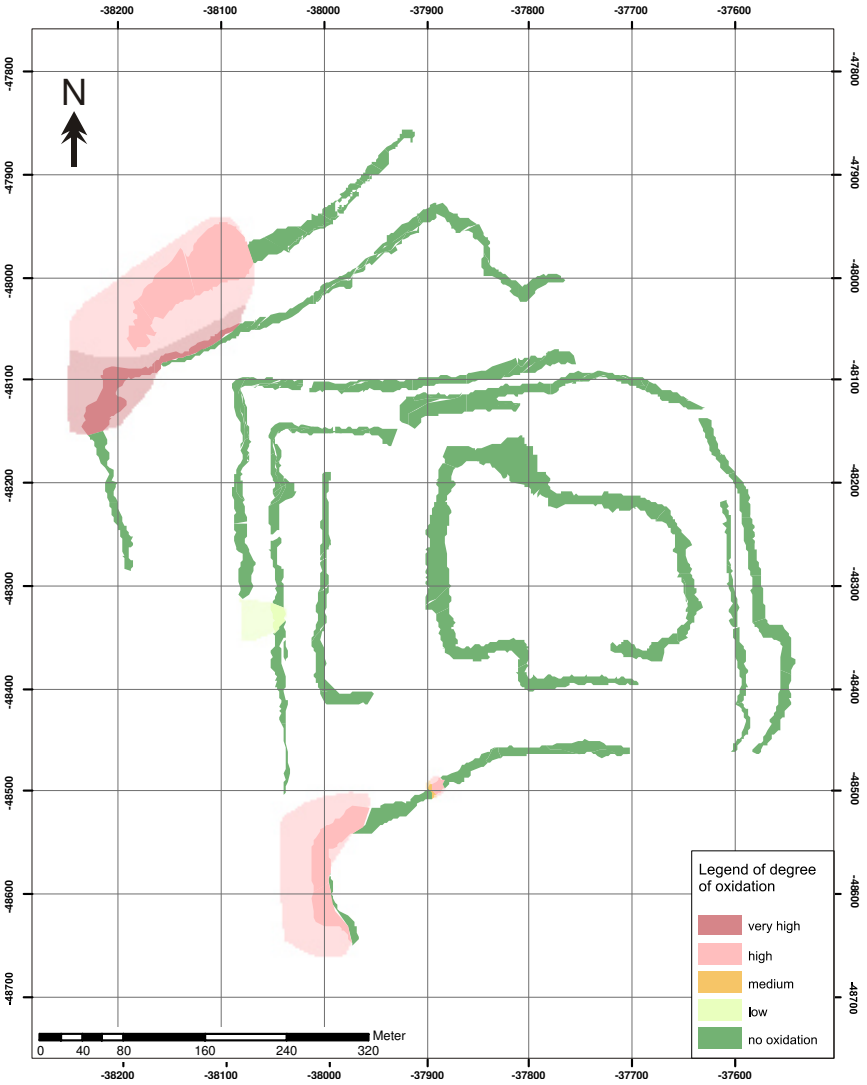

Fig. 7.20: Oxidation map of pit 3 is shown. The legend of the different stages of oxidation is displayed in the lower right corner. The brighter areas are interpolated. Only small areas of the pit, which are exclusively in the E of the pit, are oxidised. These areas were exposed near the surface.

Summary

The normal sequence of the Uitkomst stratigraphy could be evaluated. The ultramafic intrusion dips at a low angle (5°) to the NW. The calc-silicates run parallel to this direction. In some places there are stratigraphic inversion due to thrusted layers. The diabases were identified as sills with apparent dips of 10 to 15° to the E.

The biggest thrusts, which could be identified, trend from the E to the W and dip to the north pointing towards a pushing force from northern directions. The BGab is less thrusted than the PCR or LPxt unit. The main direction of the structural features is NE-SW indicating that the principal stress direction is parallel to this trend. The orientation of the bedding represents the trough to boat-like form of the Uitkomst Complex. The similar orientation of bedding

planes and the nearly horizontal shear zones indicate that the shear events occurred along the bedding planes, which acted as zones of weakness.

The occurrence of the alteration is structurally controlled. The talc-carbonate alteration is mainly linked to the PCR unit and the nearly horizontal shear zones in this unit while the serpentinisation occurs mostly in the LPxt unit. Along the NW-SE trending main faults the alteration of the rocks is especially high. The alteration also occurs around calc-silicate xenoliths. The occurrence of pyrite is linked to the alteration zones.

The oxidation is limited to portions of the pit that were exposed near the surface, where meteoric waters could interact with the igneous rocks.

8 Mineralogy and Geochemistry

8.1 Mineralogy (XRD)

Table 8.1 shows the mineral assemblages of the talc-carbonate specimens.

Tab. 8.1: Mineral assemblages of selected talc-carbonate specimens. The order of relative abundances is: chlorite > pyrite, talc > serpentine, amphibole > calcite, dolomite.

Sample	Calcite	Dolomite	Talc	Serpentine	Chlorite	Amphibole	Pyrite
H16			x	x	x	x	x
H17			x		x	x	x
H42	x	x	x	x	x	x	
H43	x	x	x	x	x	x	x
H44	x	x	x		x	x	x
H54				x	x		x
H55			x	x	x		x

Chlorite is the most abundant mineral followed by talc, pyrite and serpentine. The minerals amphibole, calcite and dolomite are less common.

Serpentine is present in the form of lizardite, a typical mineral formed under greenschist metamorphic conditions (Barnes 2000). Amphiboles are represented mostly by actinolite. The composition of chlorite ranges from chrome-rich species to leuchtenbergite and clinochlore.

The most minerals are present in the specimens H42, H43 and H44. In the samples H16 and H17 carbonates and amphiboles were not detected by the XRD facility. Pyrite is present in every sample except for H42.

Some peaks of the specimens could not be interpreted. Particularly, it was the peak at 2θ of 8.5°. A mineral, which possesses a peak in this range and is likely to occur, is palygorskite (pers. comm. Gauert 2013).

According to table 8.1 mineral assemblages of the talc-carbonate specimens are heterogeneous.

A complete overview of the XRD measurements and the formulas of the minerals are given in the appendix (Tab. A4 and A5).

8.2 Whole Rock Geochemistry (XRF)

The following description is related to all talc-carbonate measurements. All named values are in weight%. An overview of all XRF data is given in the appendix (Tab. A6).

MgO (26.16 to 37.29%) and SiO_2 (30.79 to 57.63%) have the highest contents. The values for K_2O, MnO, TiO_2, Na_2O and P_2O_5 are generally very low (usually <0.1%). Al_2O_3 (1.77 to 5.34%) and Fe_2O_3 (2.18 to 16.24%) contents are at medium values.

Fe_2O_3 (9.92 ± 4.38%), CaO (8.2 ± 7.62%) and SiO_2 (45.16 ± 9.08%) show large scatters. Al_2O_3 (3.96 ± 1.6%) and MgO (29.81 ± 3.38%) possess lower relative standard deviations. Cr_2O_3 ranges from 0.002% to 2.91%). A summary of the statistical location parameters is given in table 8.2. An overview of all XRF measurements is given in appendix table A6. The statistical location parameters of the PCR and LPxt specimens as well as the both Ca groups of the specimens and their statistical location parameters are given in the appendix (Tab. A7 to A10).

Tab. 8.2: A summary of the XRF measurements of all talc-carbonate specimens is given. The location parameters are the mean, standard deviation (SD), minimum value (Min.), and maximum value (Max.).

Element	SiO_2	TiO_2	Al_2O_3	Fe_2O_3	MnO	MgO	CaO	K_2O	Na_2O	P_2O_5	Cr_2O_3
Mean	45.16	0.004	3.96	9.92	0.02	29.81	8.2	0.04	0.01	0.01	0.45
SD	9.08	-	1.6	4.38	-	3.38	7.62	-	-	-	-
Min.	30.79	0.003	1.77	2.18	0,001	24.79	0.09	0.001	0.013	0.001	0.002
Max.	57.63	0.01	5.34	16.24	0,11	37,29	20.49	0.26	0.013	0.04	2.91

Figure 8.1 shows a scatter plot of weight% CaO against weight% MgO. The CaO content of the talc-carbonate specimens shows two clusters (fig. 8.4). The first group possesses a CaO content of <1% due very low content of carbonates. Group 2 has >1% CaO. Therefore one can distinguish between two different groups of talc-carbonate schist. This division was also applied to the pseudosections. The Mg contents of both groups plot in a similar range.

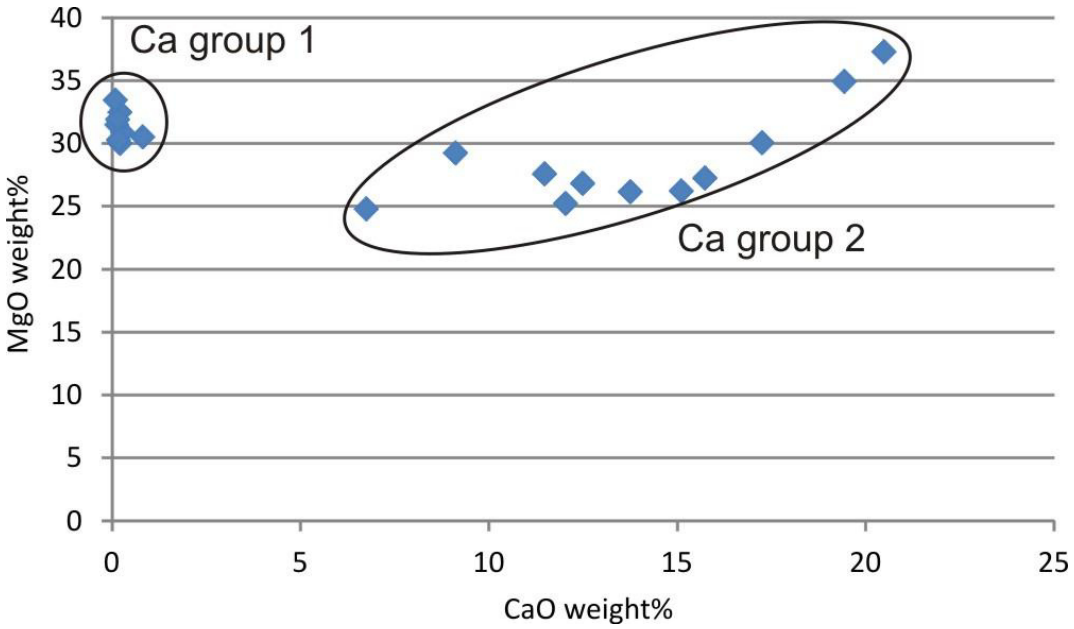

Fig. 8.1: Scatter plot depicts weight% MgO aginst weight% CaO. Two Ca populations are apparent. One population (group 1) possesses a Ca content <1%. The other population (group 2) has a Ca content >1%.

Figure 8.2 shows a scatter plot of weight% SiO_2 against weight% CaO. Element pairs of all talc-carbonate specimens are depicted. A trend between SiO2 and CaO could have been assumed due to the presence of carbonate and silicate minerals. But the correlation coefficient is 0.29 and very low. Therefore a correlation cannot be assumed, which is typical for scatter plots depicting strongly altered rocks.

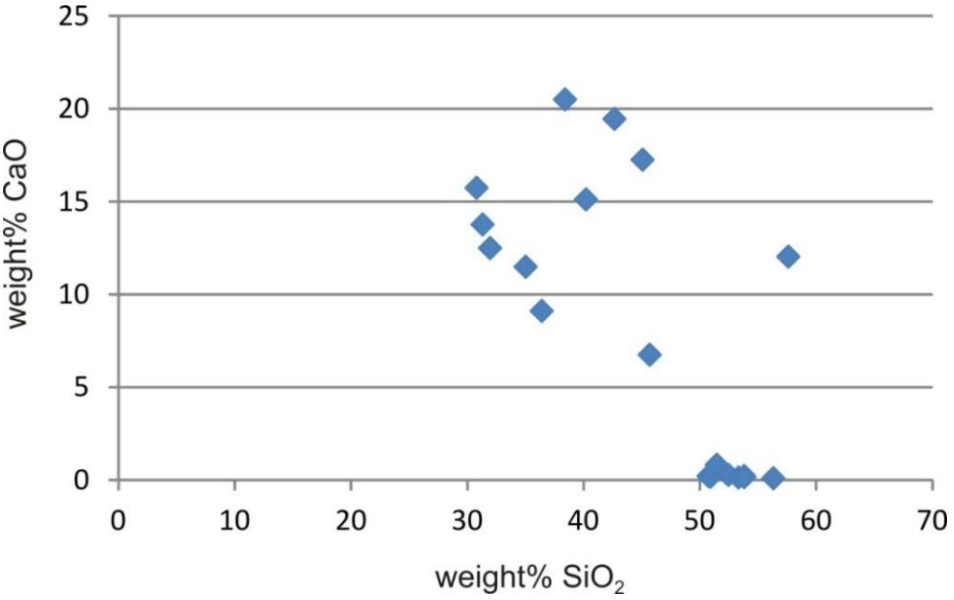

Fig. 8.2: The scatter plot SiO_2 against CaO shows a very weak correlation between SiO_2 and CaO. A trend is nearly not apparent.

Figure 8.3 shows a scatter plot of weight% MgO versus weight% Fe_2O_3. All talc-carbonate specimens are considered. Most of the Fe in the alteration mineral assemblage is incorporated in pyrite. Chlorite, talc and serpentine bear small amounts of Fe. Other Fe-bearing phases like amphibole and chromite are not present or occur in very small quantities. Talc, serpentine and chlorite possess substantial amounts of Mg. If there were a primary magmatic trend, one would assume a good correlation between MgO and Fe_2O_3. But the correlation coefficient is 0.233, which is indicative for a very weak correlation indicating that the overprint of the alteration must be very strong.

As seen in the figures 8.2 and 8.3 the measured oxides and elements mostly show mostly no or low correlations with each other. A correlation matrix is given in the appendix (Tab. A11 and A12). Primary magmatic signatures show much higher correlation coefficients between the elements and oxides (Williams 1942, Okrusch & Matthes 2010, S. 248). Poor correlation coefficients are a result of at least two different petrogenetic processes (Cox & Clifford 1982) represented by the evolution of the (ultra)mafic magma and the subsequent overprinting by alteration processes. Because of the large scatters of the oxides it can be concluded that they were mobile during the alteration process, at least to a certain extent.

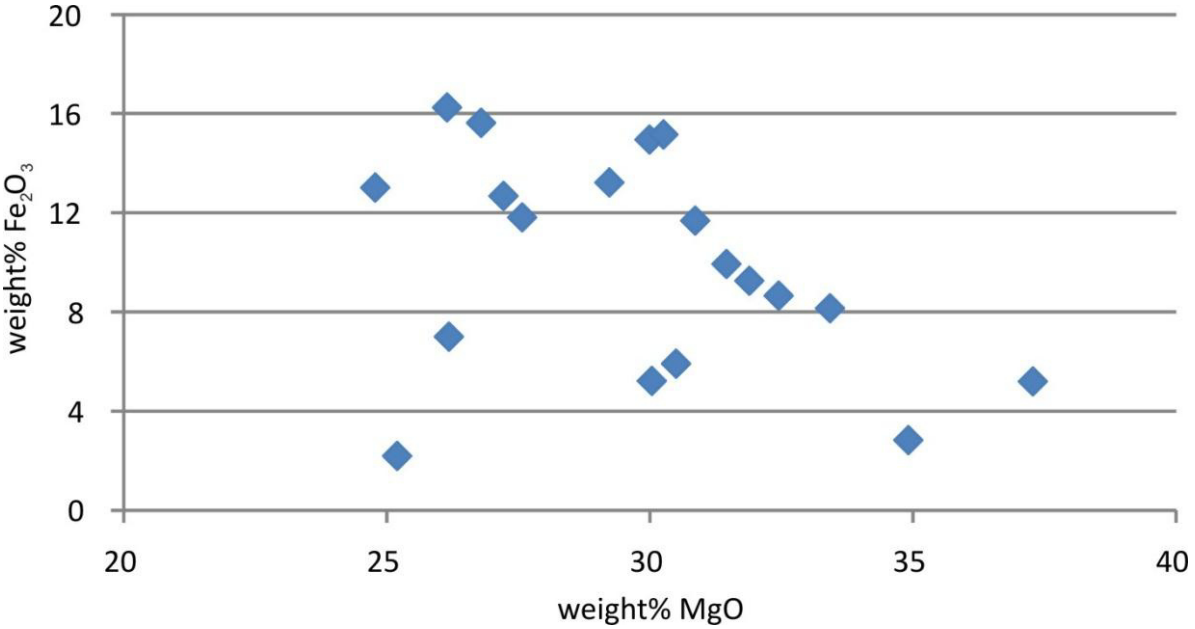

Fig. 8.3: The scatter plot MgO vs. Fe_2O_3 depects the element pairs of all talc-carbonate specimens. The original magmatic trend is strongly overprinted by another petrogenetic process (alteration) (Cox & Clifford 1982).

Figure 8.4 shows a scatter plot of CaO in weight% against LOI (loss of ignition) in weight%. All talc-carbonate and PCR specimens are considered. A part of the PCR measurements are taken from Gauerts PhD Thesis (1998). The PCR values scatter near the origin of the diagram without an apparent trend. The talc-carbonate specimens reveal a cluster at low CaO contents and a good correlation between CaO and LOI from 5% CaO. The talc-carbonate specimens, which plot along the trend, show higher values of CaO and LOI. The talc-carbonates with low CaO contents possess a higher LOI than the PCR samples. There is one outlier at 12% CaO and a LOI <2.5%.

The higher the CaO content the higher is the LOI. The trend of the talc-carbonates can be explained by the occurrence of carbonate minerals such as calcite and dolomite, which is an indicator for a higher degree of alteration. Therefore the chart shows the degree of the carbonate alteration. The talc-carbonates that plot at low CaO contents do not bear significant amounts of carbonates. Therefore they do not plot along the trend. The PCR specimens show no correlation in the chart. The outlier is a talc-carbonate with an exceptionally high content of tremolite. Therefore the LOI of this sample is relatively low.

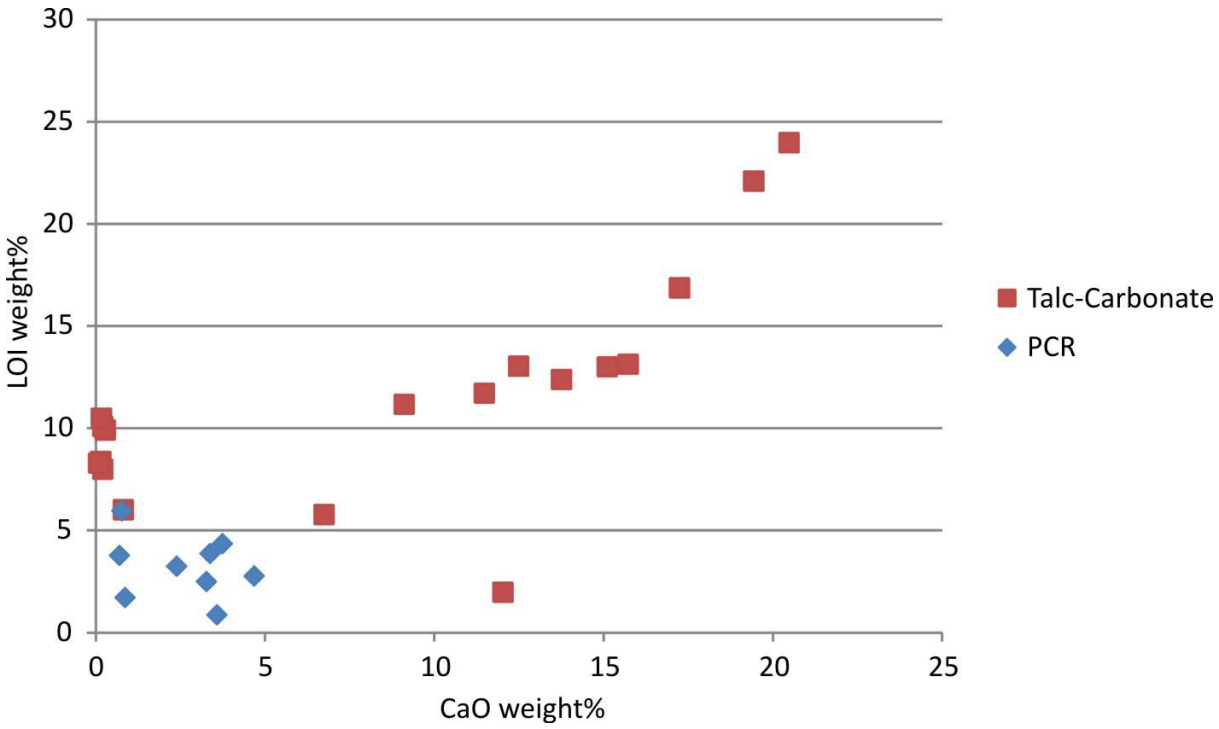

Fig. 8.4: The scatter plot CaO in weight% against LOI in % shows a good correlation between the two variables referred to the talc-carbonate specimens. A cluster of talc-carbonate values is apparent at low CaO contents. The PCR values scatter in the lower left corner.

Figure 8.5 shows the relative gain and loss of certain oxides. The talc-carbonate schists and the PCR specimens are compared with each other. The x-axis shows the mean of weight% of the main elements from all PCR specimens. The y-axis depicts the mean of weight% of the main elements from all talc-carbonate specimens. The black line symbolises the 1:1 ratio. Oxides plotting near or on the line experienced no modification in terms of concentration changes during the alteration. Oxides, which plot above the line, are relatively enriched compared to the less altered PCR rocks and oxides, which plot below the 1:1 ratio, are relatively depleted. It is evident from figure 7.4 that the PCR rocks possess a lower degree of alteration than the talc-carbonates and act as precursor rocks. Therefore the relative depletion and enrichment of certain elements is referred to the talc-carbonates.

SiO_2, MgO and CaO plot above the 1:1 ratio. Therefore they are relatively enriched in the talc-carbonates, which is a result of the formation of carbonates such as dolomite and calcite, and hydrous silicates such as serpentine and talc. SiO_2 is overestimated in the XRF measurements indicating that the enrichment is less than it would be expected based on the diagram. Al_2O_3, Fe_2O_3 and Cr_2O_3 plot below the 1:1 ratio, why they are relatively depleted in the talc-carbonates. The losses of Al_2O_3 can be attributed to the breakdown of Al-bearing phases like chromite and amphibole. The most striking feature is the very strong depletion of Cr_2O_3 caused by the dissolution of chromite. Therefore the losses of Al_2O_3 and Cr_2O_3 are linked. There is also a loss of Fe_2O_3, which can be explained by the breakdown of amphibole and chromite. Secondary formed pyrite could counteract this development but the amount of

pyrite to compensate the depletion of Fe_2O_3 is too small. One has to consider that Fe_2O_3 is also overestimated leading to the conclusion that the depletion of Fe is larger than shown in the diagram.

Major oxides with amounts of usually <1% like K_2O, Na_2O, P_2O_5, TiO_2, and MnO are relatively depleted in the talc-carbonates because they plot below the 1:1 ratio. The loss of K_2O and Na_2O can be explained by the breakdown of amphiboles. TiO_2 and MnO are depleted due to the loss of amphibole and pyroxene. P_2O_5 was measured in an amphibole grain by SEM. K_2O, Na_2O, P_2O_5, and TiO_2 cannot be integrated into one of the alteration minerals that are present in the talc-carbonate schist, why they are relatively depleted. Thus these elements were mobile during the alteration process. MnO was measured in very small amounts in carbonate minerals but they could not incorporate enough Mn to compensate the loss.

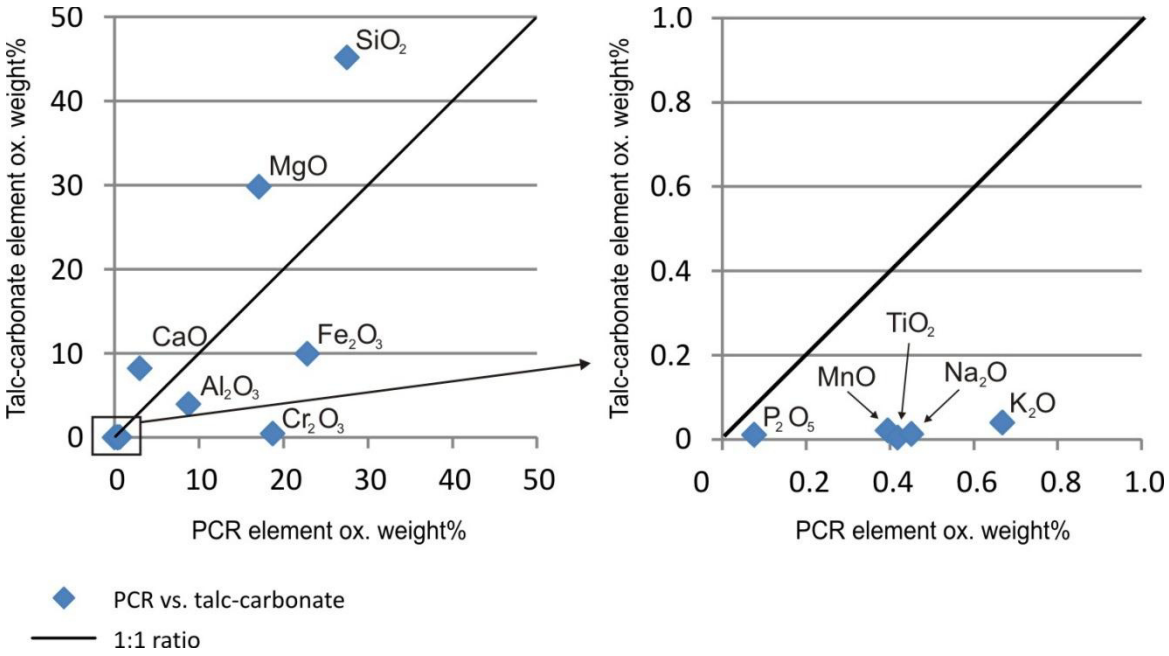

Fig. 8.5: A diagram that shows the relative enrichment/depletion of the main elements from all talc-carbonate related to the PCR specimens is depicted. The x-axis shows the mean of weight% of the main elements from the PCR specimens. The y-axis shows the same variable from the talc-carbonates. The black line represents the 1:1 ratio, which symbolises an isoconcentration line. SiO_2, MgO and CaO are enriched and Al_2O_3, Fe_2O_3, Cr_2O_3, K_2O, Na_2O, P_2O_5, TiO_2, and MnO are depleted.

Diagram 8.6 shows the alteration box plot after Large et al. (2001), in which the Ishikawa alteration index (AI) is plotted against the chlorite-carbonate-pyrite index (CCPI). The Ishikawa alteration index (Ishikawa et al. 1976) is calculated as follows:

$$equation\ 8.1: AI = \frac{100 * (K_2O + MgO)}{(K_2O + MgO + Na_2O + CaO)}$$

The formula for the chlorite-carbonate-pyrite index (CCPI) is:

$$equation\ 8.2: CCPI = \frac{100 * (FeO + MgO)}{(K_2O + MgO + Na_2O + FeO)}$$

The higher the value of the alteration index the more intense is the alteration, which is valid for both alteration indices.

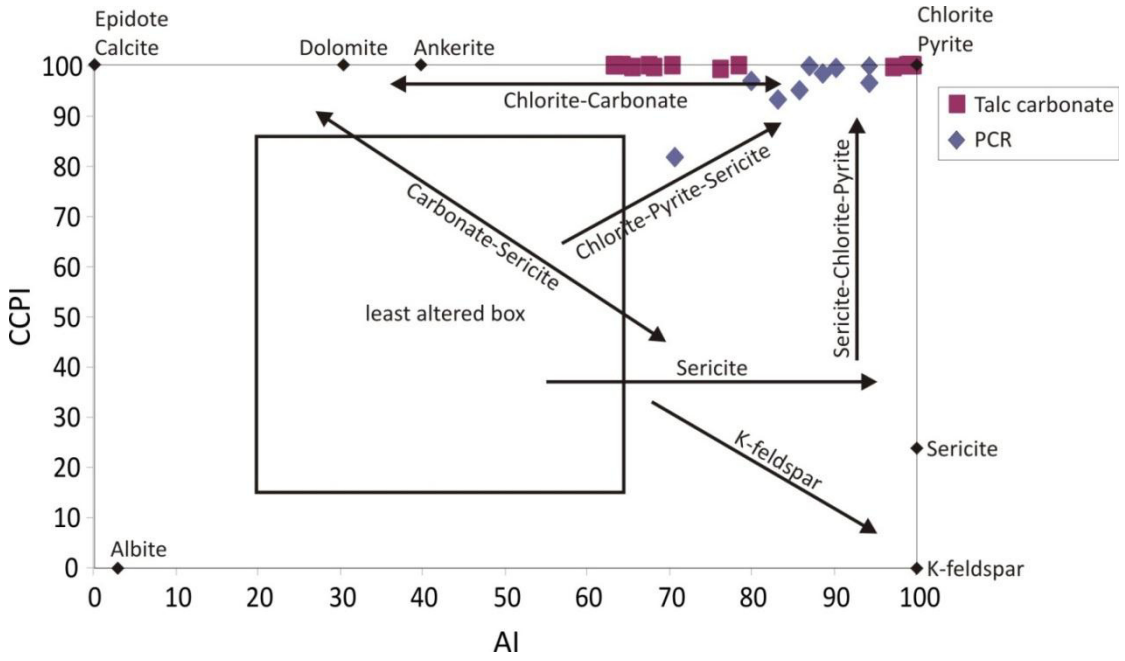

Fig. 8.6: Alteration box plot after Large et al. (2001). The Ishikawa alteration index (AI) is plotted against the the chlorite-carbonate-pyrite index (CCPI). The values plot in the right upper corner of the chart. All talc-carbonates plot along the chlorite-carbonate alteration path. The data of the PCR plot along the chlorite-pyrite-sericite alteration path.

The rock samples are highly altered. Especially the CCPI shows very high values near 100, which can be explained by the very low concentration of K_2O and Na_2O. The values for AI vary between 64 and nearly 100. This is due to the high CaO contents in the carbonate dominated specimens. The talc-carbonate specimens plot along the chlorite-carbonate alteration path. The high values can be assigned to the occurrence of calcite, carbonate, chlorite and pyrite. The PCR samples also show high degrees of alteration with lower CCPI values. The PCR specimens plot along the chlorite-pyrite-sericite path. This is due to the occurrence of pyrite and chlorite as a result of the talc-carbonate alteration. Sericite is a possible alteration product in Uitkomst but it was not observed in this study.

8.3 Mineral Chemistry (SEM)

The values in brackets are the averages and their standard deviations. The measurements of O are not considered because all OH are implemented in the O measurements. Additionally there is a high uncertainty with respect to the measurements of light elements (pers. comm. Walther 2012). Measurements with values lower than 1% are not mentioned because the precision of the SEM is limited to 1%. All values are in mol%.
A complete overview of the measurements is given in the electronic appendix.

8.3.1 Rock forming minerals

8.3.1.1 Talc

The main constituents of talc are Si (21.98 ± 1.44%), Mg (17.78 ± 1.41%) and O. Al and Fe (1.45 ± 1.19%) are minor. Talc is commonly Ni free except for three measurements with contents <1%.
Figure 8.7 shows the mineralogical classification of the pyrophyllite-talc group in the Al-Fe-Mg ternary diagram. The mol% of the Al, Fe and Mg were taken and were normalised to 100%.

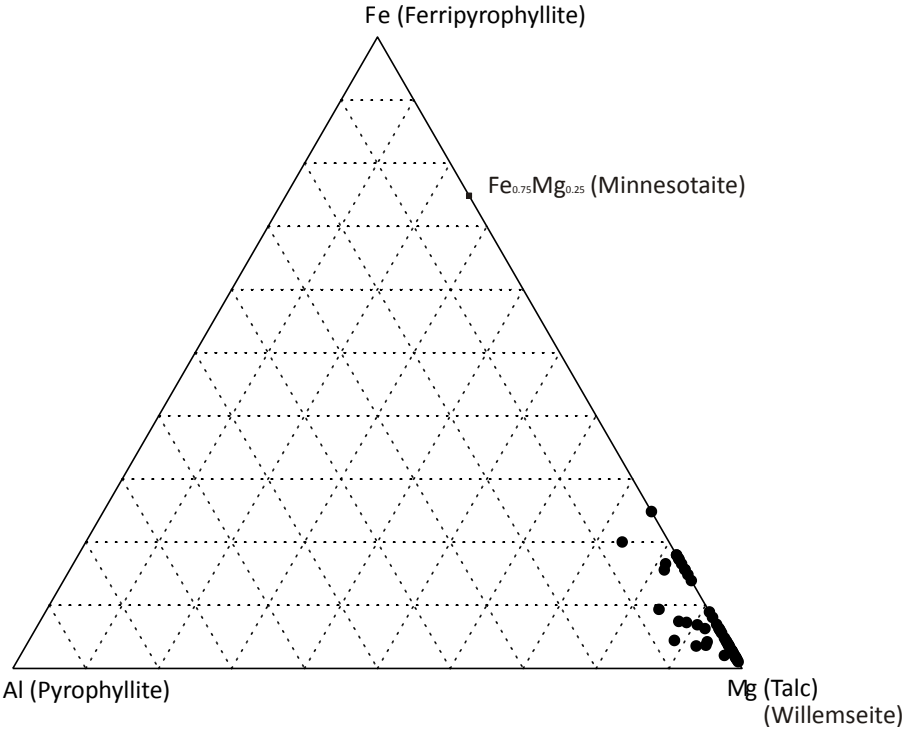

Fig. 8.7: The ternary diagram in the system Al-Fe-Mg shows the composition of all measured minerals (from talc-carbonate, sheared chromitite, LPxt) from the pyrophyllite-talc group. The depicted mol% were taken from the SEM measurements and were normalised to 100 mol%. Most of the values plot near the Mg apex, which shows the assignment to talc.

All compositions plot in or near the Mg apex identifying the minerals as talc. Some talc minerals, which can be assigned to the talc-carbonates, are more Fe rich.

8.3.1.2 Carbonate

The Ca content of calcite is 27.31 ± 1.75%. Calcite has only small quantities of Fe and Mn. Dolomite is composed of Ca (15.40 ± 1.51%), Mg (12.23 ± 0.70%). Smaller contents of Fe and Mn occur in approximately equal portions.

Figure 8.8 shows the mineralogical classification of all measured carbonates. For the construction of the ternary diagram the values (mol%) were taken from Mg, Ca, Fe and Mn and were normalised to 100 mol%. Fe and Mn are summarised in one apex due to low concentrations of Mn and Fe (usually <1%) their similar geochemical behaviour. The grey dots symbolise the ideal composition of the carbonates according to their chemical formula. The measured carbonates are from the Main Peridotite, sheared chromitite, talc-carbonate and LPxt. There is no systematic trend between the lithotypes.

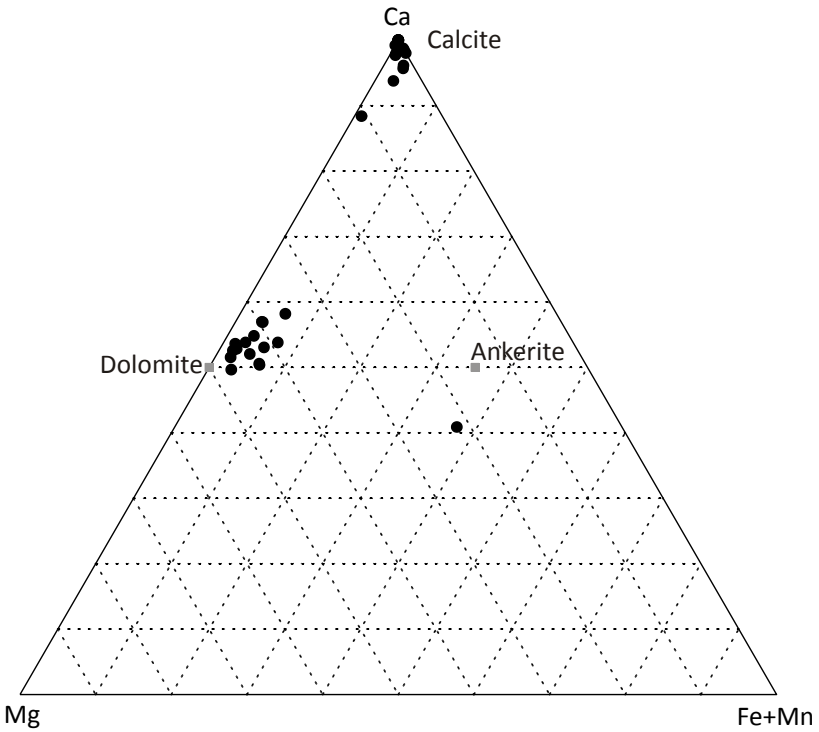

Fig. 8.8: The Mg-Ca-Fe+Mn ternary plot shows the mineralogical composition of all measured carbonates. The grey squares show the ideal composition of the carbonates according to their chemical formula. The depicted mol% of Mg, Ca, Fe and Mn were taken from the SEM measurements and were normalised to 100 mol%. The calcites and dolomites plot in the near of their ideal composition. The ankerite grain contains less Ca than the ideal composition.

All observed carbonate species are plotted in the Mg-Ca-Fe+Mn ternary diagram. The calcite grains match well with their ideal composition. The dolomites plot in the near of their ideal composition. Due to the incorporation of Fe and Mn in the dolomite the composition is shifted to the Fe+Mn apex. The measured ankerite grain does not match the ideal composition.

8.3.1.3 Serpentine and Chlorite

The element concentrations of the chlorites scatter over a wide range. The chlorites were identified as clinochlore or variations of clinochlore. The main constituents are Mg (13.33 ± 3.01%), Si (12.25 ± 2.74%), Al (6.19 ± 2.11%) and Fe (4.04 ± 2.86%).
In figure 7.9 the chlorite classification chart after Foster (1962) is shown. The diagram axis show the atomic proportions of Si against the division of the atomic proportions of Fe and all divalent cations (R^{2+}).
After the classification of Foster (Fig. 8.9) most of the chlorites are clinochlore and penninite (pennine). Some ripidolites, brunsvingites and one sheridanite are present. Some chlorites have unusually high Si contents due either to silicification or measurements of interlayers (this case is explained below). There is no systematic trend between different lithologies.

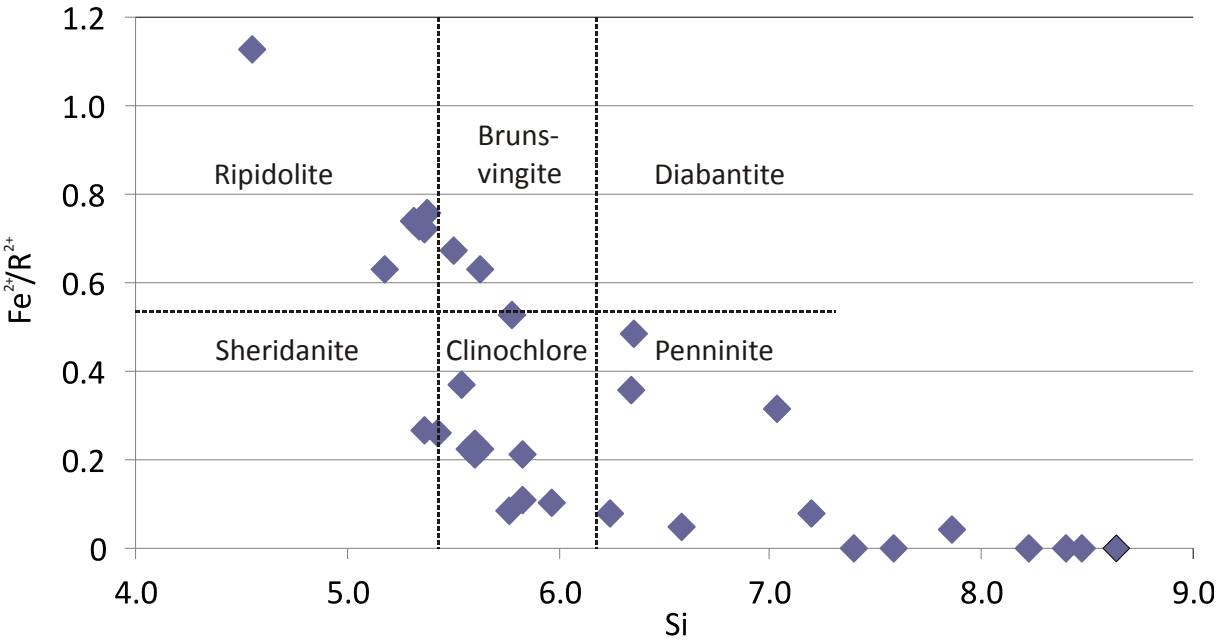

Fig. 8.9: The general mineralogical classification of chlorites after Foster (1962) shows a wide range in chlorite compositions. The atomic proportion of Si against the atomic ratio of Fe and all divalent cations (R^{2+}) is shown. All chlorite measurements from talc-carbonate, sheared chromitite and LPxt are depicted. The stated minerals in the diagram are varieties of clinochlore.

In figure 8.10 the chlorite classification chart after Hey (1954) is depicted. The chart displays display the atomic proportions of Si in chlorite against the atomic proportions of Fe and Mg calculated to Fe/(Fe+Mg).

After the classification of Hey most of the chlorites plot in the fields of ripidolite, clinochlore and talc-chlorite. Some chlorites plot in the sections of pycnochlorite, diabanite and penninite. The chlorites have a highly varying composition due either to different stages of alteration or because of the replacement of different precursor minerals (Laird 1988, S. 427). If the X-ray beam of the SEM hits a target mineral, it is possible that an interlayer of serpentine influences the measurement (Laird 1988, S. 408). Serpentine possesses a relatively higher Si content, which results in relative higher Si contents of the chlorite. Additionally chlorites show a naturally wide range in their composition, which was already indicated by the XRD measurements.

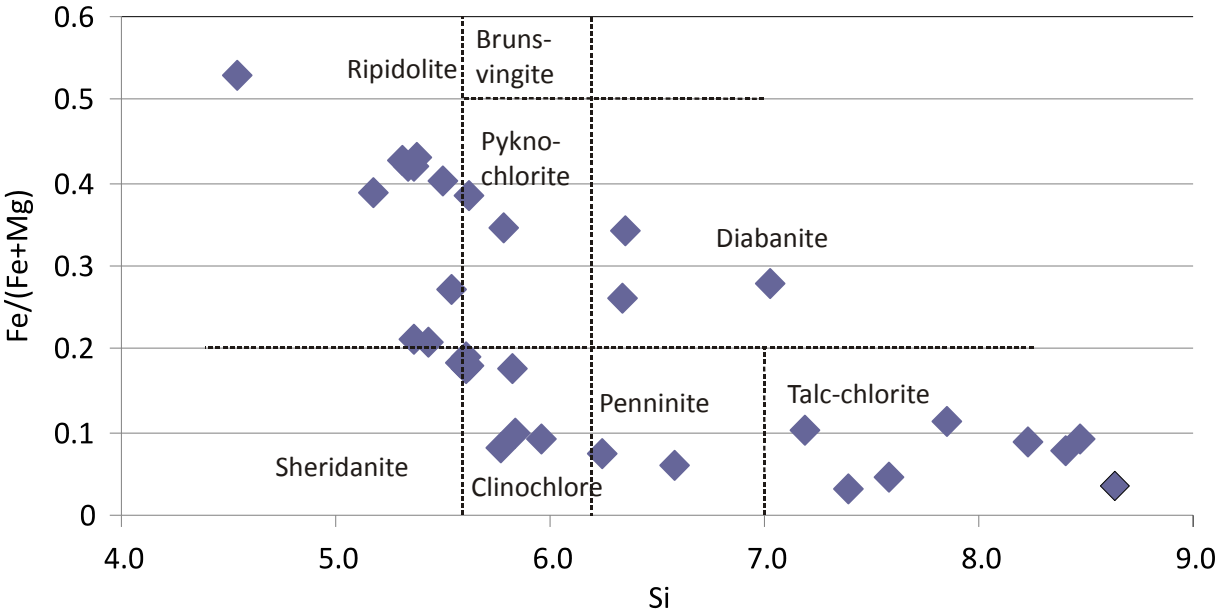

Fig. 8.10: The general mineralogical classification chart of chlorites after Hey (1954) shows a wide scatter, which can be due to silification, interlayers of serpentine or the repalcement of different precorsur minerals. The atomic proportion of Si is plotted against the atomic ratio Fe/(Fe+Mg). All chlorite measurements from talc-carbonate, sheared chromitite and LPxt are depicted. The stated minerals in the diagram are varieties of clinochlore except talc-chlorite.

Figure 8.11 shows the petrogenetic classification of chlorites according to their geological environment. The chart depicts the atomic ratio $Mg/(Mg+Fe^{2+})$ against the atomic ratio $Al/(Al+Fe^{3+}+Mg)$.

The petrogenetic classification of the chlorites shows a clear mafic to ultramafic affinity. A trend is apparent from ultramafic to mafic compositions. This trend is due to an increase of Fe or a loss of Mg because of the alteration. Chlorites tend to be more Mg rich with increasing O fugacities via the exchange reaction $Mg^{2+} \leftrightarrow Fe^{2+}$ (Caritat et al. 1993), which leads to a modification of the of the $Mg/(Mg+Fe^{2+})$ or $Fe^{2+}/(Fe^{2+}+Mg)$ values. Therefore the modification is linked to the increasing influence of more oxidising, possibly meteoric, waters (Sarkar 2008).

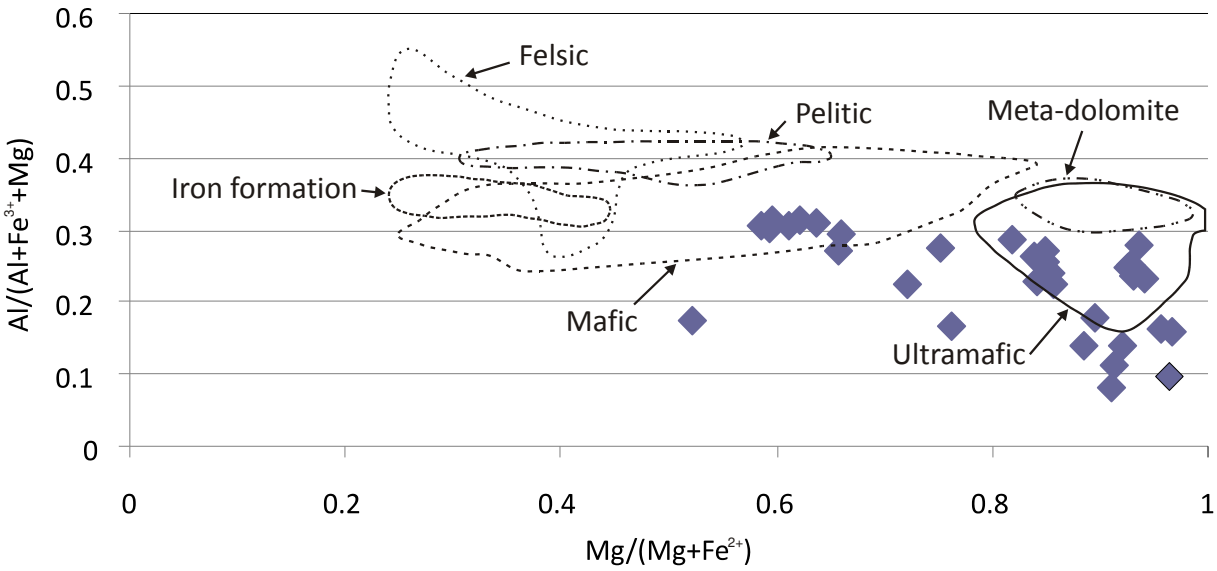

Fig. 8.11: The petrogenetic classification of chlorites after Laird (1988) and modified by Sheikhikou (1992) is depicted containing typical geological suites, where chlorites are apparent. The ratio of the atomic proportions of Mg/(Mg+Fe^{2+}) is plotted against the atomic ratio Al/(Al+Fe^{3+}+Mg). All chlorite measurements are considered. Most of the chlorites are in or around the field of mafic or ultramafic compositions, which is indicative for ultramafic to mafic precursor minerals.

Fig. 8.12 shows the chlorite compositions with respect to the alteration environment where they were formed. A large scatter is apparent. Therefore no clear assignment could be made. Around half of the measurements plot outside the fields typical for alteration (pers. comm. Gauert 2013). If they plot inside a field the chlorites can be assigned to greenschist and amphibolite metamorphic conditions.

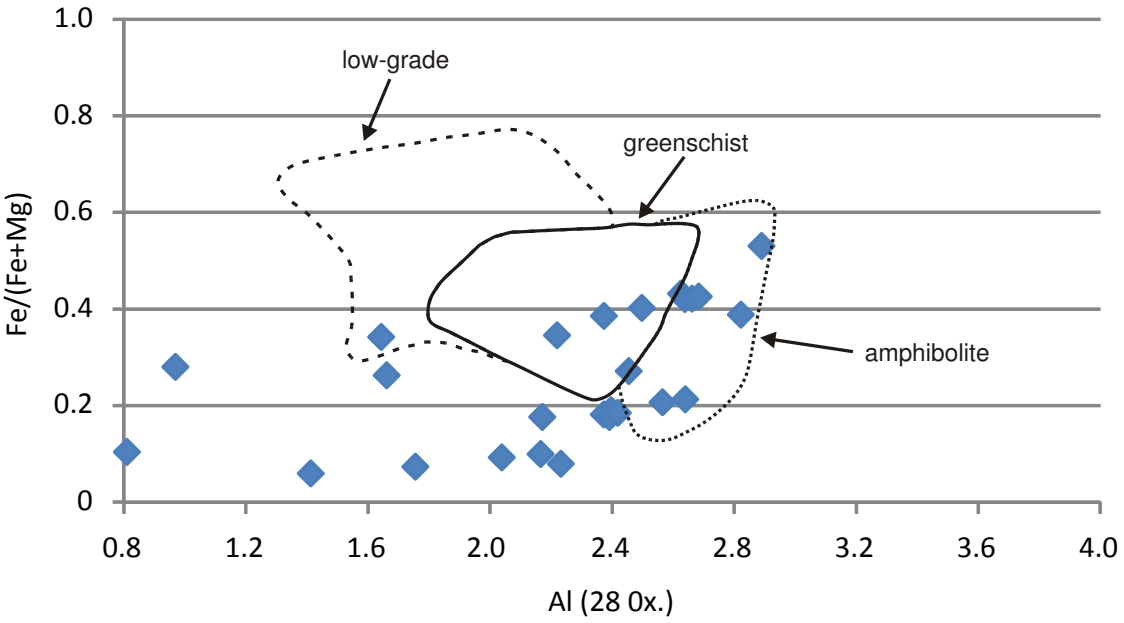

Fig. 8.12: The chlorite metamorphic classification after Nimis et al. (2004) shows different stages of metamorphism in relation to the chlorite composition. The axis are the atomic proportions of Al normalised to 28 O in the chlorite formula against the atomic proportions of Fe divided by the atomic proportions of Fe and Mg. All measured chlorites show a wide scatter and cannot be assigned to a specific metamorphic grade. The only possible statement is that there are two clusters at the rim of the greenschist field.

Most of these chlorites plot at the border between the greenschist and the amphibolite field, which is in rough agreement with the formation conditions of chromites (below), which plot at the upper end of the greenschist metamorphism field (Fig. 8.14). The upper limit of greenschist metamorphic conditions points towards temperatures between 400 and 500 °C. The large scatter is due to the aforementioned reasons (serpentine interlayer, different precursor minerals, and natural range of chlorite composition). Especially serpentine interlayers shift the chlorite compositions to lower Al values. Therefore figure 8.12 has to be regarded as a rough indicator for the alteration temperature.

Serpentines were difficult to identify in talc-carbonates. In thin sections the serpentines are clearly visible but very hard to find in SE images from the SEM because they possess a very similar composition to talc and possibly chlorite. A similar observation was recorded by Lauretta et al. (2000). Serpentines with exceptionally high Al and Fe contents were also observed by Albino (1995). Another reason could be the textural relationship between chlorite and serpentine that could have formed interlayers (Banfield & Bailey 1996). A further explanation for “non-existence” of serpentines could be that the talc measurements were confused with serpentines. Figure 8.13 rules out this case.

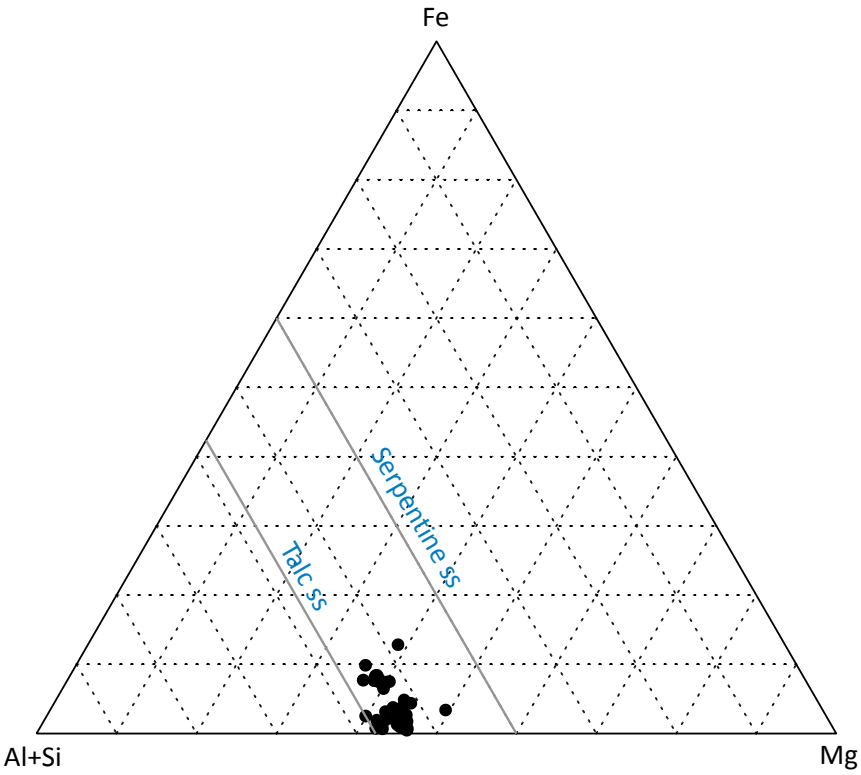

Fig. 8.13: The Al+Si-Fe-Mg ternary diagram shows the compositions of the talc minerals (modified after Furukawa et al. 2011). The blue lines represent the solid solutions of serpentine and talc. The depicted mol% of Fe, Mg, Al and Si are normalised to 100 mol%.

In figure 8.13 the attempt has been made with the Al+Si-Fe-Mg ternary diagram to evaluate the measurements of the talc minerals. Talc minerals were possibly confused with serpentines but all talc minerals (black dots) (except for two) plot along or near the talc solid solution line.

Serpentines were clearly identified in a thin section of the PCR. The main constituents are Mg (20.34 ± 1.34%) and Si (14.14 ± 0.95%). Al (0.93 ± 0.62%) and Fe (1.56 ± 0.45%) occur in minor amounts. In the near of dissolved and porous chromite grains (as described in the chapter petrography) the serpentines contain low amounts of Cr (<1%). The formation of Cr-rich serpentine is a common feature in porous chromites. Usually the serpentines do not contain Ni. This is due to the integration of Ni into the sulphide droplets during the deposition of the Uitkomst Complex (Gauert 1995). Additionally, smaller amounts of Ni could have been mobilised during the alteration process.

8.3.1.4 Quartz and amphibole

Quartz possesses generally a stoichiometric composition. The mean molar Si:O ratio is 0.61.

The water content of the amphiboles was not considered during the recalculation of the measurements for the purposes of classification because cations are considered for the classification of amphiboles. The deficit to 100%, which is linked to the absence of water in the analysis, is proportionally portioned between the distinct cations.

Because of the naturally wide-ranging composition of amphiboles only the ranges of the minerals are named. The constituents are Si (7.73 to 24.77%), Al (1.89 to 14.24%), Mg (0.83 to 14.13%), K (0.00 to 5.11%) and Fe (0.61 to 10.46%). The measured amphiboles are cummingtonite and anthophyllite.

8.3.2 Ore forming minerals

8.3.2.1 Chromite

The composition of the chromites is variable. The scatter of the divalent cations is much higher than that of the trivalent cations. The main constituents are Cr (19.58 ± 2.91%), Fe (13.36 ± 4.05%), Al (7.62 ± 1.13%) and Mg (4.72 ± 2.59%). Ti occurs in minor amounts. Fe is present as Fe^{2+} and Fe^{3+}. Mg shows a larger relative scatter than the trivalent ions.

Figure 8.14 shows the ternary diagram Cr-Fe^{3+}-Al. The grey shaded area depicts the chromite composition under greenschist facies conditions. The blue bow represents the immiscibility gap for natural chromites. It is aimed to demonstrate if the chromites plot in the field of greenschist metamorphism.

The measured chromites plot in the field or near the border of serpentinised spinels. Consequently the rocks are weakly metamorphosed. Some of the measurements do not plot in the field of greenschist metamorphism. The chromites from the PCR show a lower scatter but plot in a similar region as the chromites from the sheared chromitite sample.

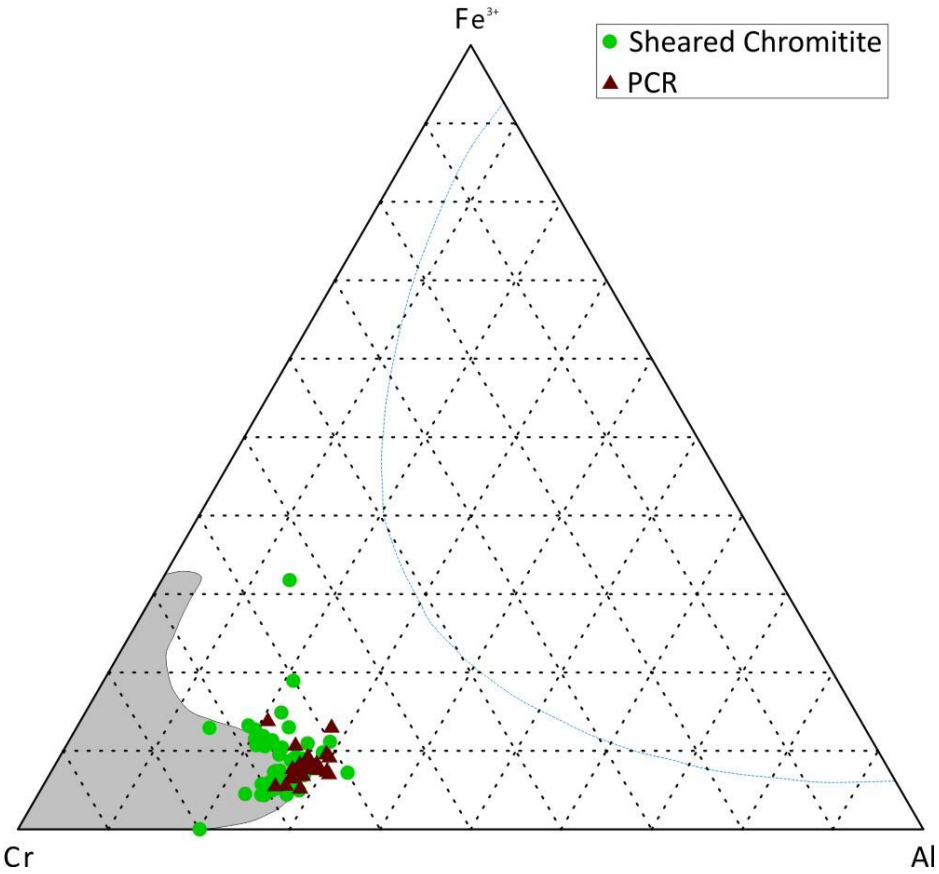

Fig. 8.14: The Cr-Fe^{3+}-Al ternary diagram shows the chromite composition under greenschist facies conditions (grey area) after Lehbib et al. (2008). The blue line represents the immiscibility gap of natural chromites. The green dots are chromites of sheared chromitite and the brown triangles are chromites from the PCR unit. The mol% of Cr, Al and Fe3+ are normalised to 100 mol%.

The figures 8.15 and 8.16 show the genetic classification of chromites (Fig. 8.15 after Lehbib et al. 2008, Fig. 8.16 after Mussalam et al. 1981), which is referred to stratiform or podiform chromite deposits. Figure 7.15 displays the atomic ratio of Mg/(Mg+Fe^{2+}) against Cr/(Cr+Al). Figure 8.16 depicts weight% Cr_2O_3 against weight% Al_2O_3. All chromite measurements of the PCR and sheared chromitite samples are considered.

The figures 8.15 and 8.16 clearly show that the sheared chromites (blue) mostly plot in the field of stratiform chrome deposits. A part of the sheared chromites is outside the stratiform field in figure 8.15. A likely reason is the geochemical overprinting due to alteration. The background of the modifications is described below. In figure 8.16 nearly all sheared chromites plot in the field of stratiform chromite deposits because only trivalent cations (Al^{3+}, Cr^{3+}), which are much less mobile than divalent ions, are plotted. Their geochemical signature is less affected by the alteration than those of the divalent cations (Fe^{2+}, Mg^{2+}).
The chromites from a PCR sample plot in the middle of the stratiform chromitite-deposit field (Fig. 8.15). This is a difference compared to the samples of the sheared chromite. The chromites from the PCR show a lower scatter and higher $Mg/(Mg+Fe^{2+})$ values. On that score one can conclude that the PCR chromites are less affected by chemical overprinting than the chromites from the sheared chromitite. Consequently the PCR chromites kept their magmatic signature. In figure 8.16 they plot in the same area as the chromites from the sheared chromtite. Therefore the trivalent cations are less modified during the alteration than the divalent cations. A reason for the different mobilisation behaviour is the release of Fe^{2+} and Mg due to the serpentinisation of olivine (Barnes 2000).
Barnes (2000) showed that greenschist metamorphosed chromites show a range of $Mg/(Mg+Fe^{2+})$ values between 0.4 and 0.7. The chromites measured in this study possess lower $Mg/(Mg+Fe^{2+})$ values varying between 0.03 and 0.45. As a result there is a stronger modification of the chromites than of those measured by Barnes (2000). Figure 8.15 shows two clusters. One cluster is between 0.03 and 0.10. The second cluster is at approximately 0.4. Thus there is heterogeneity in the composition of the chromites. The chromite grains, which plot in first cluster, possess enrichment in Fe^{2+} and a strong depletion in Mg, which could be integrated into dolomite. Additionally dolomite and calcite are not capable to carry higher amounts of Fe^{2+}. This observation was also made by Barnes (2000). The $Mg/(Mg+Fe^{2+})$ values of the chromites from the PCR unit yield are higher and plot in the observed range of Barnes (2000). The conclusion is that these chromites are less affected by the alteration. Due to the highly variable $Mg/(Mg+Fe^{2+})$ values and the low scatter of the Cr/(Cr-Al) values one concludes that the temperature of the alteration did not exceed 550 °C (Barnes 2000). Otherwise one could recognise a substantial variation of the Al content and the Cr/(Cr-Al) ratio. According to the modelled pseudosections the temperature cannot be significantly lower than 500°C (see chapter 9.1). Such would also explain the very low values of $Mg/(Mg+Fe^{2+})$ that should decrease with a higher temperature due to the supply of energy to the system and increased diffusion rates.

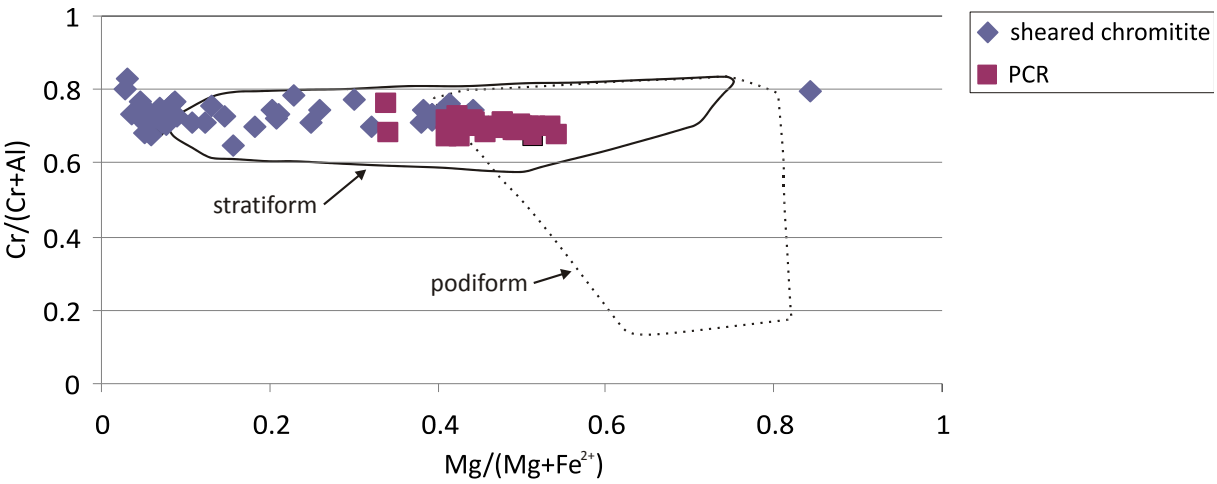

Fig. 8.15: The genetic classification chart of chromites after Lehbib et al. (2008) shows the distinction between stratiform and podiform chromitite deposits. For that purpose the atomic proportions of Mg and Fe^{2+} ($Mg/(Mg+Fe^{2+})$) are displayed against the atomic proportions of Cr and Al ($Cr/(Cr+Al)$). The PCR chromites (ruby squares) plot in the middle of the stratiform field. A part of the chromites from the sheared chromitite (blue rhombus) plot outside the stratiform field.

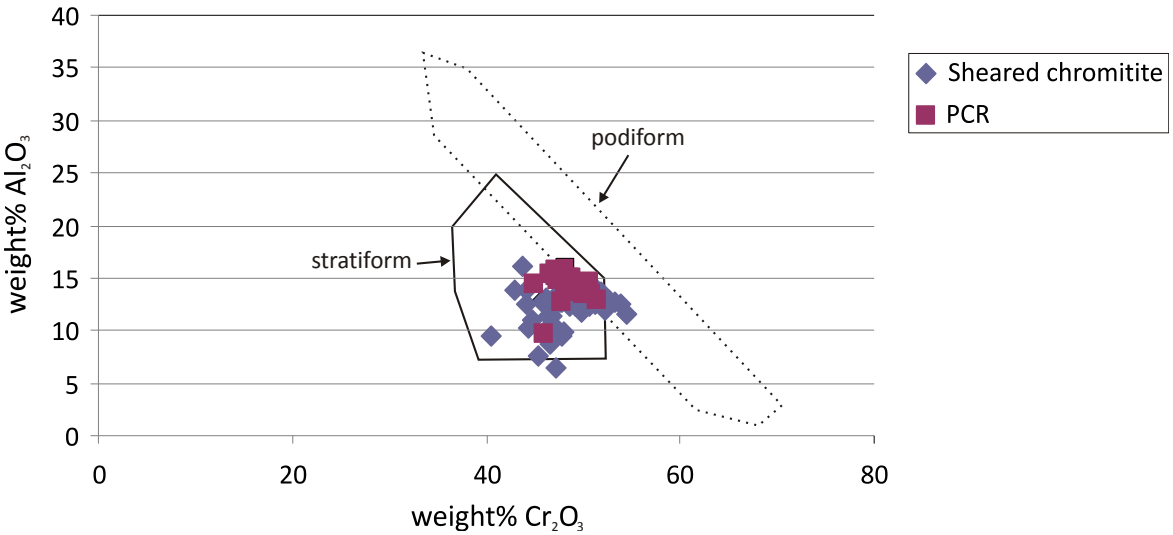

Fig. 8.16: The genetic classification chart of chromites after Mussalam et al. (1981) also shows the distinction between stratiform and podiform chromitite deposits. Weight% Cr_2O_3 are displayed against weight% of Al_2O_3. All chromites from the PCR (ruby squares) and sheared chromitite (blue rhombus) plot in the field of stratiform chromite deposits.

The Figures 8.17a to 8.17c show the distribution fields of measured chromites from all around the world (Barnes & Roeder 2001). The measured chromites of the PCR and sheared chromitite are compared with chromites from all over the world. The 50 percentile and 90 percentile define the area where 50% or 90%, respectively, of all chromite measurements are plotted. The percentile fields are valid for continental mafic intrusions.

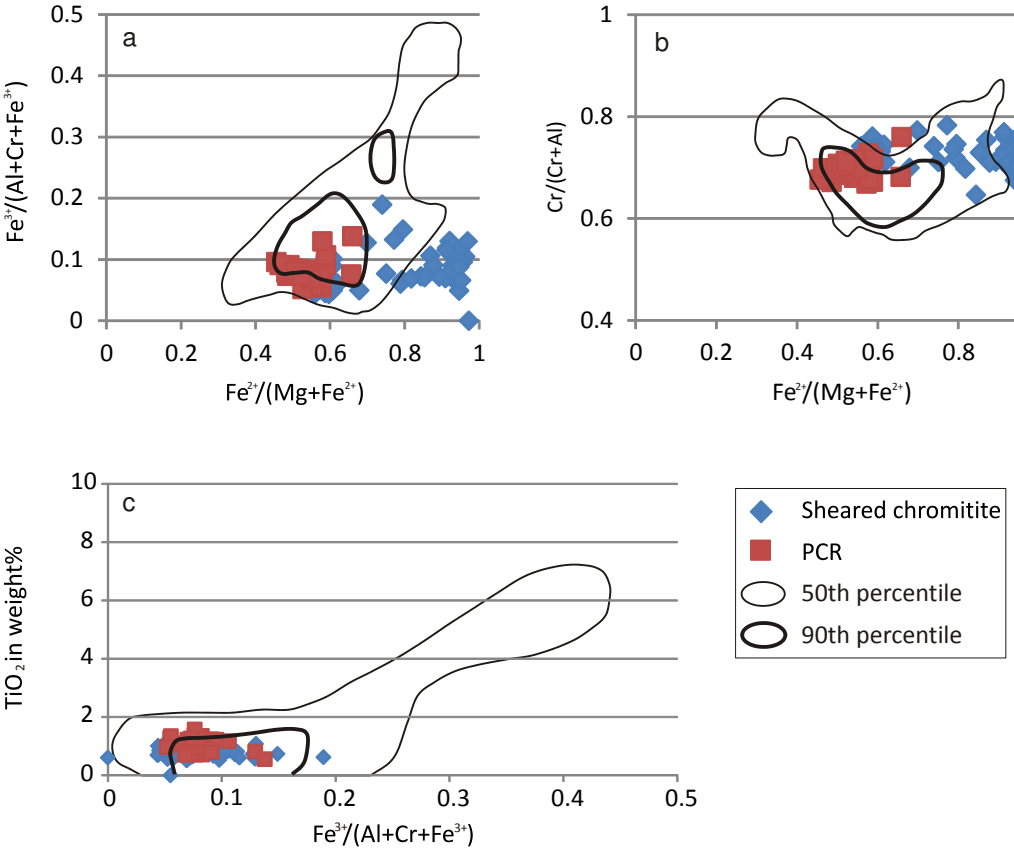

Fig. 8.17a-c: Scatter plots of chromites after Barnes & Roeder (2001) are displayed. PCR chromites (ruby squares) plot in the 90 percentile field. Chromites from the sheared chromitite (blue rhombus) plot outside the 90 percentile field. a) Atomic ratio $Fe^{2+}/(Mg+Fe^{2+})$ against Cr/(Cr+Al) is depicted. b) Atomic ratio $Fe^{2+}/(Mg+Fe^{2+})$ against $Fe^{3+}/(Cr+Al+Fe^{3+})$ is depicted. c) Atomic ratio $Fe^{3+}/(Cr+Al+Fe^{3+})$ against TiO_2 in weight% is depicted.

In figures 8.17a and 8.17b the chromites mostly plot in the 50 percentile field, while in figure 8.17c they are in the 90 percentile field, which can be explained by the different mobilisation of the trivalent and divalent cations. The measurements of the PCR sample plot mostly in the 90 percentile field in figures 8.17a to 8.17c showing that the chromites belong to a continental (ultra)mafic intrusion environment. The deviations of the sheared chromites measurements are due to the alteration processes.

In figure 8.18 an attempt has been made to illustrate the relative gains and losses of the main constituents of chromite. The chart shows the ratios of the oxides, which build up chromite, from chromite measurements of a sheared chromitite and the PCR. The chromites, which are termed as "PCR chromites" in figure 8.15, are regarded as less altered than the "sheared chromites" that were directly exposed to high fluid fluxes and fluid:rock ratios along a shear zone, which results in higher degrees of alteration (Huang et al. 1986). Therefore the "sheared chromites" are normalised to the "PCR chromites" allowing predictions on the relative enrichment or depletion of certain elements, which are incorporated into the chromite structure, between the two types of chromites. The reason for modification of the chromites is

the hot alteration fluid, which migrated along the shear zones in the PCR and provided the energy, which was necessary to mobilise certain elements.

The trivalent cations show slight modification between the two groups. The change in Fe_2O_3 and Cr_2O_3 is nearly negligible. Al_2O_3 shows a higher depletion. The change of the Al content can be explained by the entrapment into chlorite, which shows a beginning mobilisation of Al. Therefore the alteration temperature has to be close to 550°C (Barnes 2000). The divalent cations (Mg, Fe^{2+}), represented by their oxides, show a more intense modification in contrast to the trivalent cations. MgO is highly depleted and FeO is highly enriched. This behaviour was also recognised by Barnes (2000). The depletion of MgO and the enrichment of FeO can be explained by the exchange of Mg^{2+} and Fe^{2+} cations with the coexisting silicates like talc, serpentine and chlorite.

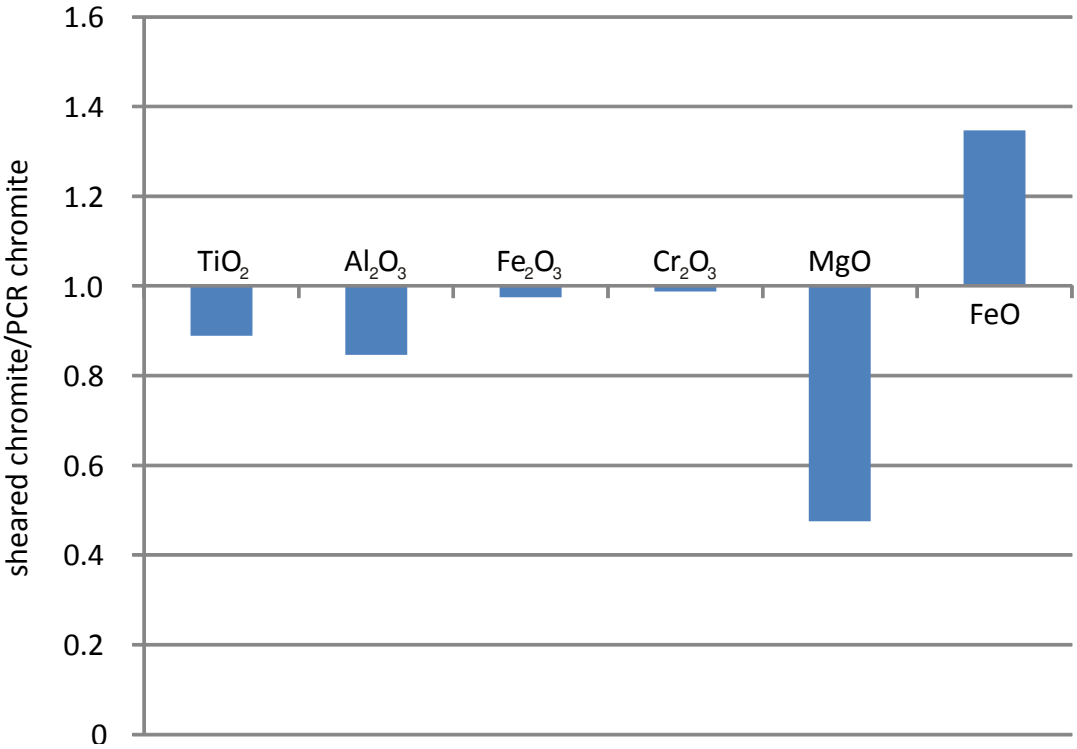

Fig. 8.18: This diagram shows the relative enrichment/depletion of TiO_2, Al_2O_3, Fe_2O_3, Cr_2O_3, MgO and FeO in two different chromite populations. Chromites from the sheared chromitite specimen are normalised to chromites from the PCR unit.

In figure 8.19 an attempt has been made to classify the chromites to different alteration environments after Barnes (2000). For that purpose the atomic ratio Mg/(Mg+Fe^{2+}) is plotted against the atomic ratio Cr/(Cr+Al).

The chromites of the Uitkomst Complex do not fit well into the alteration fields. There is a relatively large scatter of the Cr/(Cr+Al) ratio. Such can be attributed to a stronger modification of the Uitkomst chromites implying a higher degree of alteration than the chromites measured by Barnes (2000). The chromites of the sheared chromitite mostly plot

outside of the alteration areas. If they plot inside such a field, it will be mostly the talc-carbonate field. Nearly all of the PCR chromites plot outside of the alteration fields. Some samples can be assigned to the antigorite-carbonate zone. The PCR chromites cannot be assigned to a specific alteration zone. The

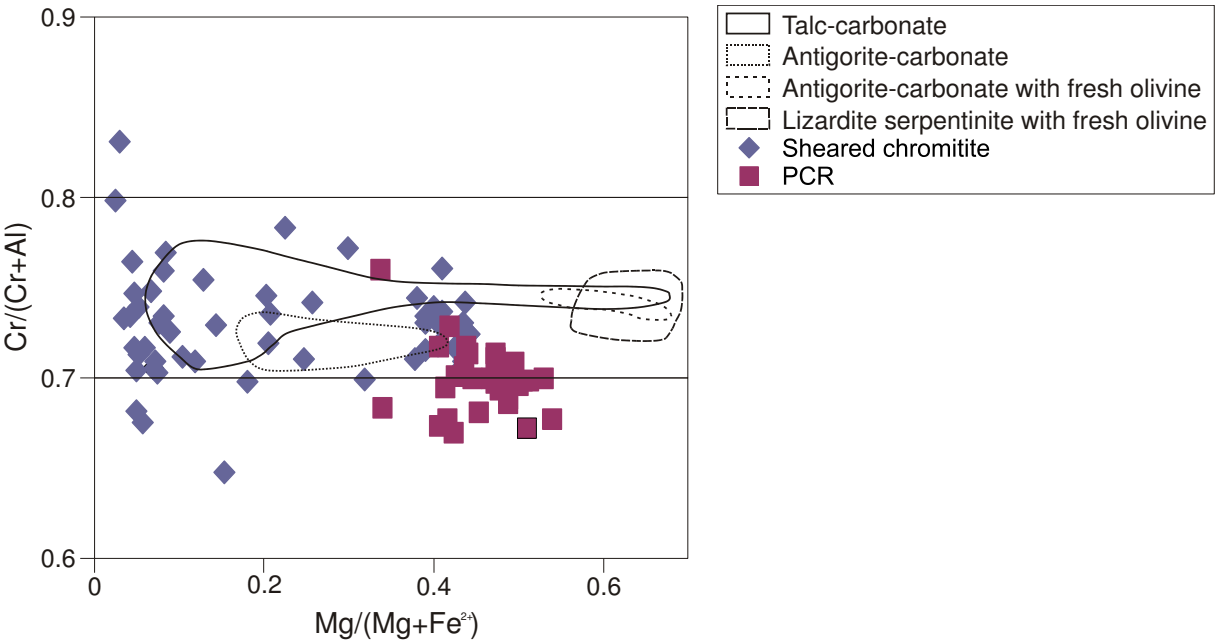

Fig. 8.19: The chromite alteration classification after Barnes (2000) is shown. Atomic ratio Mg/(Mg+Fe^{2+}) is plotted against the atomic ratio Cr/(Cr+Al). The fields are based on samples of the Black Swan deposit. The PCR chromites plot outside the alteration fields. The chromites of the sheared chromitite partially plot inside the talc-carbonate and the antigorite-carbonate field.

8.3.2.2 Sulphides

Pyrrhotite shows some variation of the Fe:S mol ratio, which ranges from 0.775 to 1.005. Pentlandite possesses variable Ni contents, which show a scatter from 27.89 to 34.19%. The Ni:Fe mol ratio varies between 1.087 and 1.612. Chalcopyrite has a Cu:Fe mol ratio of about 1. The Cu content is 23.90 ± 3.37% and the Fe content is at 25.04 ± 1.35%. In some cases pyrite contains Co (up to 2.91%).

The ternary plot of the system Ni-Fe-S (Fig. 8.20) gives an overview of the sulphide measurements except chalcopyrite, which is plotted later. All other sulphide measurements from talc-carbonates (black dots), sheared chromitites (red dots), PCR (green dots), and Lower Pyroxenite (light blue dots) are depicted. A more detailed view of pyrrhotites is shown as well.

There are three clearly defined areas, which can be assigned to pyrrhotite, pentlandite and pyrite. Pyrrhotite shows some scatter in its composition, but there seems no systematic trend between the different lithologies because the pyrrhotites of the different lithologies plot in the same area. Thus there was no modification of pyrrhotite during the alteration process. The

measurements of pyrites, which plot near their ideal composition, show a similar pattern to the pyrrhotites.

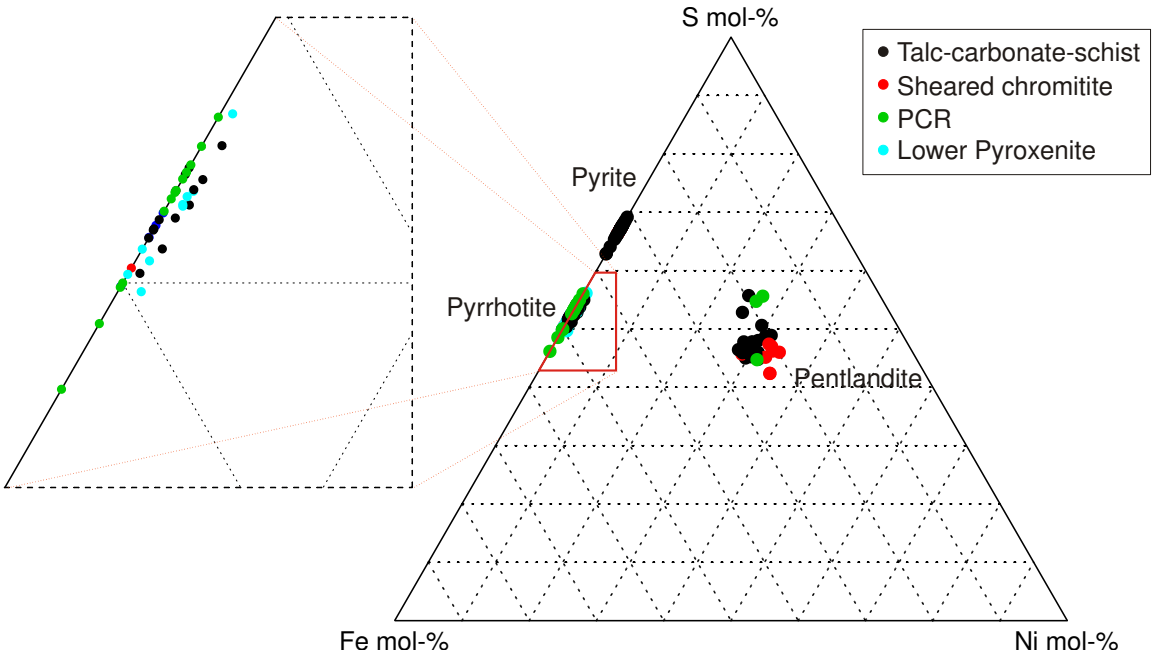

Fig. 8.20: Sulphides from talc-carbonates (black dots), sheared chromitites (red dots), PCR (green dots), and Lower Pyroxenite (light blue dots) are shown in the Ni-Fe-S ternary system. The area around pyrrhotite is magnified. The mol% from Fe, S and Ni are normalised to 100 mol%. All sulphide measurements are considered.

In figure 8.21 a more detailed view of the pentlandite measurements in the system Ni-Fe-S is displayed. It is aimed to demonstrate if there is a shift in the composition of pentlandites due to the alteration processes.

A slight shift of the pentlandite composition from the sheared chromitite (red dots) to the pentlandites from the talc-carbonate-schist (black dots) is apparent. The Fe content remains stable while a slight depletion of Ni occurs. Ni is released during the alteration of silicates (Barnes & Hill 1998). Another mechanism is the remobilisation of S due to deformation events, which become important at high temperature >500°C. The green dots are pentlandites from the PCR units. Due to the small number and high variation it is not possible to assess a trend. Assuming that the talc-carbonate schist represents a higher degree of alteration than the shared chromite then there is a depletion of Ni and a relative enrichment of S with increasing alteration within the pentlandite. Violarite as an alteration product of pentlandite is very rare.

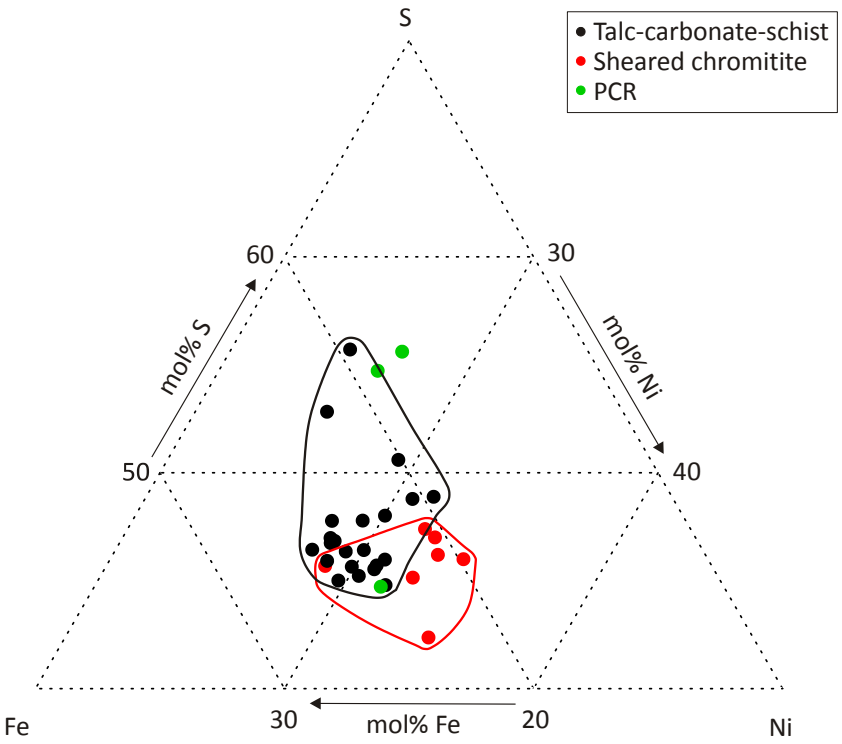

Fig. 8.21: Ni-Fe-S ternary system is shown in more detail. Pentlandites from talc-carbonates (black dots), sheared chromitites (red dots), and PCR (green dots) are displayed. The mol% from Fe, S and Ni are normalised to 100 mol%. The black arrows outside the ternary plot show the direction of increasing mol% and the corresponding element. The pentlandites from the sheared chromitite plot in a slightly more Ni rich area as the pentlandites from talc-carbonates. The pentlandites from the PCR show a wide scatter.

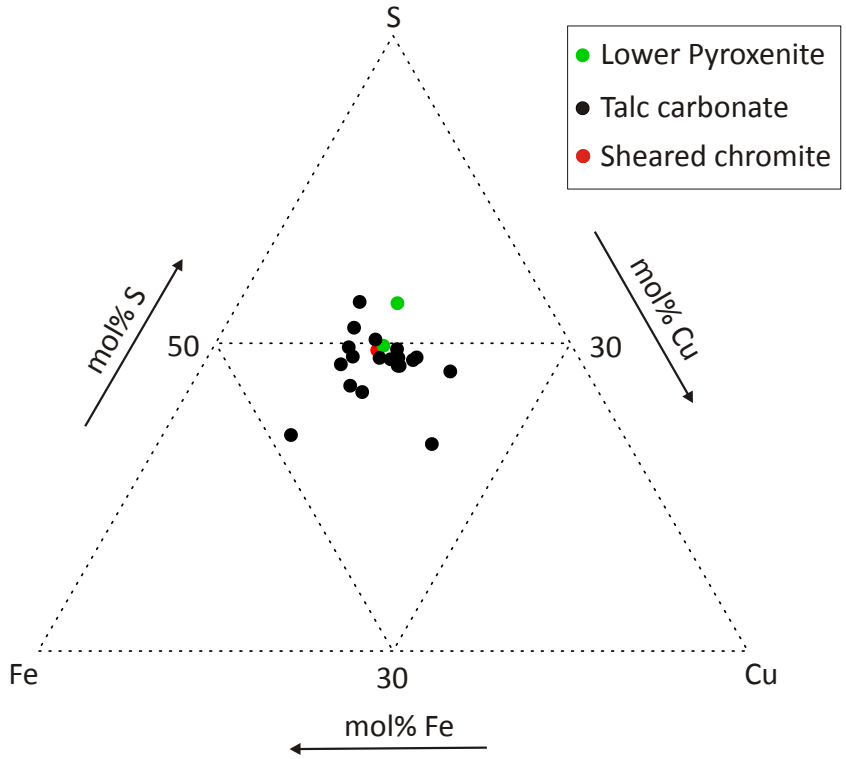

Fig. 8.22: Chalcopyrite composition in the system Cu-Fe-S. The mol% from Fe, S and Ni are normalised to 100 mol%. The black arrows outside the ternary plot show the direction of increasing mol% and the corresponding element. There is no clear trend of the chalcopyrite composition with respect to the host lithotypes (Lower Pyroxenite – green dots, talc-carbonate – black dots, sheared chromitite – red dot).

Figure 8.22 is aiming to demonstrate if there is a shift of the chalcopyrite compositions with regard to their host rocks. Because of the composition of chalcopyrite the system Cu-Fe-S was chosen.
The ternary plot Cu-Fe-S (Fig. 8.22) shows no trend in the composition of chalcopyrites. The measurements of the talc-carbonate (black dots), Lower Pyroxenite (green dots), and sheared chromitite (red dot) plot in a similar area. Therefore there was no modification of chalcopyrite during the alteration.
The sulphides mostly possess a stoichiometric composition. Therefore one can conclude that there was no or only small modification of the sulphide assemblage.

8.3.2.3 Magnetite

Magnetite, which has a typical stoichiometric content of Fe (43.16 ± 2.58%) and O, was observed in samples of the Lower Pyroxenite. There are low contents of the elements Mg, Si, Al, Ti and Mn as traces in magnetite.

8.3.2.4 Ilmenite

Ilmenite possesses a stoichiometric composition and a Fe:Ti mol ratio of about 1. The Fe and Ti contents are 18.72 ± 2.01% and 18.98 ± 2.17% respectively. Minor Mn is also present. One ilmenite grain possesses small impurities of Mg, Si, Al and Ca.

8.3.3 Other minerals

In this chapter minerals are summarized that are of minor significance. These minerals are albite, monazite, titanite, galena, apatite and stibnite.
Albite was identified in peridotite as well as monazite. Albite is most likely a product of the alteration of plagioclase. Monazite could be a primary accessory mineral because of its chemical durability.
Titanite and apatite were found in a talc-carbonate rock. Apatite can be interpreted as a mineral that was formed by alteration.
Stibnite and galena, whose modal content should be less than 0.1%, are related to a chromitite specimen. Exotic accessory minerals such as monazite and Pb-Sb-S phases in ultramafic rocks were also observed in a study by Zaccarini et al. (2006). These phases have their origin in the country rocks of the studied Campo Formoso complex. With regard to the interacting fluids the studied Campo Formoso layered ultramafic complex possesses a

similar alteration process as the Uitkomst Complex. Therefore elements such as Pb, Sb are linked to accessory minerals or sulphides, which are extremely rare.
In thin section H31 (Lower Pyroxenite) an oxide phase with an exceptional high Fe content (70.7%) was observed. The measurement could be a mixture of magnetite and native iron, which can be interpreted as a result of the very reducing nature of the fluid, which was generated by serpentinisation.

Summary

According to the XRD data the mineral assemblages are variable in the talc-carbonate schist, which gives rise to different compositions detected by the XRF measurements. The observed mineral assemblage is calcite-dolomite-talc-lizardite/chrysotile-clinochlore-tremolite-biotite-pyrite-pyrrhotite-pentlandite-chalcopyrite.
The XRF data show that there are two groups of talc-carbonates. Ca group 1 possesses a CaO content <1% due to the absence of carbonates. Ca group 2 has a CaO content >1%. The primary trends of the igneous rocks are strongly overprinted due to the modification by alteration. SiO_2, MgO and CaO were relatively enriched, and Al_2O_3, Fe_2O_3, Cr_2O_3, K_2O, Na_2O, P_2O_5, TiO_2, and MnO were relatively depleted during the alteration process. The alteration box plot (Fig. 8.6) shows that the rocks are highly altered.
Carbonates, talc, and serpentine match well with the ideal compositions. Pyrrhotite, pyrite and chalcopyrite do not show modifications because of the alteration process while the Ni content of pentlandite slightly decreased. The compositions of chromite, chlorite and amphibole are variable. Chlorite is intergrown with serpentine, which leads to relative higher Si contents and relatively lower Al and Fe contents. Additionally chlorites possess a highly variable composition. Like chromites they are susceptible to chemical overprinting during alteration processes.
The composition of chromites indicates an alteration temperature between 500 and 550°C.

9 pT-xCO_2 estimation using pseudosections

9.1 Description of the pT- and pseudosections

The pseudosections were modelled using the software Perple_X (Connolly 1990, Connolly & Petrini 2002). The Gibbs energy minimization (Connolly 2009), the thermodynamic database of Holland & Powell (1998, revised in 2003) and the Compensated-Redlich-Kwong (CORK) equation by Holland and Powell (1991, 1998) were used. Clinochlore represents all its varieties (e.g. leuchtenbergite, diabanite).

Pseudosections show the stability condition and reactions of a mineral assemblage for a specific bulk rock composition. The advantage of pseudosections is that they are less complex than standard phase diagrams and easier to interpret (Mukherjee 2011, S. 228).

The final pseudosections were modelled in the system Al_2O_3-MgO-CaO-SiO_2-CO_2-H_2O, which yields the most meaningful results. Fe_2O_3 was excluded in the modelling approaches because most of the Fe is incorporated in pyrite, which is not considered by Perple_X as a mineral phase. Therefore Fe would be incorporated in other Fe bearing phases such as siderite and daphnite, which were not observed in the Uitkomst Complex by any author. Mineral phases such as calcite would vanish because the Fe would be assigned to them.

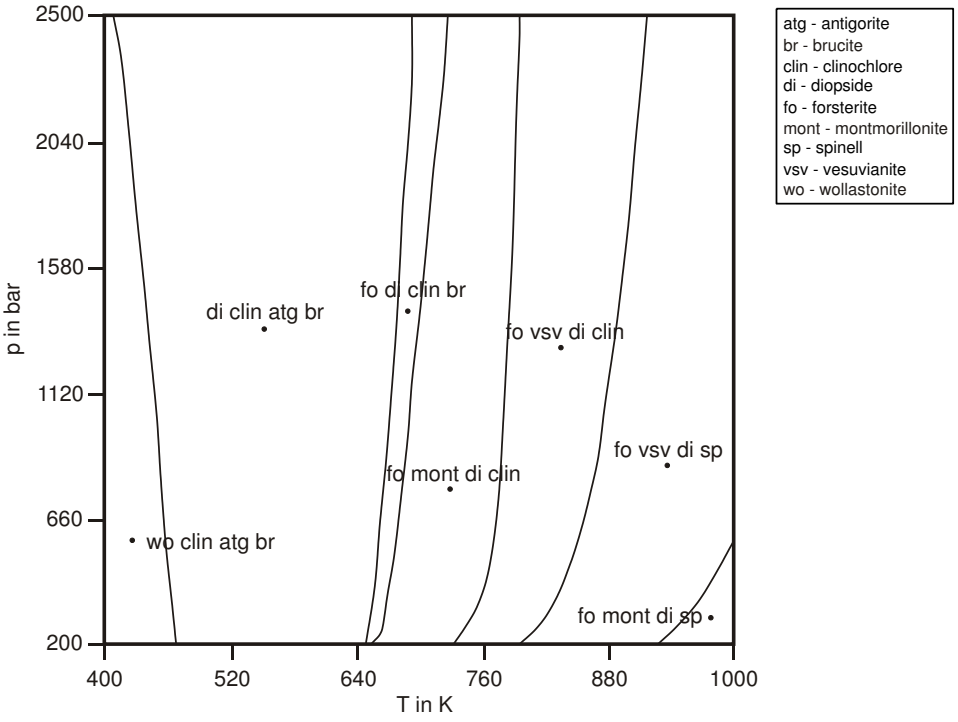

Fig. 9.1: p-T diagram in the system SiO_2-Al_2O_3-MgO-CaO-H_2O. The tie-lines are nearly vertical except for the tie-line, which separates the stability fields fo-vsv-di-sp and fo-mont-di-sp. Therefore the reactions of the system are nearly pressure independent. The abbreviations are defined in the legend in the right upper corner.

Figure 9.1 shows a p-T-diagram with a pure aqueous fluid. All tie-lines in the critical temperature range (450 to 800 K) are nearly vertical. Pseudosections with higher CO_2 values showed similar results pointing to a nearly pressure independent system. Therefore it is very difficult to estimate the pressure conditions from the modelled pseudosections. One modelled pseudosection at 2000 bar pressure, which is the twofold of the pressure of the other pseudosections (Fig. 9.2 and 9.3), showed a shift of the tie-lines of just 20 to 30 K towards higher temperatures.

The following pseudosections (Fig. 9.2 and 9.3) show the stability conditions of the observed mineral assemblages in the talc-carbonate schist.

Figure 9.2 shows the pseudosection of Ca group 1 (CaO <1 weight%). In the lower range of CO_2-contents of the fluid (0-0.1) and temperature from 400 to 750 K all tie-lines in the pseudosection have a steep, positive slope. Above 750 K they turn into a slightly negative slope getting steeper with increasing CO_2-contents. At moderate CO_2-contents (0.1-0.6) the tie-lines are nearly horizontal. With increasing CO_2-contents the tie-lines change their slopes to either positive or negative values. The occurrence of cordierite at temperatures above 760 K and high CO_2-contents seems to be possible.

The evolution paths described below (Fig. 9.2 and 9.3) are related to an internally buffered system as it was determined by Steenkamp (2012) and will be taken into account in the discussion. Externally buffered systems show only a decrease of temperature at constant CO_2 mol ratios due to the continuous supply with CO_2 rich fluids.

The starting point 1 of the evolution path is at 760 K and a CO_2 mol ratio of 0.6. The composition of the fluid is buffered along tie-line a towards the invariant point 2. From this point forsterite becomes instable and serpentine (antigorite) enters the system. Along the tie-line b the fluid is buffered until the invariant point 3, where all observed minerals (talc, calcite, dolomite, clinochlore, antigorite, tremolite) are stable. From invariant point 3 tremolite leaves the system and calcite becomes stable.

The pseudosection of Ca group 2 (CaO >1 weight%) (Fig. 9.3) shows some differences compared to the pseudosection of Ca group 1. Up to a temperature of about 760 K the pseudosections are nearly similar while significant differences can be seen at temperatures above 760 K. The stability fields are less complex and generate much different tie lines. The minerals diopside, forsterite and calcite are stable over a wide temperature and CO_2 range. Minerals such as sudoite, spinel and vesuvianite are stable according to figure 9.3 but these minerals were not observed in thin sections or by XRD or SEM measurements, because they are not stable in the critical T-CO_2 conditions. Enstatite and cordierite are not present. These differences of the pseudosections are due to the different composition of the two Ca groups. Diopside ($CaMg[Si_2O_6]$) is stable instead of enstatite ($Mg_2[Si_2O_6]$) due to the higher Ca

content. The differences at high temperatures are negligible because these areas are outside the critical T-xCO$_2$-conditions.

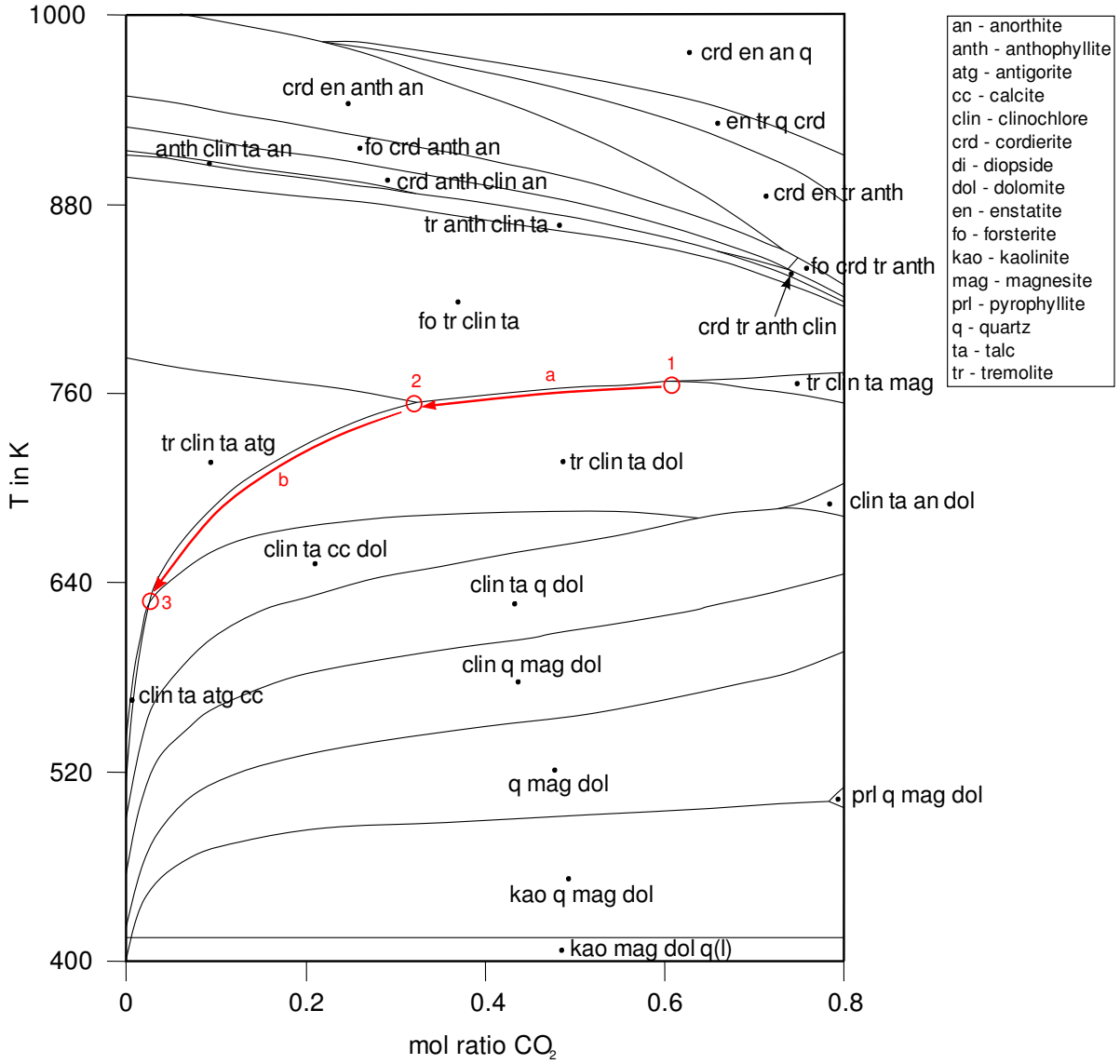

Fig. 9.2: A modelled pseudosection in the system SiO$_2$-MgO-CaO-Al$_2$O$_3$-H$_2$O-CO$_2$. The mol ratio of CO$_2$ is plotted against the temperature. The applied pressure is 1000 bar. The abbreviations are defined in the legend in the right upper corner. The red arrows represent the evolution apth of the fluid and the mineral assemblage.

To illustrate the model in the pseudosection a starting point (1) has to be estimated, which was chosen at temperatures of around 800 K and CO$_2$-contents of 0.7. The composition of the fluids is buffered along the tie-line a between the stability fields fo-di-clin-cc and fo-di-clin-dol to the invariant point 2. From this point evolution path goes along the tie-line b between the stability fields fo-tr-clin-cc and fo-tr-clin-dol to the next invariant point 3. The final step is the evolution to invariant point 4 along the tie-line c, which rests on the fields tr-clin-atg-cc and tr-clin-atg-dol.

Assuming the temperature decreased linearly the composition of the fluid changed relatively fast until a CO_2 mol ratio of 0.1. After this point the fluid composition changes much slower. The evolution paths of both pseudosections are similar. The path in figure 9.3 is more complex and begins at higher temperature (800 K instead of 760 K). The end point is the same in both modelled pseudosections.

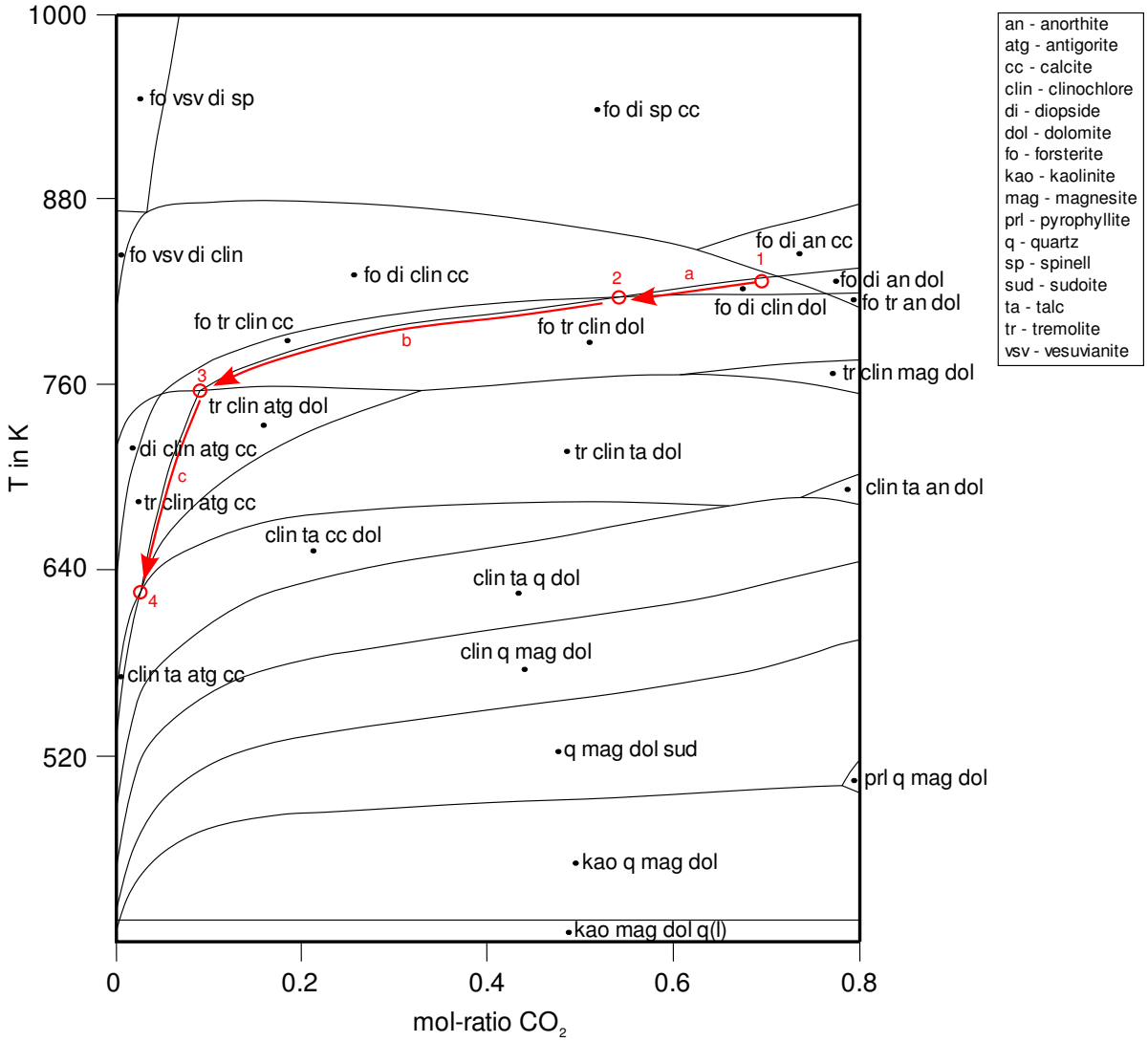

Fig. 9.3: A modeled pseudosection in the system SiO_2-MgO-CaO-Al_2O_3-H_2O-CO_2. The mol ratio of CO_2 is plotted against the temperature. The assumed pressure is 1000 bar. The abbreviations are defined in the legend in the right upper corner. The red arrows show the possible evolution path of the alteration fluid and the mineral assemblage.

9.2 Evolution of mineral assemblages

It is thought that the fluid, which interacted with the rocks, evolved over time from higher to lower temperatures and from higher to lower CO_2-contents. The fluid was initially generated by the decarbonisation reactions of the dolomites (Gauert et al. 1995, Steenkamp 2012)

leading to relative high CO_2 mol ratios of the fluid, which reacted with the ultramafic rocks to generate the talc-carbonate assemblage. The CO_2 was consumed and the fluid became depleted in CO_2. At the same time the temperatures decreased because of the cooling of the ultramafic intrusion.

The reactions, which could have taken place according to the evolution path in figure 9.3, are described below. The reactions are in the range of the temperature as it is indicated by the invariant points in figure 9.3. The red arrow in figure 9.3 shows the evolution of the mineral assemblage.

Point 1 is the starting point of the evolution path. The stable mineral assemblage is dolomite-calcite-diopside-forsterite-clinochlore. The reaction of diopside to tremolite occurs at the invariant point 2, because diopside leaves the system and tremolite becomes stable. Reaction 9.1 is taken from Goodwin-Bell (2008).

$$reaction\ 9.1\text{: } 4\ diopside + \ dolomite \ + \ CO_2 + \ H_2O \ \leftrightarrow tremolite + 3\ calcite$$

Reactions such as 9.2 and 9.3 (O'Hanley 1996, S. 137 f.) occurred at invariant point 3, in which antigorite replaces forsterite as a stable phase.

$$reaction\ 9.2\text{: } 214\ forsterite + 20\ tremolite + 40\ CO_2 + \ 321\ H_2O \leftrightarrow 11\ antigorite + 40\ calcite$$

$$reaction\ 9.3\text{: } 282\ forsterite + 20\ tremolite + 80\ CO_2 + \ 383\ H_2O \leftrightarrow 13 antigorite + 40\ dolomite$$

The reaction of chlorite to serpentine produces intergrowth textures (Banfield et al. 1994, Bailey et al. 1995) as it is evident in the thin sections.

Reaction 9.4 and 9.5 are taken from O'Hanley (1996). These reactions could have taken place at invariant point 4, where serpentine or tremolite reacts to talc.

$$reaction\ 9.4\text{: } 2\ lizardite + 3\ CO_2 \leftrightarrow talc + 3\ magnesite + 4\ H_2O$$

$$reaction\ 9.5\text{: } 3\ tremolite + 6\ CO_2 + \ 2\ H_2O \ \leftrightarrow \ 4\ quartz + 5\ talc + 6\ calcite$$

The next section describes the possible evolution of minerals, which could not be modelled in the systems applied to the pseudosections.

Chromite could not be observed by XRD, SEM or thin section investigations in the talc-carbonates, which can be explained by very high fluid:rock-ratios because the highly altered

rocks (talc-carbonates) are structurally related to the thrust faults and zones in PCR unit. Hot fluids, which are responsible for the dissolution of the chromite (Barnes 2000), could migrate along these shear zones. The released Al from the chromites was consumed by the formation of chlorite (Merlini et al. 2009, Gervilla et al. 2011) explaining the occurrence of chlorite in the talc-carbonate. Serpentine replaced the chlorite, which led to the observed intergrowth textures in the thin sections. This temporal progress is in line with the findings from the modelled pseudosections. Chromite, olivine and pyroxene released Mg during alteration. Mg can be taken into account for the formation of dolomite.

The abundance of chlorite is proportional to the Al_2O_3-content of the whole rock (Barnes 2000). If the parent rock hosts an Al-rich phase such as chromite or anorthite it is possible that chlorite will form. Therefore the talc-carbonate specimens from the LPxt host very small amounts of chlorite because chromite is missing and anorthite is very scarce as Al bearing phases in the protolith.

The occurrence of magnesite is stated in many publications (e.g. Johannes 1967). But magnesite could not be observed in the Uitkomst Complex. According to the pseudosections the surrounding temperatures are too high and the CO_2 ratio is too low.

In the pseudosections antigorite is the stable phase of the serpentine group. However, according to the XRD results serpentines are mostly present in the form of lizardite. Possibly antigorite was converted into lizardite due to decreasing temperatures, which led to an instability of the antigorite phase. After Schartz et al. (2012) the transition of antigorite to lizardite is at around 300°C at a pressure of 1 kbar.

Summary

The pseudosections indicate a retrograde alteration path buffered along tie-lines from higher to lower temperatures and from higher to lower CO_2 mol ratios typical for an internally buffered system. The starting temperature of the alteration is estimated at 500°C, which is in line with the findings of the chromite composition. The pressure was difficult to evaluate due to the nearly pressure independent reactions that occur. The CO_2 content of the starting point was also difficult to estimate due to the horizontal course of the tie-lines in the modelled pseudosections.

With decreasing temperatures and CO_2 mol ratios diopside was replaced by tremolite followed by the transition of forsterite to antigorite and carbonate. At low CO_2 mol ratios lizardite reacts to talc and tremolite is replaced by quartz, talc and calcite.

10 Discussion

In this study the talc-carbonate-pyrite alteration of the PCR was investigated with respect to its spatial distribution, geochemical characteristics and p-T-xCO_2 conditions. The original hypotheses (structural control of the alteration, retrograde evolution of alteration assemblages, T-xCO_2 conditions of the alteration fluid) regarding the origin of the alteration proved true. The only idea, which could not be confirmed, was the presence of magnesite as it is indicated by the literature (e.g. Johannes 1968), which does not mean that magnesite is absent at all.

Mapping and structure

The normal sequence of the units of the Uitkomst Complex could be confirmed. The main structural features are the thrust faults and NE-SW trending main faults as they were also observed by Hornsey (1999). This is in line with the compressive stress regime from a NE-SW direction. The small vertical displacements could also be observed in the open pit. In some places the LPxt unit is thrusted over the PCR unit, which points to continuing magma flows through the conduit. In the principal stress direction (σ_1) NE-SW a major low dipping shear zone could not be observed, which excludes an influence on the genesis of the low dipping thrust zones from this direction. Such a major thrust is apparent in the W part of the pit on the benches 23 and 24 with an E-W trend and a dip to the N (Fig. 7.13), which indicates a pushing force from a northern direction. Similar thrusts with an E-W trend were observed by Gauert (1998).

The next descriptions are aiming to demonstrate the relative temporal order of the observed structural features according to the structural model of Hornsey (1999), which is already described in the section 3.5. The layer-parallel faults and the NE-SW trending faults crosscut the diabase sills. The NW-SE trending faults crosscut the diabase sills and the thrust faults. The northernmost steeply dipping fault possibly crosscuts the shear zone, which separates the PCR from the LPxt on the benches 23 and 24 (Fig. 7.13). As a result, the oldest structures are the diabase sills, followed by the layer-parallel shear zones, which are crosscutted by the NE-SW trending main faults as the youngest structures. Therefore the findings of the face mapping are in line with the relative chronology of the evolution of the Uitkomst Complex as it was stated by Hornsey (1999).

This section discusses the structural features of the Uitkomst Complex. One problem arose from the very low dip (5 to 20°) and the adverse opportunity to measure the bedding in an exact way because of security restrictions of the Nkomati mine. Therefore it was not possible to measure the true strikes and dips of the diabase intrusions. The problem was much less

serious measuring steep dipping structures. Despite these difficulties a rough ENE-WSW trend of the bedding poles could be determined (Fig. 7.18). This finding points to a boat to trough-shaped form of the Uitkomst Complex (Gauert et al. 1995). The NE-SW trending main faults were originated by the principal stress from this direction. The overlapping areas of the bedding and the horizontal thrusts in NW-SE direction in the stereonet (Fig. 7.17 and 7.18) indicate that the thrusts follow the bedding planes, which are natural zones of weakness and susceptible to layer-parallel faulting and thrusting events. The bedding planes act as anisotropic zones in the rock, which lead to a higher susceptibility for deformation (Gomez-Rivas and Griera 2009). Additionally the presence of fluids, as they were apparent in the Uitkomst Complex, reduces the shear strength of a rock (Griggs 1936), which contributes to faulting.

It is not clear if the layer-parallel faulting (Hornsey 1999) continues in the lower three units of the Uitkomst complex. It is likely that a part of the layer-parallel faults in the igneous series are restricted to the ultramafic complex. Therefore the model of Hornsey (1999) has to be expanded by a fourth stage, which is in the temporal order between the layer-parallel thrusting of the country rocks and the emplacement of the sills and dykes. It is also possible that the layer-parallel faults, which are restricted to the ultramafic body, are syngenetic to the layer-parallel faults in the country rocks. One possible mechanism for the formation of the thrust faults in the igneous rocks is that the fluid pressure lowered the shear strength of the rocks, which led to faulting. This case would indicate a development of the thrusts independent from the layer-parallel faulting in the country rocks.

Hornsey propagated in his model “no evidence of … removal of the country rock by the Lower Harzburgite”. This finding is wrong with respect to the observed alternate bedding of pyroxenites and calc-silicates in the LPxt on bench 22. The streaming magma forced the sedimentary layers to tear. Some layers withstood the force and remained at their place, which is a clear evidence for country rock-magma interaction. Similar structures of the calc-silicates are also apparent in the Basal Gabbro, although to a lesser extent.

Due to this fact the model of Hornsey needs some modifications with respect to the lower units of the Uitkomst Complex. A mechanism, which was completely ignored by Hornsey (1999), is the thermal weakening of the country rocks. The strength of a rock decreases with increasing surrounding temperature (Handin & Hager 1958). This could have led to early fracture generation and propagation in the country rocks. Furthermore, the creation of space by the assimilation of country rock should be considered. The author proposes a model, in which both factors play a role. The massive xenoliths on the benches 22 and 23 clearly show a significant assimilation of country rock. The emplacement of the intrusion because of tension cracks originated by doming (Hornsey 1999) is feasible to assume as well as the

generation of zones of weakness by thermal weakening (Wei & Zang 2006) and contracting of the country rocks.

Joubert (2013) investigated the structure and the geochemistry of the Massive Chromitite layers. The orientation of the fracture zone in Jouberts thesis (2013) is in good agreement with main strike orientation (NW-SE) in this study. There are some deviations according to faults and joints. Some joints measured by Joubert are nearly horizontal. It is possible that the bedding was regarded as joints. The faults measured by Joubert possess similar strike directions but lower dips than these in this study. The phenomena can be explained by the different mapping areas of both studies. Joubert was focussed on the upper PCR unit and the Massive Chromitite layer while for this study the lower four units of the Uitkomst Complex were mapped, which results in shifted numbers of certain structural elements. There are more observed steep dipping faults in this study than in the thesis of Joubert. Therefore the differences in both studies are mostly of relative nature and structural findings of Joubert (2013) could partially be evaluated.

Steenkamp (2012) concluded that the shear zones in the Massive Chromitite of the PCR unit were generated by the volume increase due to the talc-carbonate alteration, which is in conflict with the findings of Hornsey and this study. An increase in volume would generate radial extension cracks in the hanging units (Hornsey 1999) and an upwards movement but the theory after Steenkamp does not explain the horizontal motion, which led to a considerable thickening of the Massive Chromitite (Hornsey 1999, Joubert 2013)

The mine geologists of the Nkomati joint venture stated that a major vertical displacement in NE-SW direction is apparent in pit 3 but nobody did recognise a fault (pers. comm. Edwards 2012, pers. comm. Mandiwana 2012). During the mapping numerous faults with vertical displacements of up to 50 cm were recognised. Therefore there is the possibility that the small displacements aggregate to a large displacement, which is the reason that nobody found a large displacement.

It is possible that not all of the faults were recognised due to their small vertical displacements and overprinting by joints which were produced by blasting operations.

The face mapping resulted in the conclusion that the alteration is structurally linked to the thrust faults in the PCR unit and to the steeply dipping NE-SW trending main faults. Around calc-silicate xenoliths alteration occurrences are apparent as well. Donaldson (1981) also observed structural controls on the distribution of the talc-carbonate schist in dunites of the Archean Norseman-Wiluna greenstone belt in the NE of the Yilgarn Block. It is likely that fluids of meteoric origin migrated along the NE-SW trending faults as it is proposed by Sarkar et al. (2008).

The closer a rock is to a fault the higher is its degree of alteration, which is linked to higher water:rock ratios along joints, faults and shear zones. The mapped alteration is to be regarded as the smallest area which is affected by this process because investigations of thin section showed alteration characteristics in specimens, which were thought to be fresh. Therefore it is very likely that the alteration is more pervasive than mapped.

Geochemistry, mineralogy and alteration

The XRF measurements reveal a high variability. During the milling of rock samples it cannot be ruled out that there were some contaminations from the jar mill that is lined with a WC alloy. This would result in slightly higher W and Mo contents of the rock powder. The XRF gadgetry measured too high SiO_2 contents due to contaminations in the facility. The impact of these deviations is of minor character with respect to the evaluation of the measurements. The most important diagrams do not consider SiO_2. The calculated alteration indices (CCPI – chlorite-carbonate-pyrite-index, AI – Ishikawa alteration index) generally yielded very high values for all samples, which is indicative for very high degrees of alteration. In the alteration box plot (Large et al. 2001) the specimen plot along the chlorite-carbonate alteration path and the chlorite-pyrite-sericite path. The talc-carbonates possess higher degrees of alteration than the PCR measurements. The LOI (loss of ignition) correlates with the Ca content indicating higher degrees of alteration with increasing LOI and Ca values. Mobility diagrams (Fig. 8.5) indicate depletion of Al_2O_3, Cr_2O_3, Fe_2O_3, TiO_2, MnO, K_2O, Na_2O, and P_2O_5 and enrichment of SiO_2, MgO, and CaO of the talc-carbonates in comparison to the PCR specimens. The total loss Al_2O_3, Cr_2O_3, and Fe_2O_3 can be attributed to the dissolution of chromite, which can only be achieved if the fluid:rock ratio is very high (Barnes 2000). Due to the structural control on the occurrence of the talc-carbonate schist by the horizontal shear zones it is likely that large volumes of fluid passed the shear zones. The dissolution of chromite is apparent in BSE images from the SEM measurements (fig. 6.17). Chlorite and serpentine could not incorporate the entire Al which led to a total loss of Al_2O_3. The loss of the minor elements (TiO_2, MnO, K_2O, Na_2O, P_2O_5) can be attributed to the breakdown of amphiboles and partially of pyroxenes. The enrichment of SiO_2 and MgO is due to the formation of serpentine and talc. However, the enrichment of SiO_2 should be smaller than it is detected due to the overestimation in the XRF measurements. The findings do not consider the change in density during the alteration process. Steenkamp (2012) tried to demonstrate the mobility of oxides and elements based on the study of Grant (1986) but the results were very heterogeneous with changing depletion/enrichment patterns from sample to sample.
According to investigation of thin sections, XRD and SEM measurements the observed mineral assemblage of the talc-carbonate schist is calcite-dolomite-talc-serpentine-chlorite-

tremolite-biotite-pyrite-pyrrhotite-pentlandite-chalcopyrite. Minerals, which compose less than 5 % of the rock, cannot be measured or only few peaks are apparent. This can be an explanation for a peak, which could not be assigned in many measurements. Its 2Θ position is 8.5°. A mineral, which possesses a peak in this range and is likely to occur, could be palygorskite but this does not imply a guarantee that palygorskite is present in the talc-carbonate schist. A possible formation of palygorskite in the Uitkomst Complex is possible because palygorskite is an alteration product of Mg silicates (Anthony 1995). Serpentine occurs mostly in the form of lizardite, which is indicative for greenschist facies conditions (Donaldson 1981). Magnetite is not present in the talc-carbonate-schist despite the fact that magnetite is a common mineral in altered ultramafic rocks. The magnetite could have been broke down during the talc-carbonate alteration. The Fe could have been released by the reaction with H_2, which is generated during serpentinisation processes. The addition of S from S bearing fluids (Sarkar et al. 2008) led to the formation of secondary pyrite.

The carbonates (dolomite and calcite) were identified by scanning electron microscope (SEM), which has a highly limited accuracy if light elements like O or C are analysed. The deviation is at least 5 %. If the specimens contain carbonate minerals and minerals with a high OH content (talc, serpentine) the analysis in only reliable for the heavier cations in the compounds. The accuracy for heavier elements is 1% (pers. comm. Walther 2012).

The formation temperature of the talc-carbonate schist was 500 to 550°C, which is evident by the modelled pseudosections in chapter 9. The pressure was difficult to assess because of the nearly pressure independent nature of the mineral reactions but was estimated at 1000 bar, which is in line with Gauert (pers. comm. 2012) and the findings of Hulley (2005). The overall appearance of the modelled pseudosections is in good agreement with the experimentally determined phase diagrams of Johannes (1967) and Barnes & Hill (2000), but one has to consider that the pseudosections were modelled with the assumption that the system is in equilibrium. According to Klein & Garrido (2011) serpentinisation processes occur under disequilibrium conditions, which are also visible in thin sections. The minerals are very fine-grained and did not have the possibility to form larger aggregates or smooth crystal boundaries (e.g. Fig. 6.20, 6.24). Additionally replacement structures are apparent in nearly all thin sections (e.g. Fig. 6.12, 6.16, 6.20). Especially along the rim of veins and cracks minerals like chromite and olivine (Fig. 6.16) are replaced. These disequilibrium conditions may lead to small deviations between the observed mineral assemblage and the results of the modelled pseudosections. Additionally it is assumed that there is no major element transport into or out of the closed system. Minor constituents such as TiO_2, K_2O, Na_2O and P_2O_5 were not considered because of their low concentrations and for reduction of occurring phases, which excludes the consideration of alteration minerals like biotite or sericite. Cr_2O_3 could not be considered by the option file which was used in Perple_X during

the modelling, which excludes the appearance of chromite or fuchsite in the pseudosections. Fe_2O_3 was not regarded because Perple_X cannot consider sulphides as mineral phases. As a result metals such as Fe and Ni would be incorporated into siderite and olivine, which are not present or stable in the regarded sections. The disadvantage is that only the pure Mg end-members of olivine (forsterite) and clinopyroxene (diopside) are considered. Another point is that the rocks possess their original magmatic compositions at very high temperatures (directly after the emplacement of the ultramafic magmas). At this temperature the alterations fluids were not already produced. Therefore the system, which was modelled, is not applicable for original conditions during the initial emplacement of the Uitkomst Complex.

The mineral geochemistry of chromites points to a similar temperature from 500 to 550 °C. At temperatures above 550 °C the trivalent cations become mobile (Barnes 2000). This would result in a scatter of Al, Cr and Fe^{3+}, which is not apparent. Therefore the temperature could not have exceeded 550°C in the rocks, where chromite is present. There is a substantial scatter of divalent cations (Mg, Fe^{2+}), which is a result of cation exchange during alteration processes with the surrounding silicates (Barnes 2000). Joubert (2013) explained the scatter in divalent cations by primary magmatic events. In this study the atomic ratio $Mg/(Mg+Fe^{2+})$ of the chromites from the sheared chromitite is between 0.03 and 0.45 with a cluster between 0.03 and 0.1 (Fig. 8.15) while the $Mg/(Mg+Fe^{2+})$ atomic ratio measured by Joubert (2013) is at least 0.28 and possesses a cluster between 0.4 and 0.5, which shows that the chromites measured in this study reveal a scatter that cannot be explained by primary magmatic events alone. A second petrogenetic event must have taken place to produce the large scatter. The SEM data of the PCR chromites are in good agreement with the findings of Joubert (2013) but the chromites of the sheared chromitite show a substantial difference. The samples of Joubert are mostly from the Massive Chromitite. The question is, if he also investigated sheared chromitite samples. If this is not the case the difference to the data of Joubert is due to sampling effects.

In a ternary plot Cr-Fe^{3+}-Al the chromites plotted at the rim of the field of greenschist metamorphism which indicates temperatures around 500°C.

The determined alteration temperatures (500-550°C) are in rough agreement with the findings of Steenkamp (2012), who determined the temperatures at 540-660°C with modelled pseudosections. Gole et al. (1987) estimated similar temperatures (550°C) at a pressure of 3 kbar for alteration of the komatiites from the Agnew nickel deposit but it is shown in figure 9.1 that the influence of pressure on the reactions in the relevant temperature range is of minor character. Hence the determined temperatures of this study and the study of Gole et al. (1987) can be compared. The komatiites from the Agnew nickel deposit also intruded into carbonate country rocks, which were responsible for the generation of a CO_2 enriched fluid,

which led to a talc-carbonate alteration of the ultramafic rocks. Therefore the talc-carbonate alteration of the Uitkomst Complex can be compared to the alteration of the komatiites in the Agnew nickel deposit.

The sulphides do not show a significant modification during the alteration process. Only pentlandite reveals a small trend of Ni depletion and the (relative) enrichment of S, which can be explained by diffusion mechanisms triggered by deformation events (McQueen 1987) and Ni mobilisation during to the alteration of silicate minerals (Barnes & Hill 1998) but this observation is in conflict with the findings of e.g. Groves et al. (1974) or Donaldson (1981), which determined an upgrading of Ni ores in similar geological settings as the Uitkomst Complex possesses. However, to upgrade a Ni bearing sulphide assemblage substantial amounts Ni bearing silicates are necessary. Gauert et al. (1995) showed that olivine crystals of the PCR unit are Ni poor. Therefore there is not enough Ni to upgrade the observed sulphide assemblage in the PCR unit, why the depletion mechanisms prevail and pentlandite becomes Ni poorer. Nevertheless, not all olivines are depleted in the Uitkomst Complex (pers. comm. Gauert 2013). Possibly, the temperature was not high enough to upgrade the Ni bearing minerals due to low diffusion rates.

The idea of a retrograde evolution trend is derived from the modelled pseudosections and the investigations of thin sections. The evolution follows roughly a decrease in temperature and CO_2 content of the fluid, which is buffered along nearly horizontal tie-lines until a CO_2 mol ratio of 0.1 (Fig. 9.3). After this point the tie-lines become much steeper and the composition of the fluid changes only in small amounts. Assuming the temperature decreased linearly the composition of the fluid changed relatively fast until a CO_2 mol ratio of 0.1. After this point the fluid composition changes much slower with constant decrease of temperature. According to the pseudosection magnesite is not present because of the high temperatures, which must have been much lower for the formation of magnesite. The system is regarded as internally buffered. The same finding was made by Steenkamp (2012). If one started at high CO_2 mol ratios and assuming a decrease in temperature without a decrease in CO_2 mol ratios (typical for externally buffered systems) then observed minerals like serpentine or calcite would not become stable. Therefore there has to be a decrease in CO_2 mol ratios, which can be achieved by internally buffered mineral reactions. Nevertheless, one has to consider that the CO_2 necessary for the reactions was derived from an external source. Therefore an externally buffered part is also apparent but it cannot be evaluated, why an internally buffered system is assumed.

According to the investigated thin sections the primary minerals were replaced during the alteration processes (e.g. Fig. 6.20). Pyroxene and olivine are replaced by serpentine. There is a possibility that the replacement proceeded over an interim stage, which would induce that pyroxene was replaced at first by amphibole and amphibole was replaced by serpentine.

Later serpentine was replaced by talc. The magmatic textures are mostly still apparent. The occurrence of quartz can be attributed to a late stage, low temperature interaction with an oxidizing fluid of possibly meteoric origin (Sarkar et al. 2008).
Concluding one can say that the talc-carbonate schist is a completely secondary originated rock unit. Primary, magmatic textures are preserved but all primary minerals are replaced by secondary ones. In some cases even the magmatic textures are destroyed.
According to the Nkomati geological department the rock density of peridotite is 3.14 g/cm³. The mean density of the rock powders is 3.21 g/cm³. Consequently there is a small overestimation of the rock density. The density of the talc-carbonate rocks is 2.89 g/cm³. Therefore a mass deficit or an increase in volume (Steenkamp 2012) must have had to be evolved during the talc-carbonate-alteration.

Alteration model

The supposed model for the alteration of the PCR unit is shown in figure 10.1 as a flow chart in the most likely temporal order of events.
The lowermost two units of the Uitkomst Complex (Basal Gabbro and Lower Pyroxenite) were deposited until the pyroxenite reached the level of the Malmani Dolomites. The detailed emplacement of the lithotypes is already describes in chapter 3.7. The dolomites were partially assimilated, decarbonised and passed through contact metamorphism. During the contact metamorphism the dolomite xenoliths degassed and released substantial amounts of CO_2 to the aqueous, deuteric fluid (de Waal et al. 2001, Steenkamp 2012), which was generated by serpentinisation processes. It is also likely that the country rocks directly decarbonised without being assimilated by the magma.
The Lower Pyroxenite was affected by talc-carbonate alteration due to CO_2 in the fluid. Therefore a smaller part of the produced CO_2 was used for this process. The rare development of a talc-carbonate assemblage in the Lower Pyroxenite can be explained with the buoyancy-driven rise of the fluids. Some amounts of CO_2 likely left the system along cracks into the country rocks. Afterwards the PCR unit was deposited. The Chromitiferous Peridotite was strongly affected by the alteration due to the upwards migration of the fluids. Most of the CO_2 was used for the formation of the carbonates in the PCR unit. The Massive Chromitite Layer on the top could have acted as a barrier or an upper 'seal' for the alteration fluids. The fluids cooled during the upward migration and the decrease in temperature of the surrounding rocks. The lower temperatures and CO_2 levels of the fluids led to the formation of serpentine in the PCR unit and the lower portions of the Main Harzburgite.

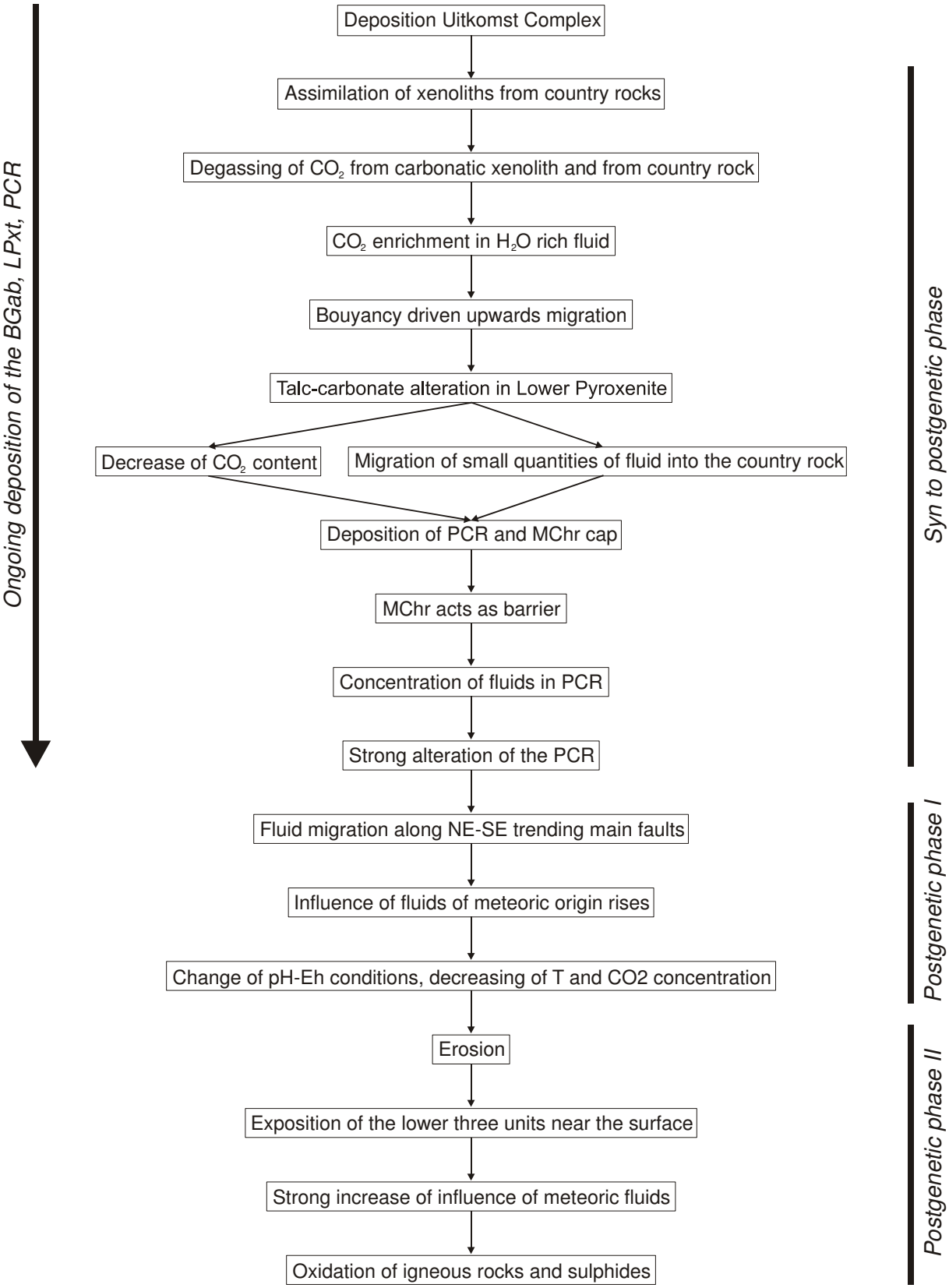

Fig. 10.1: The developed genetic model in temporal order of the events is shown.

The postgenetic phase I begins with the migration of aqueous, meteoric fluids into the complex along the NE-SW trending main faults (Sarkar et al. 2008). It is feasible to assume that the deuteric fluids and meteoric fluids mixed. Because of the likely oxidising properties

such meteoric fluids could have changed the pH-Eh conditions of the rock facies and the highly reducing serpentinisation fluids.

Due to erosion the complex is exposed near the surface, which introduces the postgenetic phase II. At present there is a strongly increased influence of meteoric waters, responsible for the oxidation haloes around the secondary pyrite cubes.

The proposed model is in agreement with the conclusions of Steenkamp (2012).

The findings of the thesis can be applied to the spatial assessment of the metallurgically problematic talc-carbonate schist. Enrichment processes of the Ni ore could not be evaluated. Therefore it is problematic to admix the talc-carbonate schist to the Ni ore. It is suggested to separate the talc-carbonate schist from the rest of the ore in-situ and dump it. A good assessment of the talc rich portions of the pit is critical to the mining operations in the LPxt and PCR unit (Bowers & Smit 2007) The structural models of Hornsey (1999) and Joubert (2013) could be largely confirmed. The suggestions of Steenkamp (2012) could be partially evaluated. New findings were made according to the mineralogical evolution of the talc-carbonate schist. Additionally the first continuous geological map of open pit 3 in the lower units of the Uitkomst Complex was produced.

11 Conclusions

Based on the investigations and observations the following conclusions can be made:

- The observed mineral assemblage of the talc-carbonate-schist is calcite-dolomite-talc-serpentine-chlorite-tremolite-biotite-pyrite-pyrrhotite-pentlandite-chalcopyrite.

- The degree of alteration of the rocks is very high. The alteration is very pervasive throughout the three lower units of the Uitkomst Complex.

- According to the different alteration zones in ultramafic rocks which were grouped by Johannes (1967) the talc-carbonates cannot be directly assigned to one of these groups. The talc-carbonate-schist is between the group magnesite + talc and magnesite + quartz, which can be regarded as the highest degree of alteration.

- According to the modelled pseudosections, mineral chemistry of the chromites and the observed mineral assemblage in the talc-carbonates the surrounding conditions during the formation of the altered rocks can be assigned to higher greenschist facies conditions. The temperatures were between 500 to 550 °C.

- Due to the dissolution of chromite it is feasible to assume that the fluid:rock ratios were very high during the talc-carbonate alteration.

- The evolution path of the alteration is retrograde. The path trends from higher to lower temperatures and from higher to lower CO_2-ratios.

- The alteration was initiated by H_2O- and CO_2 rich fluids. These fluids were derived from the country rocks due to devolatisation processes.

- The alteration was overprinted by late stage meteoric fluids which led to an oxidation of the sulphides in the talc-carbonate-schist.

- The alteration was a multi-stage process and cannot be reduced to one event.

- The massive chromitite layer at the top of the PCR unit could have been acted as a barrier for the fluids which caused the alteration. But this barrier was not compact enough to completely hold back the fluids. This is evident by carbonate minerals in specimen H 5 which was sampled directly above the top of the massive chromitite layer.

- The talc-carbonate-alteration is structurally controlled by the thrust faults and layer-parallel faulting in the PCR. The NE-SW trending faults also contributed to the alteration process. Along these structures in the LPxt highly altered rocks were observed, but no carbonate mineralisation was detected indicating that the fluids were of aqueous nature.

12 Outlook and review

Due to the fact that the talc-carbonate-schist was already mined out during the face mapping it is suggested to perform further mapping campaigns. The questions regarding the spatial distribution, structural control, geochemistry, and T-x_{CO2} conditions could be clarified.

The occurrence of chlorite in the talc-carbonate-schist could be used to identify the strongly altered portions of the PCR unit by airborne or terrestrial remote sensing techniques, which would improve the mine planning process and the processing of these rocks.

A big question is the depth during the deposition of the Uitkomst Complex and the formation of the alteration. For that purpose a geobarometry of the country rocks could be carried out. Until now only estimates were performed on this topic.

Further research could contain the comparison between the pyrites in the Lower Pyroxenite and the pyrites in the talc-carbonate schist in terms of composition, zonation, inclusions and S- and O-isotopes. A study like this could contribute to the nature of the fluids which are responsible for the alteration.

A further question is the origin of the quartz and calcite veins in the pit. Are they a result of serpentinisation or did they develop under the influence of external, country-rock-derived fluids?

A subsequent topic is the influence of meteoric fluids on the deuteric fluids and how they changed the Eh-pH-conditions. This topic can be investigated with numerical simulations and mixing experiments as well as from a mineralogical view with respect to theoretically forming mineral assemblages.

Another interesting issue which could be investigated is the formation of secondary copper mineralisation of the Lower Pyroxenite unit how it was observed by the author on bench 24. This work could contribute to the understanding of the late-stage ore genesis of the Uitkomst Complex.

13 Acknowledgements

I want to thank Professor Gauert for his support and organisation of the project as well as Professor Borg for his support and the initiation of this Master Thesis.
I want to show gratitude to the staff of the Nkomati Ni Mine. Especially I would like to express my thanks to the geology department and its staff Mr. Mark Davidson (Head of Department), Mr. Karel Coetzer (Manager of the Geology Department), Takalani, Bryn, Vincent, Jeffrey Jimmy and Thabiso. They helped whenever they could and answered questions concerning the project. My thank goes to Solly and Fuller for their support during surveying.
I also want to thank Andreas Kamradt and Marco Fiedler for their support and long as well fruitful discussions. Additional thanks goes to Sabine Walter for her support during the SEM measurements.
I also want to show gratitude to Professor Ian Lerche for the correction of the orthography.
And last but not least I want to thank my girlfriend Christine for her mental support in stressful times.

14 Literature

Anhaeusser, C.R., Robb, L.J., Barton, J.M. (1979): Mineralogy, petrology, and the origin of the Archaean Boesmanskop syenite, Barberton Mountain Land, South Africa. – Information Circular of the Economic Geology Research Unit, University of Witwatersrand, v. 139: 15 pp.

Anthony, W.A. (1995): Handbook of mineralogy: 446 S., Tucson (Mineral Data Publishing).

Bailey, S.W., Banfield, J.F., Barker, W.W. (1995): Dozyite, a 1:1 regular interstratification of serpentine and chlorite. – American Mineralogist, v. 80: 65-77.

Banfield, J.F., Bailey, S.W. (1996): Formation of regularly interstratified serpentine-chlorite minerals by tetrahedral inversion in long-period serpentine polytypes. – American Mineralogist, v. 81: 79-91.

Banfield, J.F., Bailey, S.W., Barker, W.W. (1994): Polysomatism, polytypism, defect microstructures and reaction mechanisms in regularly and randomly interstratified serpentine and chlorite. – Contributions to Mineralogy and Petrology, v. 117: 137-150.

Barnes, S.J., Hill, R.E.T. (2000): Metamorphism of Komatiite-Hosted Nickel Sulfide Deposits. – in: Spry, P.G., Marshall, B., Vokes, F.M. (Eds.): Reviews in Economic Geology: Metamorphosed and Metamorphogenic Ore deposits: 203-215, Littleton (Society of Economic Geologists).

Barnes, S.J., Wells, M.A., Verrall, M.R. (2009): Effects of Magmatic Processes, Serpentinization, and Talc-Carbonate Alteration on Sulfide Mineralogy and Ore Textures in the Black Swan Disseminated Nickel Sulfide Deposit, Yilgarn Craton. – Economic Geology, v. 104: 539-562.

Bowers, R.L., Smit, D.S. (2007): Process development of the Nkomati PCMZ base metals sulphide ore. - The Fourth Southern African Conference on Base Metals, symposium series S47: 415-432.

Bricker, O.P., Nesbitt, H.W., Gunter, W.D. (1973): The stability of talc. – American Mineralogist, v. 58: 64-72.

Button, A. (1973): A regional study of the stratigraphy and development of the Transvaal Basin in the eastern and northeastern Transvaal: 351 S., PhD-Thesis, Johannesburg (University of the Witwatersrand).

Caritat, P., Hutcheon, I., Walshe, J.L. (1993): Chlorite Geothermometry: A Review. – Clays and Clay Minerals, v.41: 219-239.

Cawthorn, R.G., Eales, H.V., Walraven, F., Uken, R., Watkeys, M.K. (2006): The Bushveld Complex. – in: Johnson, M.R.; Anhaeusser, C.R.; Thomas, R.J. (Eds.): Geology of South Africa: 261-281, Johannesburg (Geological Society of South Africa).

Clendenin, C.W. (1989): Tectonic influence on the evolution of the early Proterozoic Transvaal Sea, Southern Africa: 734 S. PhD-Thesis, Johannesburg (University of Witwatersrand).

Cox, K.G., Clifford, P. (1982): Correlation Coefficient Patterns and Their Interpretation in Three Basaltic Suites. – Contributions to Mineralogy and Petrology, v. 79: 268-278.

De Nooy, D.: Mineralogy of the MSB Ore from the Nkomati Mine: Implications to Beneficiation. – in: Rammlmair, D., Mederer, J., Oberthür, T., Heimann R.B., Pentinghaus, H. (Eds.): Applied Mineralogy in Research, Economy, Technology, Ecology and Culture: 277-281, Rotterdam (Balkema).

De Waal, S.A., Gauert, C.D.K. (1997): The Basal Gabbro Unit and the identity of the parental magma of the Uitkomst Complex, Badplaas, South Africa. – South African Journal of Geology, v. 100: 349-361.

De Waal, S.A., Maier, W.D., Armstrong, R.A., Gauert, C.D.K. (2001): Parental magma and emplacement of the stratiform Uitkomst Complex, South Africa. – The Canadian Mineralogist, v. 39: 557-571.

Deer, W.A., Howie, R.A., Zussman, J. (1992): An Introduction to rock forming minerals: 696 S., Harlow (Longman Verlag).

Donaldson, M.J. (1981): Redistribution of Ore Elements during Serpentinization and Talc-Carbonate Alteration of Some Archean Dunites, Western Australia. – Economic Geology, v. 76: 1698-1713.

Ehlmann, B.L., Kelemen, P.B., Pinet, P., Mustard, J.F., Launeau, P., Ceuleneer, G. (2012): Aqueous alteration of ultramafic rocks in Oman: an analog for understanding carbonate and serpentine on Mars. – 43rd Lunar and Planetary Science Conference, Contribution No. 1659.

Frost, B.R., Beard, J.S. (2007): On Silica Activity and Serpentinization. – Journal of Petrology, v. 48: 1351-1368.

Furukawa, Y., Sekine, T., Kakegawa, T., Nakazawa, H. (2011): Impact-induced phyllosilicate formation from olivine and water. – Geochimica et Cosmochimica Acta, v. 75: 6461-6472.

Gauert, C.D.K., De Waal, S.A., Wallmach, T. (1995): Geology of the ultrabasic to basic Uitkomst complex, eastern Transvaal, South Africa: an overview. – Journal of African Earth Sciences, v. 21: 553-570.

Gauert, C.D.K. (1998): The Petrogenesis of the Uitkomst Complex, Mpumalanga Province, South Africa: 315 S., PhD thesis, Pretoria (University of Pretoria).

Gauert, C.D.K. (2001): Sulphide and oxide mineralisation in the Uitkomst Complex, South Africa: origin in a magma conduit. – Journal of African Earth Sciences, v. 32/2: 149-161.

Gervilla, F., Fanlo, I., Kerestedjian, T.N., Castrovielo, R., Gonzalez-Jimenez, J.M., Padron, J.A., Rodigues, J.F. (2011): Alteration Mechanism of Chromite in Podiform Chromitites

from two Metamorphosed Ophiolitic Complexes: Golyamo Kamenyane (Bulgaria) and Tapo (Peru). – Geophysical Research Abstracts, v. 13.

Gomez-Rivas, E., Griera, A. (2009): Influence of mechanical anisotropy on shear fracture development. – Trabajos de Geologia, v. 29: 305-311.

Gole, M.J., Barnes, S.J., Hill, R.E.T. (1987): The role of fluids in the metamorphism of komatiites, Agnew nickel deposit, western Australia. – Contributions to Mineralogy and Petrology, v. 96: 151-162.

Goodwin-Bell, J.A.S. (2008): Delineation of isograds in siliceous dolomitic marbles along the Sharbot Lake – Frontenac terrane boundary of the Grenville Province, southeastern Ontario. – Canadian Journal of Earth Sciences, v. 45: 669-691.

Grant, J.A.: The isocon diagram; a simple solution to Gresens' equation for metasomatic alteration. – Economic Geology, v. 81: 1976-1982.

Griggs, D.T. (1936): Deformation of rocks under high confining pressures. – Journal of Geology, v.44: 541-577.

Groves, D.I., Hudson, D.R., Hack, T.B.C. (1974): Modification of Iron-Nickel Sulfides During Serpentinization and and Talc-Carbonate Alteration at Black Swan, Western Australia. – Economic Geology, v. 69: 1265-1281.

Handin, J., Hager, R.V. (1958): Experimental deformation of rocks under confining pressure: Tests at room temperature on dry samples. – American Association of Petroleum Geologists Bulletin, v. 41: 1-50.

Hornsey, A.E. (1999): The genesis and evolution of Nkomati mine Ni-sulfide deposit, Mpumalanga Province, South Africa: 224 S., M.Sc. Thesis, Durban (University of Natal).

Huang, W.L., Bishop, A.M., Brown, R.W. (1986): The effect of fluid/rock ratio on feldspar dissolution and illite formation under reservoir conditions. – Clay Minerals, v. 21: 585-601.

Hulley, V. (2005): Reactions between Country Rock Xenoliths and the magma of the Uitkomst Complex, with Implications for the Origin of the Sulphide Mineralisation: 117 S., M.Sc. Thesis, Pretoria (University of Pretoria).

Janousek, V., Farrow, C.M., Erban, V. (2006): Interpretation of whole-rock geochemical data in igneous geochemistry: introducing Geochemical Data Toolkit (GCDkit). – Journal of Petrology, v. 47: 1255-1259.

Johannes, W. (1967): Zur Bildung und Stabilität von Forsterit, Talk, Serpentin, Quarz und Magnesit im System MgO-SiO_2- H_2O-CO_2. – Contributions to Mineralogy and Petrology, v. 15: 233-250.

Johannes, W. (1968): Experimental Investigation of the Reaction Forsterite + H_2O ↔ Serpentine + Brucite. – Contributions to Mineralogy and Petrology, v. 10: 309-315.

Joubert, P.L., Gauert, C.D.K. (2013): The deposition of the Massive Chromitite layer of the Uitkomst Complex in South Africa: 49 S., BSc Hon. Thesis, Bloemfontein (University of Free State).

Kenyon, A.K., Attridge, R.L., Coetzee, G.L. (1986): The Uitkomst nickel-copper deposit, Eastern Transvaal. – in: Anhaeusser, C.R.; Maske, S. (Eds.): Mineral Deposits of Southern Africa Vol. I & II: 1009-1017, Johannesburg (Geological Society of South Africa).

Klein, F., Garrido, C.J. (2011): Thermodynamic constraints on mineral carbonation of serpentinized peridotite. – Lithos, v. 126: 147-160.

Mattauer, M. (1993): Strukturgeologie: 353 S., Enke Verlag (Stuttgart).

Merlini, A., Grieco, G., Diella, V. (2009): Ferritchromite and chromian-chlorite formation in melange-hosted Kalkan chromitite (Southern Urals, Russia). – American Mineralogist, v. 94: 1459-1467.

Mposkos, E., Baziotis, I. (2010): Study of the metamorphic evolution of a carbonate-bearing Metaperidotite from the Sidironero Complex (Central Rhodope, Greece) using p-T and p(T)-X_{CO2} pseudosections. – Bulletin of the Geological Society of Greece, v. 5: 2667-2679.

Mukherjee, S. (2011): Applied Mineralogy: Applications in industry and Environment: 562 S., Springer (Berlin).

Naldrett, A.J. (1966): Talc-Carbonate Alteration of some Serpentinized Ultramafic Rocks south of Timmins, Ontario. – Journal of Petrology, v. 7: 489-499.

Nesbitt, H.W., Bricker, O.P. (1978): Low temperature alteration processes affecting ultramafic bodies. – Geochimica et Cosmochimica Acta, v. 42: 403-409.

O'Hanley, D.S. (1996): Serpentinites: Records of Tectonic and Petrological History: 277 S., Oxford University Press (Oxford).

Okrusch, M., Matthes, S. (2010): Eine Einführung in die spezielle Mineralogie, Petrologie und Lagerstättenkunde: 658 S., Springer (Berlin).

Power, M.R., Scott, P.W. (1995): Talc-Carbonate alteration of some basic and ultrabasic intrusions in Cornwall. – Proceedings of the Ussher Society, v. 8: 392-397.

Sarkar, A., Ripley, E.M., Li, C., Maier, W.D. (2008): Stable isotope, fluid inclusion, and mineral chemistry constraints on contamination and hydrothermal alteration in the Uitkomst Complex, South Africa. – Chemical Geology, v. 257: 129-138.

Sarkar, A., Ripley, E.M., Li, C.: Oxygen and hydrogen isotopic studies of the Uitkomst Ni-Cu sulfide deposit, South Africa: Evidence of selective crustal contamination, multiple magma injection, and hydrothermal alteration. – Geological Society of America Abstracts with Programs, v. 37: 451.

Schandl, E.S., Naldrett, A.J. (1992): CO_2 metasomatism of serpentinites, south of Timmins, Ontario. – Canadian Mineralogist, v. 30: 93-108.

Schandl, E.S., Wicks, F.J. (1993): Carbonate and Associated Alteration of Ultramafic and Rhyolitic Rocks at the Hemingway Property, Kidd Creek Volcanic Complex, Timmins, Ontario. – Economic Geology, v. 88: 1615-1635.

Schwartz, S., Guillot, S., Reynard, B., Lafay, R., Debret, B., Nicollet, C., Lanari, C., Auzende, A.L. (in press): Pressure-temperature estimates of the lizardite/antigorite transition in high pressure serpentinites. – Lithos: 14 p.

Streit, E., Kelemen, P., Eiler, J. (2012): Coexisting serpentine and quartz from carbonate-bearing serpentinized peridotite in the Samail Ophiolite, Oman. – Contributions to Mineralogy and Petrology, v. 164: 821-837.

Trommsdorff, V., Connolly, J.A.D. (1990): Constraints on phase diagram topology for the system CaO-MgO-SiO_2-CO_2-H_2O. – Contributions to Mineralogy and Petrology, v. 104: 1-7.

Walraven, F., Martini, J. (1995): Zircon Pb-evaporation age determinations of the Oak Tree Formation, Chuniespoort Group, Transvaal Sequence: implications for Transvaal-Griqualand West basin correlations. – South African Journal of Geology, v. 98: 58-67.

Wei, R.Q., Zang, S.X. (2006): Effects of temperature and strain rate on fracture strength of rocks and their influence on rheological structure of the lithosphere. – Chinese Journal of Geophysics, v.49: 1576-1584.

Whitney, D.L., Evans, B.W. (2010): Abbreviations for names of rock-forming minerals. – American Mineralogist, v. 95: 185-187.

Whitney, G., Eberl, D.D. (1982): Mineral paragenesis in a talc-water experimental hydrothermal system. – American Mineralogist, v. 67: 944-949.

Williams, H. (1942): The geology of Crater Lake National Park, with a reconnaissance of the Cascade Range southward to Mount Shasta: 162 S., Carnegie Institution of Wahington publication (Wahington).

Wunder, B., Schreyer, W. (1997): Antigorite: High-pressure stability in the system MgO-SiO_2-H_2O (MSH). – Lithos, v. 41: 213-227.

Zaccarini, F., Garuti, G., Martin, R.F.: Exotic accessory minerals in layered chromitites of the Campo Formoso Complex (Brazil). – Geologica Acta, v. 4: 461-469.